GEOMORPHOLOGY AND METAL CONTAMINATION OF AN URBAN FLOODPLAIN ALONG WILSON CREEK, SPRINGFIELD, MISSOURI

A Masters Thesis

Presented to

The Graduate College of

Missouri State University

In Partial Fulfillment

Of the Requirements for the Degree

Master of Science, Geospatial Sciences in Geography and Geology

By

Aubree Vaughan

August 2014

GEOMORPHOLOGY AND METAL CONTAMINATION OF AN URBAN FLOODPLAIN ALONG WILSON CREEK, SPRINGFIELD, MISSOURI

Department of Geography, Geology, and Planning

Missouri State University, August 2014

Master of Geospatial Science

Aubree Vaughan

ABSTRACT

Elevated concentrations of toxic metals in sediments represent an environmental threat, but can also be used as tracers for dating floodplain deposits, particularly if the pollution history is known. Following, metal profile variations within floodplain soil cores affected by urban releases can provide an understanding of human-related watershed changes and geomorphic history. Wilson Creek in Springfield, Missouri drains the old industrial center of the city that dates back to the mid-1800s. The purpose of this study is to investigate the geomorphic history of urban floodplain deposition along a 597 m long reach of Wilson Creek, located immediately below a USGS discharge gaging station. The sub-basin of this study area drains 96 km^2 of southern Greene County. Metal analysis of floodplain surface samples indicate that landform elevation, proximity to the channel, and channel capacity contribute to sedimentation patterns. Field and LiDAR data in combination with a NRCS soil map allowed for accurate identification of valley floor landforms and associated distribution patterns of anthropogenic metals Cu, Pb, and Zn and the naturally occurring metals Ca and Fe. Aerial photographs supported these findings based on width measurements from select channel locations over a 57-year period. Results suggest that channel widening due to greater flow energy occurred throughout most of the study reach since 1953, except for cross-sections affected by bedrock control.

KEYWORDS: floodplains, fluvial sediments, urban pollution, topographic control, Wilson Creek, Missouri

This abstract is approved as to form and content

_____

Robert T. Pavlowsky, PhD
Chairperson, Advisory Committee
Missouri State University

GEOMORPHOLOGY AND METAL CONTAMINATION OF AN URBAN FLOODPLAIN ALONG WILSON CREEK, SPRINGFIELD, MISSOURI

By

Aubree Vaughan

A Masters Thesis
Submitted to the Graduate College
Of Missouri State University
In Partial Fulfillment of the Requirements
For the Degree of Master of Science, Geospatial Sciences in Geography and Geology

August 2014

Approved:

_____
Robert T. Pavlowsky, PhD

_____
Xiaomin Qiu, PhD

_____
Matthew Pierson, PhD

_____
Thomas Tomasi, PhD, Associate Dean Graduate College

ACKNOWLEDGEMENTS

I would like to thank Dr. Pavlowsky for the numerous educational opportunities he provided for me in the classroom and in the field. This project would not have succeeded without his guidance and support. I also want to thank him for allowing me to work with OEWRI, where I not only learned a lot, but also made lifelong friendships and memories. Another key influence in this research was Marc Owen. Marc helped with nearly all of the fieldwork involved in this project and was always prepared with words of encouragement. Thank you to my committee members Dr. Qiu and Dr. Pierson for your meaningful input and guidance. Thank you to my parents, who have always supported my adventures and encouraged me to achieve my goals. I would also like to thank my best buddy, and dog, Hattie Mae. She patiently sat by my desk for hours on end while I worked on this project. I am thankful for all of these wonderful influences, and owe the success of this project to them.

TABLE OF CONTENTS

LIST OF TABLES

LIST OF FIGURES

CHAPTER ONE: INTRODUCTION

Floodplains are constructed by the river itself through the influence of both hydrological and sediment transport processes (Wolman and Leopold, 1957; Magilligan, 1985; Walling, Quine, and He, 1992; Jain, Fryier, and Brierly, 2008). These depositional landforms form along the sides of the channel when rivers overflow their banks and deposit sediment (Wolman and Leopold, 1957). Floodplains are primarily composed of sedimentary materials that were supplied from upstream sources including upland soil erosion, landslides, and stream bank erosion. Therefore, floodplains represent both a sink and source of sediment in a watershed (Magilligan, 1985). In addition, sediment-associated contaminants released from urban, industrial, and mining sources can be stored in floodplains for long periods of time, and remobilized 10 to >100 years later (Sekabira, Origa, Basamba, Mutumba, and Kakudidi, 2010). Land use changes within a watershed such as urbanization or agriculture can alter the geomorphic processes controlling floodplain sedimentation and erosion, creating the potential for the remobilization of floodplain sediment back into the stream (Knox, 1977; Magilligan, 1985; Walling and He, 1999). The release of excess sediment and associated contaminants can in return degrade water quality and harm biological life within the watershed (Paul and Meyer, 2001).

Floodplains provide important areas for both aquatic and terrestrial life within riparian corridors through increased habitat connectivity and biodiversity (Paul and Meyer, 2001). These natural functions of a floodplain can become altered by human interference, causing stress on biological life. When biota is exposed to contaminants,

those contaminants then enter the biogeochemical pathways that can lead to human exposure (Förstner and Wittman, 1981). Better knowledge of how floodplains form in urban watersheds and how they interact with contaminant pathways is needed in order to improve management practices and achieve the maximum environmental benefit of floodplains (Wolman and Leopold, 1957). Understanding how human activities, as opposed to natural processes, influence floodplain formation, erosion, and remobilization of stored alluvial sediment is needed for better environmental management (Chin, 2006; Gale, Adams, Wixson, Loftin, and Yue-Wern, 2002; Galster et al., 2006; Graf, 1975; Harber, 1999; Knox, 1977; Knox, 2006; Leopold, 1968; Magilligan, 1985; Pavlowsky, 2004; Sekabira, 2010; Bernard and Laverdiè, 2001; Wang, Kim, Dionysiou, Sorial, and Timberlake, 2004).

Wolman and Leoplold (1957) suggest that the area subject to inundation by the highest discharge in a given year is considered the floodplain, or in terms of probabilities, the land subject to flood with a reoccurrence interval of one to two years. Floodplains can be described in different ways. In topographic studies, a floodplain is the flat land adjacent to a stream, while hydrologically, floodplains are defined as the landforms subject to periodic flooding by parent streams, and geomorphically, the floodplain is the landform comprised of depositional materials derived from upstream (Schmudde, 1968).

Floodplain topography and sedimentology vary spatially, acting as both an end product and functional part of maintaining equilibrium within a drainage network. Equilibrium in geomorphology refers to the self-correcting balance among materials (sediment/detritus), process (erosion, transport, deposition), and form (geometry, curvature) (Schmudde, 1968). As an integral part of the stream system, a floodplain must

adjust to meet the requirements of sediment load and discharge imposed upon it by the drainage basin. Adjustments that alter surface configuration of a floodplain are a result of initial sediment supply conditions and the subsequent transport history of that supply (Knighton, 1998). Types of adjustments include changes in width and height of the floodplain, which is associated with surface configuration (Schmudde, 1968).

Purpose

This geomorphological study identifies the floodplain as a valley floor landform, influenced by various upstream anthropogenic actions since the late 1800's. These land use alterations have influenced sedimentation, erosion, and contamination of the urban floodplain under investigation. The purpose of this study was to investigate the geomorphology, sedimentology, and geochemistry of a floodplain landform along an urban-affected stream in the Missouri Ozarks region. The main goal was to describe where metal contaminants are stored within historical floodplain deposits and to evaluate the role of floodplains as a control on water quality in Wilson Creek through storage and remobilization of sediment and metal contamination. The Wilson Creek watershed is located within the James River Basin Watershed in southwest Missouri within the Springfield Plateaus of the Ozark Plateaus Province of the Interior Highlands. The entire Wilson Creek watershed drains 218 km^2 of the west-central position of Greene County and flows south to the confluence of the James River in Christian County and is comprised of both urban and agricultural land use. The stream is listed in the Total Maximum Daily Load Report (TMDL) as impaired by multiple point sources and urban nonpoint sources (TMDL, 2011). The pollutants causing impairment to the stream are

listed as unknown, but geomorphic alterations and toxicity from multiple pollutants is likely a result of excessive storm water runoff from impervious surfaces (TMDL, 2011).

The Springfield Plateau Ozark Highlands is one of the fastest growing areas in Missouri and home to Wilson's Creek National Battlefield. Many tourists are attracted to this area for the Civil War history and outdoor recreation and the Ozark region in general is economically dependent on tourism. In order to support the tourism economy, the James River and its receiving water body Table Rock Lake must be protected from non-point source contamination including sediment and pollutants released from bank erosion. Management strategies to improve water quality need to be implemented at those locations, which are determined to produce significant nonpoint source loads. This study will evaluate the potential for nonpoint source loads from floodplains to influence water quality in urban areas.

The study area drains a smaller 96 km^2 sub-basin within the Wilson Creek watershed that is affected largely by urban runoff and nonpoint pollution (TMDL, 2011). Previous studies along Wilson Creek have found heavy metal contamination of mercury, zinc, and lead in channel and floodplain sediments (Shade, 2003; Rodgers, 2005). The floodplain studied for this study is located within a recent Nonpoint Source 319 riparian easement project that aims to improve the riparian corridor and water quality that suffers impairment from urban and agricultural land uses within the watershed.

Objectives

The objectives of this study are:

1) Sample surface and subsurface floodplain sediment to describe the stratigraphy and geochemical profiles across the valley floor;

2) Identify and interpret historical site characteristics and disturbance that influence floodplain morphology;

3) Analyze historical and recent hydrological data to determine influence on historical channel and floodplain change; and

4) Distinguish patterns of elevation and valley floor landforms to aid in the analysis of metal distribution.

Understanding historical land use changes and the effects on soil contamination can help provide a baseline for better environmental management in the future (Knox, 1977; Lenat and Crawford, 1994; Bernard and Laverdière, 2001; Paul and Meyer, 2001). Analysis of valley floor response to historical anthropogenic change is an important factor in attempting to restore or maintain the dynamic equilibrium of a river system. Identification of heavy metal distribution throughout floodplain surface and sub-surface sediments can provide better insight as to how floodplains store sediment, and moreover respond to hydrological changes caused by human actions. Knowledge obtained by this study will not only benefit Ozark streams, but could also aid in the environmental management of urban streams everywhere. Once floodplain response to urbanization is understood, potential for remobilizing stored floodplain contamination into the stream can be reduced (Gale et al., 2002; Martin, 2004; Sekabira et al., 2010). Ecological habitats can be preserved, and outdoor enthusiast can enjoy the recreation of a healthy Ozark watershed.

CHAPTER TWO: BACKGROUND

This chapter reviews previous research and background information to provide a framework for this study, as well as its limitations. The primary focus of this chapter is to introduce the following areas of study: structure of valley floor landforms, geomorphic response of floodplains, urban influence on watersheds, floodplains as both sediment sinks and sources, and rates of floodplain deposition, including sections along Wilson Creek.

Floodplains and other Valley Floor Landforms

Interactions among basin geology, hydrology, and the inputs of organic and inorganic material from adjacent hillslopes and vegetation result in the formation of valley floor landforms, including floodplains (Figure 1) (Gregory, Lamberti, and Moore, 1989; Gregory, Swanson, McKee, and Cummins, 1991). Due to the force required to alter geomorphic surfaces at various spatial scales, valley-floor landforms are ranked hierarchically in a temporal sense that is directly linked to the recurrence intervals for floods or other geological events of similar magnitude such as earthquakes, landslides, hurricanes, and tornadoes (Frissell, Liss, Warren, and Hurley, 1986; Gregory et al., 1991). Floodplains are a type of valley floor landform and their formation and spatial distribution within a river system is a result of downstream variations in the stream power threshold (Jain et al., 2008). This is the available energy in a stream, also defined as the rate of liberation of kinetic energy from potential energy generally defined as the product of stream slope and flow depth (Bagnold, 1966; Jain et al., 2008). Floodplain formation is controlled by basin variables including drainage area, drainage density, relief, and

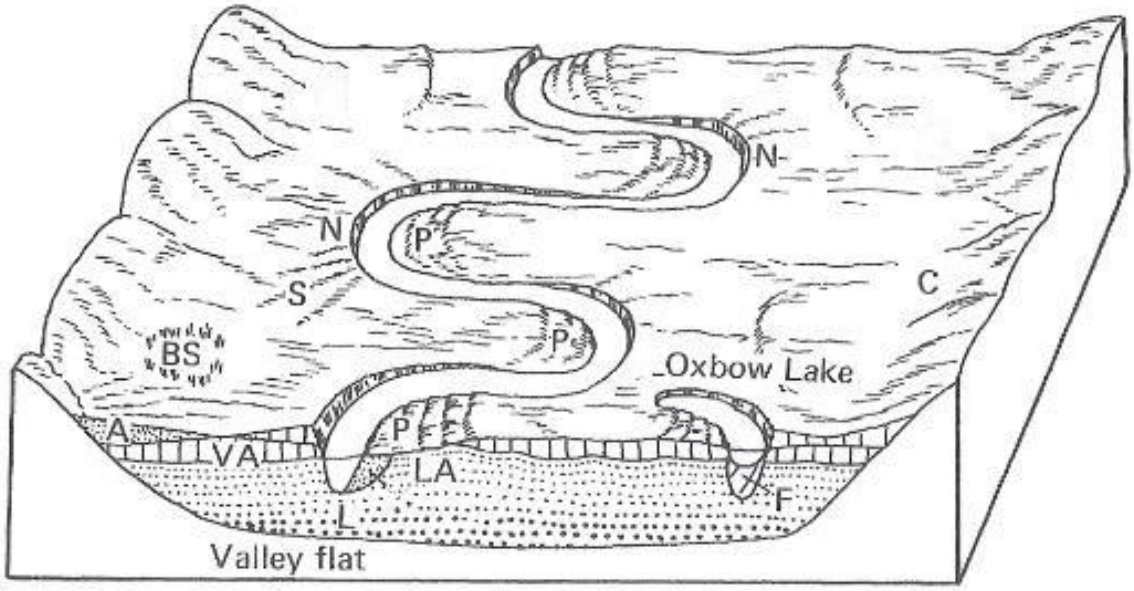

Figure 1. Typical representation of valley floor landforms. A-Alluvial fan; BS-Backswamp; C-Colluvium; F-Channel fill; L-Lag deposit; LA-Lateral accretion; N-Natural levee; P-Point bar; S-Splay; VA-Vertical accretion.
(Source: Bloom, 1998)

more local scale variables such as slope, valley width, and sediment supply (Jain et al., 2008)

Floodplains form along streams across the valley floor. The base of the valley floor and channel are comprised of lag deposits. In the channel, this material is only moved during the highest peak flows. Lag deposits can consist of gravel to boulder-sezed clasts, waterlogged plant material, and partially consolidated mud blocks that were eroded from the channel wall (Galloway and Hobday, 1996). Above the lag, sand is transported as the typical bed load. Above these lag deposits, the valley floor is comprised of colluvium and alluvium deposits.

Colluvium is unconsolidated sediment deposited by rainwash, sheetwash, slope failure, or continuous downslope creep that collects at the base of slopes or hillsides (C in Figure 1). These deposits are a result of mass wasting, gravity, and friction (Bloom, 1998). Accumulated deposits can form a colluvial wedge, or interfingering deposits along valley margin slopes. Alluvial fans are formations on terraces and floodplain surfaces that result from tributary sediment and debris-flow deposits (A in Figure 1) (Gregory et al. 1991). They are greatly diverse in size, slope, types of deposits, and source-area characteristics. Abrupt widening and shallowing of a channel cross-section are important factors in the formation of alluvial fans (Bloom, 1998). The abrupt loss of competence at the mouth of the valley through widening, infiltration, and loss of depth, results in increased alluvial deposition.

Older floodplains, typically not involved in contemporary floodplain process, may remain on the valley floor as fluvial terraces. Terraces typically represent the former levels of valley floors or flood plains (Bloom, 1998). The two types of fluvial terraces

are depositional (alluvial) and erosional (strath). Alluvial terraces are formed by alluvium deposition, but occur less often than strath terraces (Cotton, 1940; Howard, Fairbridge, and Quinn, 1968). Strath terraces are eroded out of preexisting formations caused by river meandering, or lateral planation (Cotton, 1940; Howard et al., 1968). Different types of terraces are best classified by the stratigraphy of deposits. A fill-cut terrace is comprised by a layer of coarse debris and boulders with the finer particles having been removed during the scouring process (Howard et al., 1968). A strath terrace often has a thin layer of alluvium over a bedrock bench, representing a previous channel bed. Both strath and fill terraces can be found within the same valley.

An oxbow lake is a lake in an abandoned channel found atop a floodplain. Natural process or human activity can cause a channel meander to be cut off, forming an oxbow lake (Figure 1). A neck cutoff can form if a meander recurves until it intersects with an upstream portion of the channel (Bloom, 1998). This locally abrupt shortening of channel length will increase the gradient and velocity in the cutoff, and eventually closes off the abbreviated ends of the abandoned meander with bank deposits (Bloom, 1998).

When channel discharge cannot be contained within channel banks, floodwaters with high velocity can erode chutes atop the floodplain, which act as secondary channels to contain and convey the excess discharge (Figure 1). From a geomorphic perspective, chutes and secondary channels serve to attenuate flood flows in the main channel, and from an ecological perspective, they serve as an important function of nutrient exchange, primary production, and riparian habitat development (Ellis, Church, and Rosenau, 2004). Chutes create a shortcut across a meander during a flood event, and sometimes cut-offs occur in chute locations. These areas can be free of vegetation due to frequent

use, but are not present at all streams. Streams with large, well-established natural levees or where alluvium contains substantial binding material may not develop chutes.

Floodplains consist of various combinations of sand, silt, and clay, which are often underlain by pebble and cobble gravels (Wolman and Leopold, 1957). Lateral (point bar) and vertical (overbank) deposits are the two main types of sedimentary deposits within floodplains. Lateral accretion of floodplains occurs as the channel migrates back and forth across the valley floor (LA in Figure 1). Erosion due to lateral shifting in a channel is compensated by deposition on the opposite side of the channel, forming a point bar. Point bars are typically formed on the inside bend of a river by lateral accretion of relatively coarse sediment at various elevations, often reaching all the way to the floodplain surface (P in Figure 1). Lateral migration of the channel across the valley floor over time helps control floodplain elevation by erosion of banks, but rates vary upon location due to variation in slope, discharge, and materials being transported. The size of particles found in bar deposits is also dependent on channel form, particularly slope (Knighton, 1998). Steeper channels typically transport coarser sediments. Point bars can be comprised of materials with varying sizes and textures. Although, in general, sediment size decreases exponentially downstream from the headwaters to the mouth of the river system (Knighton, 1998). As bar height increases, inundating flows become less frequent and result in vertical gradation sizes from coarsest to finest (Knighton, 1998). Thus, there is a vertical transition, often abrupt, from buried coarser channel bar deposits upward to finer overbank deposits.

The vertical accretion of floodplains occurs by overbank deposition (VA in Figure 1) (Wolman and Leopold, 1957). Overbank deposition occurs when channel flow

exceeds bankfull stage and drops suspended sediments on the floodplain, causing floodplain elevation to increase as a result of sediment accumulation (Knox, 2006). Presumably, as floodplain elevation increases, flood frequency should decline (Wolman and Leopold, 1957). Vertical accretion deposits can vary in texture due to source materials within a specific basin, but become gradually finer from the bottom to the top of the floodplain. Resistance to flow increases as floodwaters spread further across the floodplain, leaving textures of overbank deposits coarser and thickest near the stream bank or higher energy channel. This pattern is typically found within one to two stream widths of the parent stream (Schmudde, 1968).

Where a channel has stable banks and relatively slow lateral movement, repeated deposition can result in a natural levee (N in Figure 1). Natural levees often develop when alluvial streams flow over floodplains, creating a low, wide ridge located immediately adjacent to the channel (Bloom, 1998). Once a system of natural levees is established, overbank flows do not typically inundate the levees, but instead locally breach them and spread out across the floodplain behind them. The point of breaching is known as a crevasse in the levee, which can result in splay being spread far across the backswamp (S in Figure 1; BS in Figure 1) (Bloom, 1998). A backswamp is a depression in elevation atop the floodplain where silt and clay accumulate during overbank flows. This breach in a natural levee can become a full-size flood-time channel, and may even become a new permanent channel (Bloom, 1998). If a new master channel is developed, the old channel will begin to fill with channel deposits and form a curved oxbow lake (F in Figure 1).

Geomorphic Response of Floodplains

Fluvial systems can retain a geomorphic history of their adjustments to environmental and anthropogenic disturbances (Schumm, 1977; Knighton, 1998). Present conditions of river systems are a result of both current and previous geomorphic events. The current events reflect the relatively constant inputs over time to the fluvial system, which tend to produce characteristic forms (Knighton, 1998). Historical events such as the last glaciation had a direct effect on streams in both glaciated and unglaciated areas, leaving a lasting influence on many fluvial systems (Knighton, 1998). During the late Wisconsin glacial stage between about 20,000 and 14000 ^{14}C yrs BP, uplands and hillslopes throughout the Upper Mississippi Valley region immediately south of the continental glacier experienced accelerated mass wasting that caused colluvial aggradation by as much as 10 m in small headwater tributaries of a few square kilometers or less (Mason and Knox, 1997; Stuiver, Reimer, and Braziunas, 1998; Webb, Bartlein, Harrirson, and Anderson, 1993; Knox, 2006). Knox (2006) suggests that modest changes in climate can produce large changes in the magnitude-frequency characteristics of floods, and therefore in the level of fluvial activity.

Climatic change and human influences are important factors in geomorphic response of floodplains. Climate is an important source of energy for fluvial systems and affects the amount of deposition on floodplains. Many rivers throughout the world have experienced increased flooding from what many believe is a result of climate change (Pielke, Downton, and Miller, 2002; Wilby, Beven, and Reynard, 2008; Laforce, Simard, Leconte, and Brissette, 2011). The general trend explaining increased flood disasters in Canada is the increase of flood magnitude in the second half of the 20th Century

compared to the first half, and greater development on flood-prone areas as a response to the growing population (Laforce et al., 2011). The hydrological cycle is accelerating in response to the evident increasing precipitation at continental and global scales, leading to greater flood disasters and geomorphic response (Huntington, 2006; Laforce et al., 2011). In combination with greater urbanization and impervious surfaces, increased precipitation as a result of climate change will increase peak discharge, bankfull discharge, and surface runoff (Espey, Morgan, and Mash, 1965; Leopold, 1968; Arnold and Gibbons, 1996; Booth and Jackson, 1997; Paul and Meyer, 2001). Physical responses to hydrological changes include dramatic change in channel planform and channel enlargement by widening and/or incision (Dunne and Leopold, 1978; Booth and Jackson, 1997, Paul and Meyer, 2001).

Agricultural practices can also lead to geomorphic change of floodplains (Knox, 1977; Trimble 1993; Knox, 2006). Converting natural land cover to agricultural use typically increased both runoff discharge and sediment supply to stream channels (Knox, 1977; Matisoff, Bonniwell, and Whitling, 2002; Loczy, 2011). Knox (2006) determined that post-settlement row cropping practices caused accelerated overbank flooding that led to greater floodplain sedimentation and bank erosion in the Upper Mississippi Valley from 1900 to1950. The watershed was also exposed to zinc-lead mining, but the greatest influence on sedimentation was linked to human activities related to agriculture. Pre-agriculture vertical accretion rates within tributary watersheds with less than 700 km^2 averaged about 0.2 mm yr^{-1}, and rates with areas increased to approximately 170,000 km^2 were about 0.9 mm yr^{-1} (Knox, 2006). In contrast, vertical accretion rates from the past 200 years that possess the highest agricultural production in the same areas averaged

between 2 and 20 mm yr^{-1} (Knox, 2006). In preparation for cultivation, natural forest vegetation within a watershed is destroyed, reducing habitat and root protection. The cultivation and tilling practices reduce soil filtration capacity of uplands, which can result in increased floodplain erosion and sediment into streams (Knox, 1977; Matisoff et al, 2002). After a single thunderstorm event, approximately 6 to 10 times more sediment resulted from predominately-tilled sub basins than sub basins with no exposure to tilling practices in the Old Woman Creek watershed in Ohio (Matisoff et al, 2002). Till farming and land cultivation results in greater soil erosion and an increase in suspended sediment discharges when compared to uncultivated lands (Matisoff et al, 2002).

Livestock can also act as important geomorphic agents in the fluvial environment (Trimble, 1993). The cattle industry in the United States increased vastly in the two decades following the civil war and resulted in geomorphic changes of floodplains. Trimble (1993) discovered that cattle grazing increased bank erosion along a small stream in the Central Basin of Tennessee and that uncontrolled grazing of cattle caused approximately six times the amount of bank erosion as was seen along a controlled stretch with no grazing.

Urban Influence

Urban development affects hydrologic and geomorphic characteristics in watersheds (Chin, 2006; Galster et al., 2006; Graf, 1975; Leopold, 1968; Paul and Meyer, 2001; Pavlowsky, 2004; Sekabira et al., 2010). Greater urbanization leads to an increasing amount of impervious surfaces, which result in decreasing infiltration rates and increasing surface runoff, thus impervious surfaces cause more frequent and larger

floods (Leopold, 1968; Dunne and Leopold, 1978; Paul and Meyer, 2001). Flooding has been found to peak more rapidly and occur for shorter periods of time in urban environments in proportion to the percentage of impervious surface cover in a given catchment area (Espey et al. 1965; Seaburn, 1969; Hirsch, Walker, Day, and Kallio 1990; Arnold and Gibbons, 1996). The increased discharge caused by urbanization can lead to more erosion, poor aquatic habitat, and landform alteration (Galster et al., 2006). Part of the issue with increased flooding is related to inability of storm sewer systems to successfully. Storm sewer systems were not built to handle the increased magnitude of runoff as a result of increased impervious surfaces. Drainage efficiency is a crucial determinant of hydrological change (Leopold, 1968). As cities continue to grow, their storm sewer systems are insufficient at directing water into natural drainage systems. Similar to agriculture, urbanized areas cause greater erosion and sedimentation yields (Graf, 1975; Arnold, Boison, and Patton, 1982; Paul and Meyer, 2001; Chin, 2006; Galster et al., 2006).

Urbanization has the potential to cause various geomorphic changes such as aggradation and erosion (Dunne and Leopold, 1978; Booth and Jackson, 1997, Paul and Meyer, 2001). Aggradation occurs in the construction phase of urbanization as hillslope erosion increases, and increased sediment supply leads to bed aggradation and increased overbank deposition rates (Dunne and Leopold, 1978; Arnold et al. 1982; Booth and Jackson, 1997; Paul and Meyer, 2001). Channel pattern change has also been observed during the construction phase, and streams change from meandering to braided, or to more channelized forms during the period when watershed surface erosion rates are restricted by landscaping and storm drain systems (Arnold et al. 1982; Paul and Meyer,

2001). The erosional phase takes place post-construction. Hillslope sediment supply decreases, but the frequency of bankfull flows increase due to increased impervious surfaces and storm water drainage rates. As a result, increased stream power causes incision and widening of the channel to make room to accommodate increased bankfull discharge (Paul and Meyer, 2001). Chin (2006) found that a floodplain's initial response to urban development is an increase of sediment production and deposition, followed by a decline. The decline in energy required to transport sediment causes an increase of excess stream power in the channel, resulting in channel enlargement. Urban streams can increase from two to three times the size of the original channel and floodplains can expand within two years, and eventually by 270 percent the initial size (Chin, 2006). Excess runoff flows across cleared lands that have not yet been developed, causing soil erosion and increased sediment production that fills channels. Since soil conservation practices were implemented in the 1940's, researchers have been able to use the temporal control to study how such conservation efforts can alter floodplain sedimentation rates (Magilligan, 1985).

Large woody debris is also reduced in urban channels as a result of washout, down-cutting, and direct removal by people (Booth and Jackson, 1997; Paul and Meyer, 2001). Altered channel form and processes, greater sediment fluxes, quicker bank erosion and incision, and loss of heterogeneity in bed morphology can result from a loss of large woody debris (Booth and Jackson, 1997).

Floodplains as Sediment Sinks and Sources

Floodplains protect water quality with the ability to trap and remove nutrients and

heavy metals from polluted runoff by sedimentation, infiltration, and vegetative removal. Typically, the efficiency of contaminant removal by floodplains is directly related to fine-grained sedimentation rates on the floodplain surface (Horowitz, 1991). Overbank sedimentation and storage rates vary among undisturbed and disturbed watersheds, and are affected by frequency of inundating flows and their sediment load (Knighton, 1998; Knox, 2006). Knox (2006) compared natural Holocene floodplain aggradation of the mainstem upper Mississippi River (UMR) along western Wisconsin to the undisturbed Driftless Area watersheds in southwestern Wisconsin and northwestern Illinois (Knox, 2006). The sedimentation rate of the UMR was higher in comparison to the Driftless Area watershed as a result of drainage area and the size of the floodplain, indicating that valley size correlates with amounts of sediment accumulation (Magilligan, 1985; Knox, 2006). Wide valleys are associated with greater floodplain sediment accumulations while narrow valleys are associated with lower sedimentation rates since narrow valleys typically are steeper with higher velocity flows over floodplains (Magilligan, 1985).

Bridge and Leeder (1979) reported long-term sedimentation rates from 0.2 to 10 mm yr^{-1} with a simulation model of alluvial stratigraphy beneath a floodplain traversed by a single major river, but with the tendency for rates to vary even within short reaches of a river. Over the last 35 years, rates of sedimentation along the lower Severn have ranged between 0 and 10 mm yr^{-1} (Walling et al., 1992; Knighton, 1998), while floodplains in the Amazon region have reached almost 6 m yr^{-1} (Mertes, 1994; Knighton, 1998). These variations once again demonstrate how flood frequency and sediment load can influence sedimentation rates.

Evidence of change in the fluvial system can come from morphological remnants

in the floodplain, including relict or buried channels and from sediment sequences that reveal a complex and typically incomplete record of changing conditions (Knighton, 1998). Analysis of pollutant storage of major nutrients and heavy metals in the floodplain can also be used to indicate changes in the fluvial system (Förstner, 1990; Magilligan, 1992; Walling et al., 1992; Knighton, 1998; Owen, Walling, and Leeks, 1999; Paul and Meyer, 2001; Matisoff et al. 2002; Pavlowsky, 2004; Pavlowsky, Owen, and Martin, 2010). Sediment-trace element chemistry can be affected by a number of factors such as surface area, surface charge, and porosity, but the most significant factor for concentrating and retaining trace elements is grain size (Horowitz, 1991). A very strong positive correlation most commonly exists between decreasing grain size and increasing trace element concentrations (Horowitz, 1991), resulting in floodplains being widely recognized as significant sinks for storing pollutants adsorbed to suspended sediments (Lecce and Pavlowsky, 1997; Lecce and Pavlowsky, 2004). Further analysis of spatial distribution of nutrients and heavy metals in floodplain soils can help understand fluvial responses to land use changes within a watershed (Lecce and Pavlowsky. 2001; Owen et al., 1999).

Alluvial sediments with contamination from known anthropogenic factors, such as mining, can be employed to determine floodplain sedimentation rates and patterns (Lewin, Davies, and Wolfenden, 1977; Brewer and Taylor, 1997; Lecce and Pavlowsky, 2001). Analysis of pre-mining (1830-1900) and post-mining (1920-1997) alluvium in the Blue River Watershed, Wisconsin suggests alterations to channel form and floodplain sedimentation rates caused by the mining industry (Lecce and Pavlowksy, 2001). Sediment contamination levels of Pb and Zn and their spatial distribution helped

acknowledge that lateral channel migration and development of meander belts during the mining period (1900-1920) increased transport capacity of sediments, reducing overbank flooding and sedimentation.

Identification of floodplains containing high concentrations of pollutants that are also affected by high rates of bank erosion is important for protecting water quality. Remobilization of contaminants at concentrations of concern can harm aquatic life, potentially ending with the greatest harm inflicted on people through the process of bioaccumulation. The Ozarks has a history of heavy Pb and Zn mining. When studying Ozark streams, these metals can often be identified in sediment samples as a result of natural mineralization and/or anthropogenic influence. The United States Environmental Protection Agency (USEPA) defines contamination levels of Pb in floodplain soils used as residential soils to be greater than 400 ppm.

Floodplain Deposition Rates in Wilson Creek

Cesium-137 (Cs^{137}) is a radionuclide tracer that can be used to date floodplain deposits and determine sedimentation rates (Walling and Woodward, 1992; Walling and He, 1993; Owen et al., 1999; Bernard et al., 2001; Sekabira et al., 2001; Matisoff et al., 2002; Ritchie, Finney, Oster, and Ritchie, 2004). Radioactive fallout from nuclear testing in the 1950s and 1960s resulted in the deposition of aerial Cs^{137} by rain and stratification in the soil profile. Once deposited, Cs^{137} strongly absorbs to soil particles and is then trapped in the sediment profile. The strong absorption to surface sediment causes Cs^{137} to remain relatively stable in the soil profile, making the isotope a significant tracer for dating sediment throughout a floodplain. Gamma spectrometer analysis can be used to

identify the first Cs^{137} occurrence in a core and assign the layer a date of 1954 (Walling and He, 1993). Following, peak concentrations are identified and the layer containing the greatest Cs^{137} is dated 1963 (Shade, 2003; Rodgers, 2005).

Shade (2003) collected soil cores along a reach of Wilson Creek within the Nation Battlefield. Results for Cs^{137} in Shade's (2003) study indicate the beginning of Cs^{137} deposition at approximately 40 cm near the channel. Peak deposition near the channel was discovered at about 10 cm while upland soils displayed a typical undisturbed profile with most of the Cs^{137} confined to the top 13 cm. Average sedimentation rates between 1954 and 2002 were 0.8 cm/yr, rates between 1963 and 2002 were 0.4 cm/yr, and rates between 1954 and 1963 were 2.3 cm/yr (Shade, 2003). Hillslope erosion was significant between 1954 and 1963 as indicated by sedimentation rates at the sample nearest to the terrace (Shade, 2003).

Rodgers (2005) also studied overbank deposition along various segments of the Wilson Creek, including a sample located approximately 60 m south of FR 156 and 20 m off the east bank of Wilson Creek. Sedimentation rates were calculated for historical deposits between the 1963 surface and the buried soil surface. The buried soil surface was given an estimated date of 1870 based on land use changes and industrial growth within the watershed. Overall, the Cs^{137} profiles generally peaked at the floodplain surface near 15 to 30 Bq/kg and decrease to 0 Bq/kg by 40 cm depth. The core profile closest to this studies sampling location for Rodgers' (2005) analysis showed initial Cs^{137} presence at 20 cm and peak concentration at 0 cm. The sedimentation rate for the 94-year timespan at Rodger's (2005) sampling site near FR 156 was 0.59 cm/yr.

Previous studies have analyzed floodplain morphology, heavy metal contamination of surface and/or sub-surface sediment, and stream hydrology, but few have combined all of these areas of study to understand floodplain response to land use history. Further, none have evaluated the three dimensional geometry of floodplain formation and contaminated deposition in Wilson Creek, or any other urban stream in the Ozarks. This thesis combines the hydrology, sedimentology, and geochemistry of floodplain deposition to understand their geomorphic development since the 1950s.

CHAPTER THREE: DESCRIPTION OF STUDY AREA

The study area is located in the middle segment of Wilson Creek within the James River Basin (Figure 2). At the study reach, the Wilson Creek drains 96 km^2 of southern Greene County in Missouri, including storm water runoff from Springfield, the third largest city in Missouri. The length of the study reach is 0.6 km and is located 3.5 km downstream from the Springfield city limits. Wilson Creek flows into the James River about 11.2 km downstream from the study area.

Geology

Sedimentary rocks underlie the Wilson Creek watershed and include the Burlington-Keokuk Limestone and Warsaw Formation (Figure 3) (Thompson, 1986). Differentiation of the Burlington with the lithologically similar overlaying Keokuk is often difficult, so this sequence of Osagean limestones is often referred to as Burlington-Keokuk Limestone. These limestones are typically coarse-grained, crystalline, crinoidal limestone. Chert fragments compose 35-80% of inset floodplains' subsurface horizons (Hughes, 1982; Owen, Pavlowsky, and Olson, 2012). The small area of Warsaw Formation outcropping in the study area is comprised of a lower geode-bearing argillaceous dolomite and shale unit and an upper shale-dominated unit (Anderson, 1998). As a result of this limestone bedrock being distributed throughout the watershed, a karst landscape is formed, consisting of sinkholes, losing streams, and springs (Vineyard and Feder, 1982). Exposed limestone formations with chert beds are exposed along the bed of the project segment.

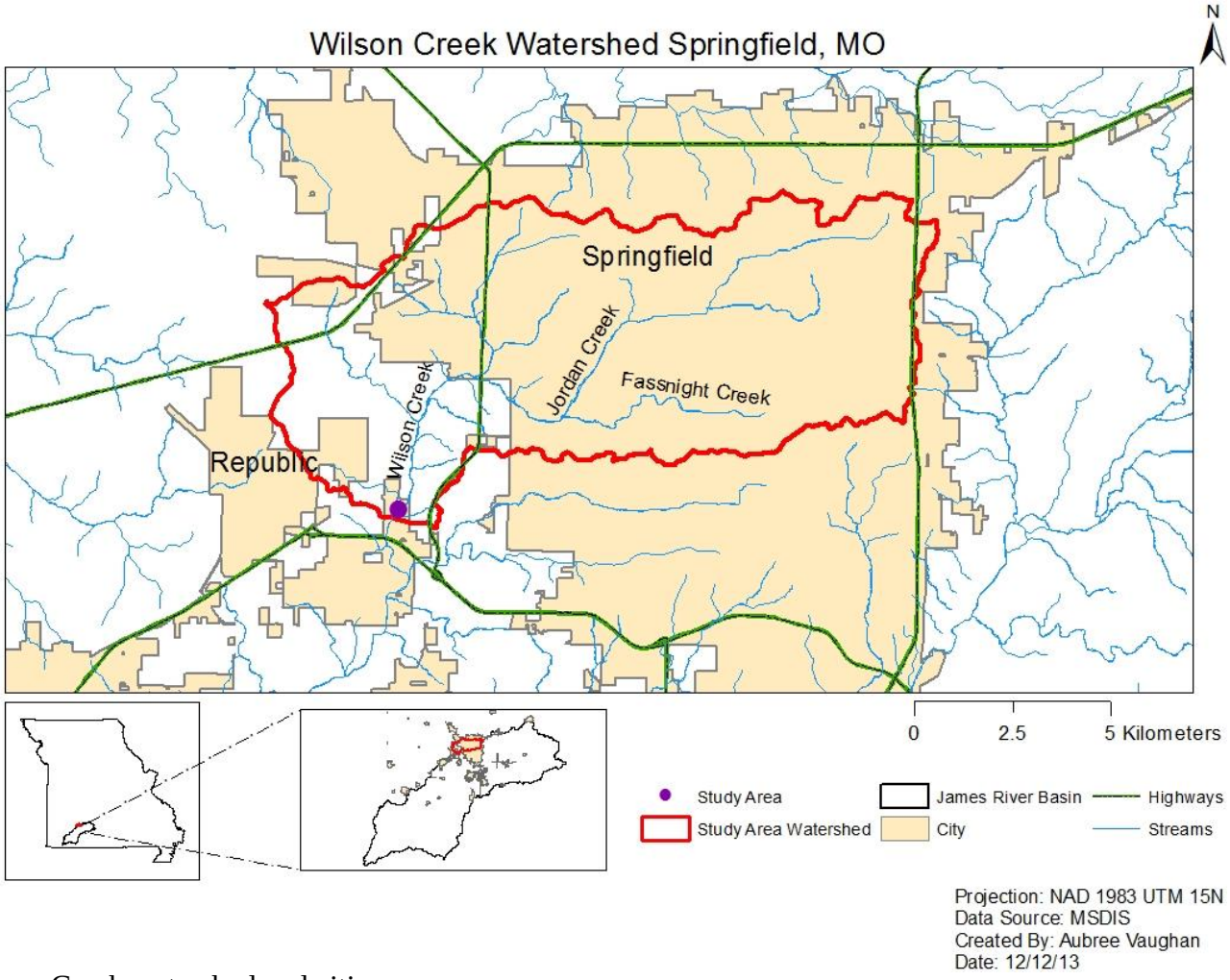

Figure 2. Wilson Creek watershed and cities.

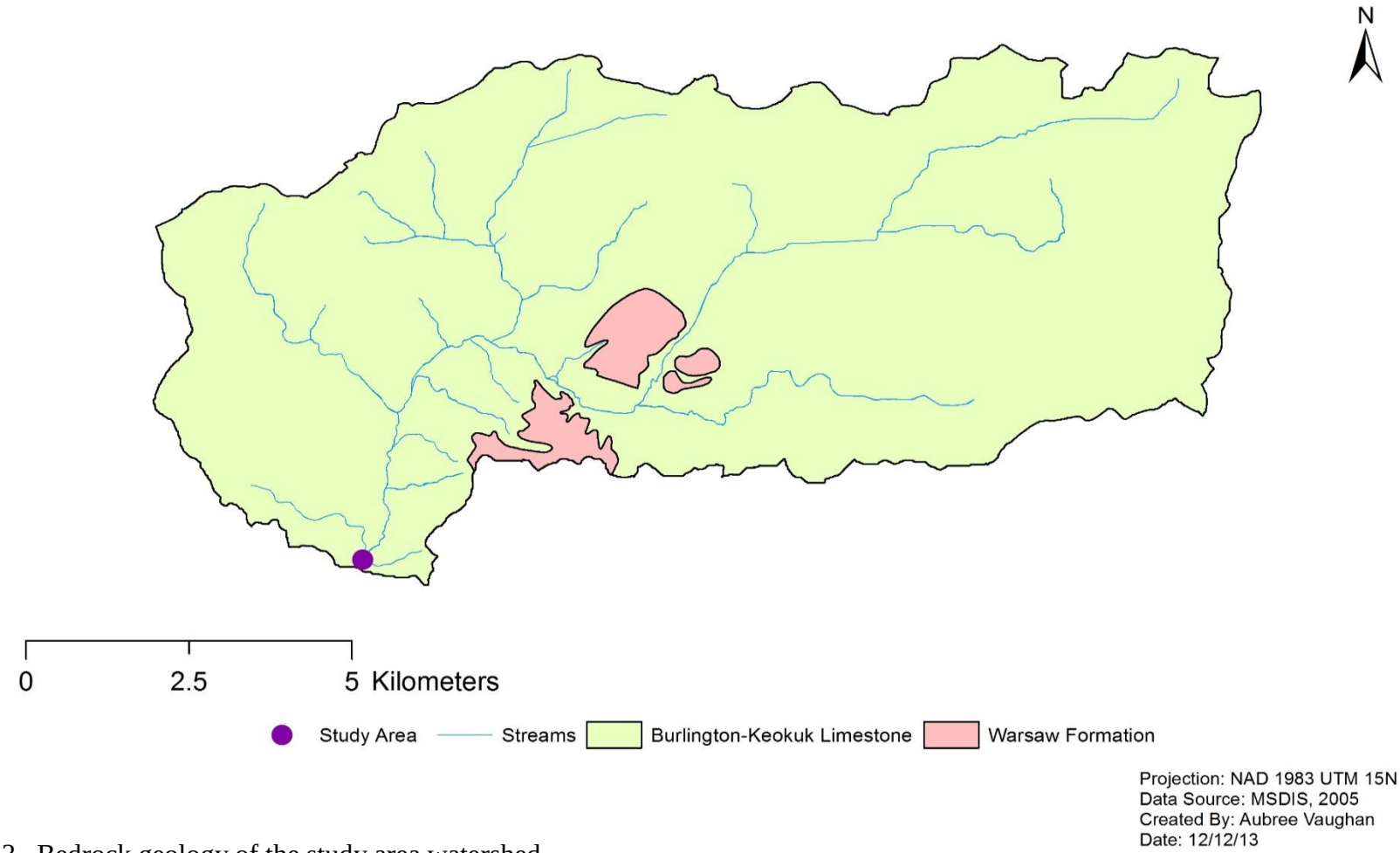

Figure 3. Bedrock geology of the study area watershed.

Soils

The fertility and physical properties of soils in the Ozarks vary greatly. Factors of parent material, climate, topography, drainage, and vegetation all affect soil formation. Parent materials for soils in the study area are comprised of limestone, dolomite, and shale residuum and Pleistocene Loess, colluvium, and alluvium (NRCS, 2008). Most of the soils throughout the Springfield Plateau are alfisols, ultisols, and mollisols. A total of six soil series were mapped by the Natural Resources Conservation Service (NRCS) near the sampled segment of the study area, labeled with corresponding landform type (Figure 4) (NRCS, 2008). Table 1 provides characteristics for slope (%), landform type, horizon, texture, and particle size at various depths for the soil classifications at the study site. The Goss-Gassconade complex is formed on steeper hillslopes along the valley at the study site (NRCS, 2008). Goss gravely silt loam, Peridge silt loam, and the karst Keeno-Bona complex were identified as terraces, and both Dapue silt loam and Cedargap silt loam are identified as floodplain units (Hughes, 1982; NRCS, 2008). Sample cores for this study were all collected from soils within the floodplain unit (Figure 4). The development of floodplain soils and sediment transport within stream channels at the study area are strongly influenced by the fluvial geomorphic processes of erosion, transportation, and deposition (Rogers, 2005). Exposure to agriculture, land clearing, and urbanization has been proven to bury floodplain soils at various locations within the southwest Missouri region (Carlson, 1999; Shade, 2003; Rodgers, 2005; Owen, Pavlowsky, and Womble, 2011).

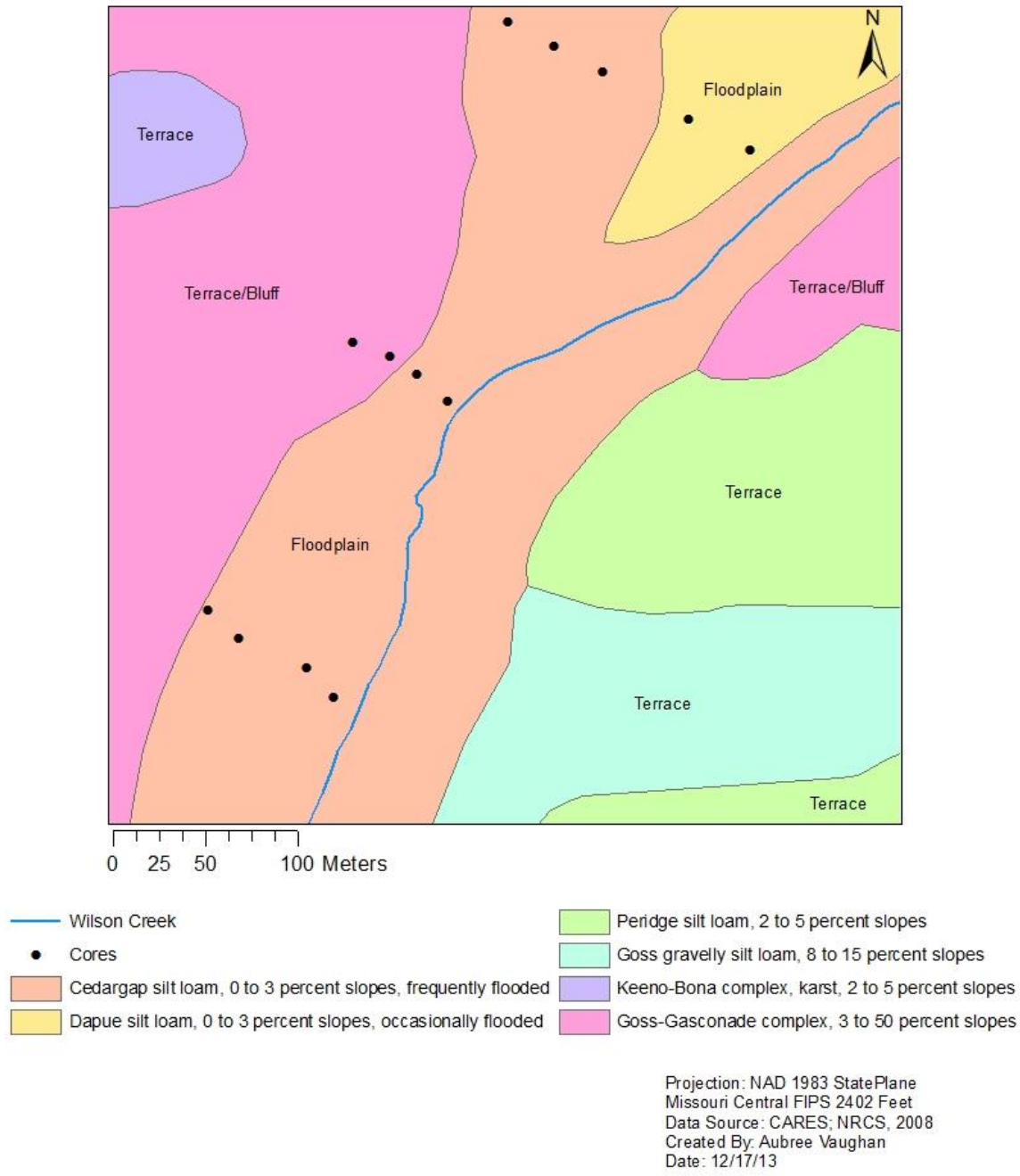

Figure 4. Soil series within the study area.

Table 1. Soil classification characteristics at study site (Hughes, 1982; NRCS, 2008).

Soil Classification	Slope %	Landform	Depth (cm)	Horizon	Texture	Particle Size		
						Clay %	Silt %	Sand %
Goss-Gasconade complex	3-50	Terrace/ Bluff	0-7.6	Ap	Cherty Silt Loam	17	54	29.3
			7.6-38	BA	Cherty Silty Clay	26	50	23.6
			38-163	Bt	Cherty Silty Clay	38	55	7.5
Goss gravelly silt loam	8-15	Terrace	0-15	A	Cherty Silt Loam	15.6	70.5	13.9
			15-48	E	Cherty Silty Clay	16.1	66.4	17.5
			48-152	Bt1	Cherty Silty Clay	38	44	18
			152-203	2Bt2	Cherty Clay	70	20	10
Peridge silt loam	2-5	Terrace	0-20	Ap	Silt Loam	11.6	68.2	20.2
			20-48	Bt	Silty Clay Loam	20.8	65.4	13.8
			48-152	2Bt2	Silty Clay Loam	34.5	49.8	15.7
Keeno-Bona complex, karst	2-5	Terrace	0-28	A	Cherty Silt Loam	20	53.5	26.5
			28-71	Bt	Cherty Silty Clay	31.5	48.5	20.0
			71-99	2Btx	Cherty Silty Clay Loam	26	50.4	23.6
			99-152	3Bt	Cherty Clay	60	27.9	12.1
Dapue silt loam	0-3	Floodplain	0-23	Ap	Silt Loam	13	62	25
			23-38	A	Silt Loam	19	69	12
			38-203	Bw	Silt Loam	20	69	11
Cedargap silt loam	0-3	Floodplain	0-20	Ap	Silt Loam	21	60	19
			20-117	Bw	Silt Loam	25	42	33

Climate

Both mid-continent and mid-latitude locations of the Ozarks influence the seasonal variations of temperature, precipitation, and humidity. Most precipitation in the study area sub-basin falls as rain, averaging 111.8 to 114.3 cm/yr ("United States", 2006). Approximately 57 percent of the average annual rainfall occurs during the 6 warmest months of the year. Annual snowfall averages nearly 30.5 cm and melts fairly quickly after accumulation (Rafferty, 2001). The latitudinal location of the Ozarks favors more sleet and freezing rain.

Hydrology

The maximum relief of the sub-basin containing the study area is 78 m with an average slope of 0.0015 m/m for the 597 m study reach. The study area segment of Wilson Creek is a third order stream that originates in Springfield and transports water and sediment into the James River (Shade, 2003). The water and sediment eventually empty into the White River system at Table Rock Lake. Average runoff at the mouth of the Wilson Creek that influences the study area is approximately 2.5 m^3/s (U.S. Army Corps of Engineers, 1968). Approximately 1 m^3/s of that total is discharge from the Southwest Waste Water Treatment Plant (SW WWTP). A total of seven United States Geological Survey (USGS) gages have been collecting discharge data along the Wilson Creek and its tributaries (Table 2), but only the gages 07052000, 07052050, and 07052100 were analyzed in this study. Gaging station 07052100 is located at FR 156, which is approximately 239 m upstream from the first cross-section in the study. The datum of the gage is 350.41 m above National Geodetic Vertical Datum of 1929.

Table 2. Drainage area and discharge at USGS along all of Wilson Creek.

USGS Gage	Description	Period of Record	Drainage Area	Average Q for Period of Record	Max Q for Period of Record and Date
7052000	Wilson Creek at Scenic Dr. N 37°11'13.1", W 93°19'52.8" NAD83	10/1/1932 to 9/30/1939; 6/28/1973 to 9/22/0977, 6/4/1998 to 2012 n=26 years	17.8 mi^2	0.55 m^3/s	191.1 m^3/s 7/12/2000
7052050	N. F. Wilson Creek at Hwy 13 and 160 N37°12'17.61", W 93°20'54.52" NAD83	6/26/73 to 9/30/77 n=4 years	5.1 mi^2	0.18 m^3/s	42.5 m^3/s 5/20/1979
7052100	Wilson Creek near Springfield N 37°10'06.7", W 93°22'13.0" NAD83	9/21/1972 to 9/30/1982; 5/28/1998 to 2012 n=25 years	31.4 mi^2	0.6 m^3/s	181.5 m^3/s 6/13/2008
7052120	South Creek Near Springfield N 37°09'13.1", W 93°21'46.0" NAD83	6/1/1998 to 9/30/2012 n=14 years	10.5 mi^2	0.14 m^3/s	81.3m^3/s 6/12/2000

Table 2 Continued. Drainage area and discharge at USGS along all of Wilson Creek.

USGS Gage	Description	Period of Record	Drainage Area	Average Q for Period of Record	Max Q for Period of Record and Date
7052150	Wilson Creek below Springfield	4/1/67 to 9/30/1972	47.2 mi^2	1.1 m^3/s	105m^3/s
	N 37°08'49", W 93°22'26" NAD27	n=5 years			12/21/1967
7052152	Wilson Creek near Brookline	8/1/2001 to 9/30/2012	51 mi^2	1.9 m^3/s	269.9 m^3/s
	N 37°08'49.7", W 93°22'31.7" NAD83	n=11 years			6/13/2008
7052160	Wilson Creek near Battlefield	3/1/1968 to 9/30/70; 9/20/72 to 9/30/82; 8/3/99 to present	58.3 mi^2	2.6 m^3/s	205 m^3/s
	N 37°07'03.9", W 93°24'13.9" NAD83	n=25 years			5/20/1979

Wilson Creek and its tributaries within the City of Springfield have been straightened and rerouted through concrete tunnels due to increasing urbanization in several areas. The Jordan Creek is a tributary to Wilson Creek that has been enclosed in a concrete tunnel that runs underneath downtown Springfield. The tunneling occurred in the 1920's as a last resort to protect the stream from urban runoff and dumping of various types of waste directly into the channel. Channelization is another result of construction and human activities in the watershed. These alterations create the flashy flooding and low baseflow associated with the Wilson Creek watershed (Kiner and Vitello, 1997; Rogers, 2005; Shade, 2003).

The hydrology of the Wilson Creek watershed is influenced by karst features (Vineyard et al. 1982). Karst aquifers contain dissolution generated conduits that permit rapid transport of ground water. Several geological characteristics are needed for the formation of karst features, such as soluble rock with a preferred thickness of several hundred feet, moderate to heavy rainfall to aid in the solution process, and available relief for solution to occur (Shade, 2003; Thomson, 1987). Large, well-established, jointed or fractured limestones or dolomites are the best-suited rocks for the formation of karst features. These carbonate rocks form various surface and sub-surface karst features including caves, karrs, sinkholes and tunnels that result in unusual subsurface hydrology (Delina, Babre, Popovs, Sennikovs, and Grinberga, 2012). The conduit systems receive localized water inputs from losing streams and runoff through sinkholes. These systems interconnect with groundwater stored in bedrock fractures and granular permeability (White, 2002). These karst pathways accept water during dry seasons and emit water as springs in the rainy seasons (Vineyard et al., 1982).

Land Use

Reports and accounts of early settlers' surveys suggest that forested vegetation was much less in the Ozarks than what is present today. Survey notes of Greene County demonstrate equally divided land consisting of prairie and woodland. Prairies covered uplands while trees occupied valley floors and slopes (Rafferty, 2001). The primitive land of the Ozarks was three-fourths forested with the remaining consisting of tall-grass prairie, particularly the bluestem grasses that were described by Rafferty (2001) to have grown as high as a man on horseback.

Osage Indians occupied the area until approximately 1830. The Native tribes set fire to forest and grasslands to drive out wild game and to prepare land for agricultural production. Following displacement of the Indians from the Ozarks, the maintenance and fires of the land became irregular. Some farmers still practiced the slash and burn method, but the natural vegetation distribution was forever altered.

River-bordering areas and the Springfield Plain were inhabited by general farming around 1870. Annual burning and maintenance of grasslands took place during the spring seasons, but this practice became less common as more settlers arrived and the risk of burning down neighbor's fences increased (Rafferty, 2001). The lack of controlled fires allowed for underbrush to take over and kill off native grasses.

The arrival of railroads in the Ozarks created transformations in both agriculture and industry. The period between 1870 and 1920 brought railroads and improved roadways that allowed for more affordable and quick transportation of goods, creating a transition from subsistence to commercial agriculture. Railways were also a draw for employment, which brought even greater populations to the area. The development of

the railroad and increased population growth caused great demand for wood construction materials. This demand caused the Ozark timber boom, a period of deforestation that lasted until the 1920's.

Wilson Creek has a long history of pollution from industrial sources and wastewater effluent from Springfield. The Wilson Creek watershed became a popular dumping ground for industrial wastes in the late-1800s to mid-1900s (Shade, 2003; Rodgers, 2005). The 1904 plat book of Greene County, MO describes industries surrounding Wilson Creek and its tributaries. These businesses included Springfield Gas Light Co., Foundry and Machine Shop, Kansas City and Southern Lumber Co., and various railroad shops. Springfield Wagon Co. was also located along the Jordan Creek in downtown Springfield between the years 1873 to 1941. In 1873, the Brookline mining District became one of the four main lead and zinc producing areas in Greene County, Missouri. Production near Brookline dropped to low levels in 1876 and eventually ceased around 1898 ("Missouri Lead Mining," n.d.). The deposits are hosted locally in fractures in the Burlington-Keokuk Limestone, which underlie the study area along the Wilson Creek. When these businesses and others in the area became flooded, floodwaters transported contaminants from storage and dump sites to downstream areas (Figure 5).

As of 2012, approximately 30% of land cover in the watershed was impervious, with 47% urban, and nearly 16% grassland (TMDL, 2011). The rest of the area was comprised of small percentages of cropland, forest, and herbaceous cover (TMDL, 2011). Today's land use of the watershed ranges from low to high density urban in the upper watershed, to residential, livestock grazing, and forage crop production ouside the city

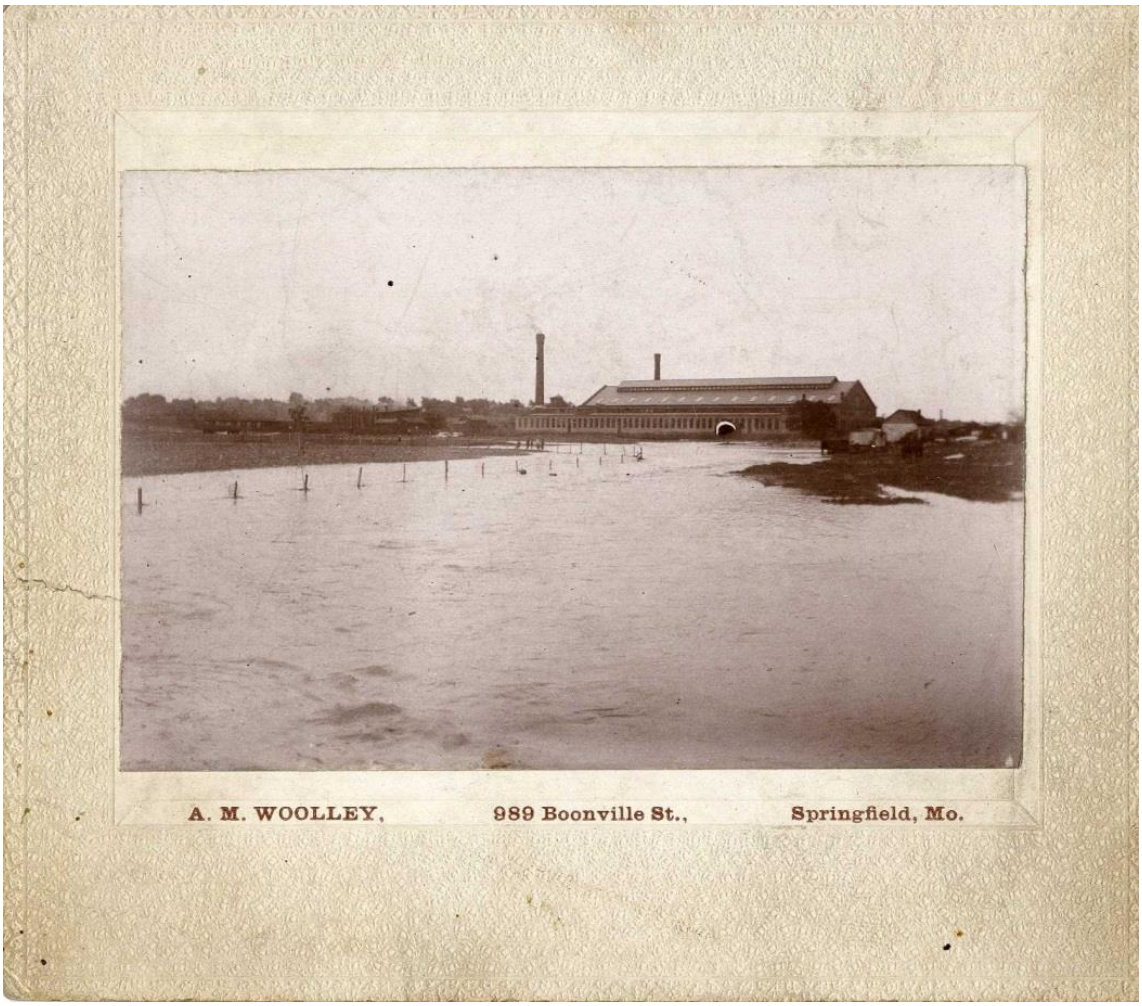

Figure 5. Springfield Wagon Co. Flooded by Jordan Creek Ca. 1900.

limits (Figure 6). Most of the area is comprised of farms and ranches where forage and grain are grown for livestock within the lower portion of the study watershed.

Table 3 provides a chronological history of the city of Springfield's development. All of these major land use and industry changes could have influenced fluvial geomorphology within the Wilson Creek watershed. This information helps to identify rapid land use changes for industry and residential construction, and how resources might have been utilized in the 185-year time span. When analyzing sedimentation and fluvial changes, these historical land use changes could provide important insight into any sedimentation patterns and channel morphology. A better understanding of the more recent (post-1953) land-use changes immediately surrounding the study area can be acquired through analysis of aerial photographs.

Aerial photographs from 1953, 1970, and 2010 display land cover changes around the study area (Figure 7 through 9). Between 1953 and 1970, a few more structures were built along the terrace on the east side of the channel. Tree removal is also evident between the years 1953 and 1970, which can be seen north of FR 156 and along the east terrace. The most recent aerial from 2010 displays an increase in vegetation on the terrace along the west side of the valley floor as well as the area north of FR156 where tree removal previously occurred. To the far west of the 2010 aerial, some rooftops can be seen from a nearby neighborhood that was developed between 1970 and 2010. From 1950 to 1980, the population of Greene County increased nearly 20% every 10 years (Forstall, 1995). The construction of this neighborhood and others to meet the demands of the growing population of Greene County may have influenced the hydrology an sedimentation of the study area (Dunne and Leopold, 1978; Paul and Meyer, 2001).

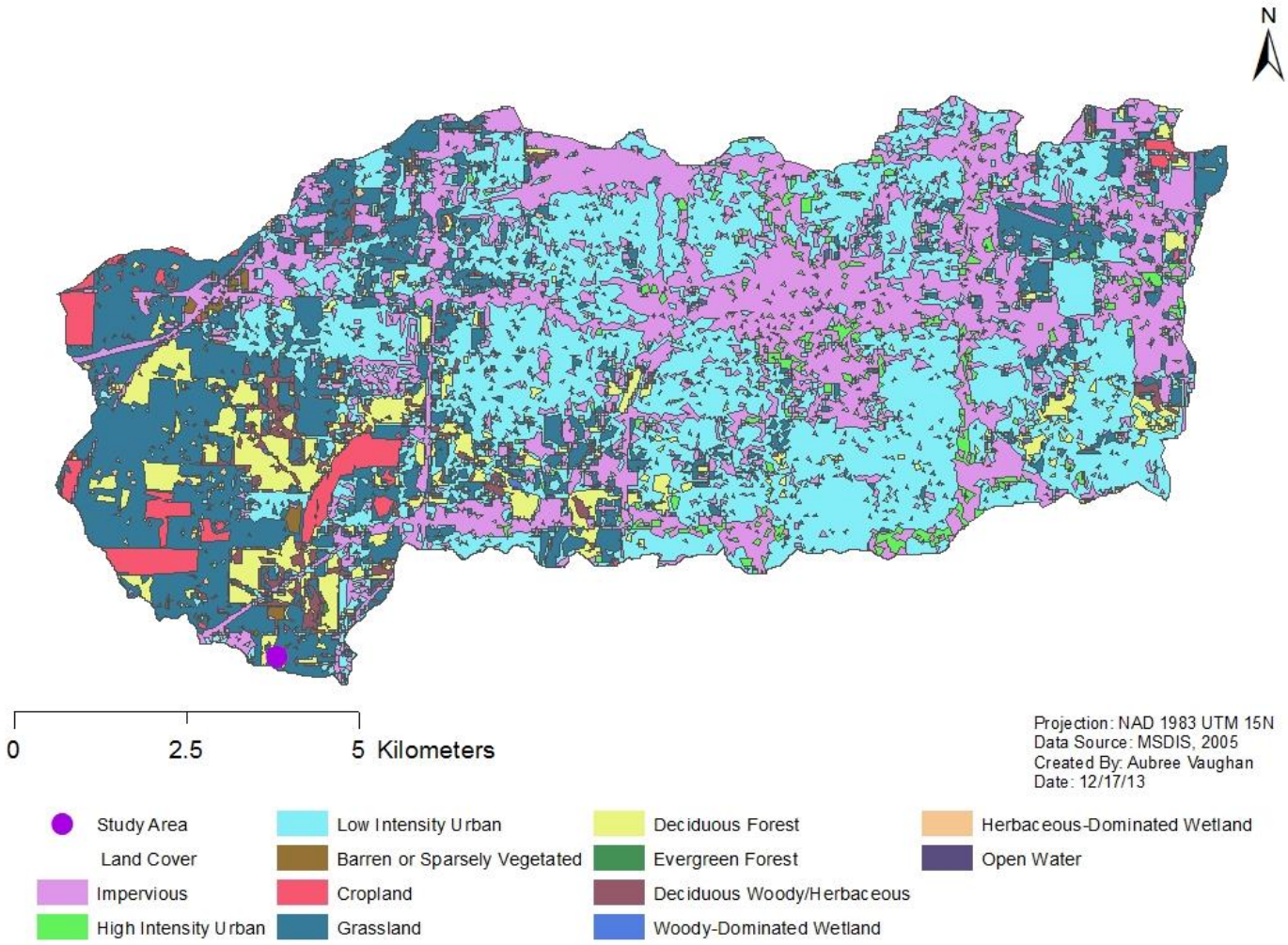

Figure 6. Land cover of the Wilson Creek Watershed in 2005.

Table 3. Chronology of development and urbanization of Springfield, MO (Boyle and March, 1997; Dark, 1981; Dark, 1984; Fairbanks and Tuck, 1915; Holcombe, 1883; Shade, 2003; TMDL, 2011).

Year	Event
1828	John Polk Campbell travels to the area and stakes a claim
1835	Springfield is named
1850	Greene County population is 12,799 in commercial and industrial economy
1870	Atlantic and Pacific railroad reached North Springfield
1878	Springfield total population is 6,878
1881	The Kansas City, Fort Scott & Memphis Railway was completed from Kansas City to Springfield
1926	Highway 66 completed; gives Springfield a paved highway connection from Chicago to Los Angeles
1945	First Springfield-Branson Regional Airport opens
1945	Residential construction boom begins
1945	City of Springfield purchases Springfield Gas and Electric Companies and became City Utilities
1955	Lake Springfield built for cooling James River Power Station
1957	James River Power Station online
1957	City Utilities takes over Springfield City Water Company
1958	James River Power Station unit # 3 online
1963	James River Power Station unit # 4 online
1965	Wilson Creek Battlefield open to public
1966	Paul Mueller Company plant expansion to 306,000 sq. ft.
1970	James River Power Station unit # 5 online
1974	Southwest Power Station online
2010	Population of Springfield is 159,498

Table 3. Chronology of development and urbanization of Springfield, MO (Boyle and March, 1997; Dark, 1981; Dark, 1984; Fairbanks and Tuck, 1915; Holcombe, 1883; Shade, 2003; TMDL, 2011).

Year	Event
2011	Total Maximum Daily Load established by the EPA for Wilson Creek and Jordan Creek
2013	James River Riparian Corridor 319 Restoration and Protection

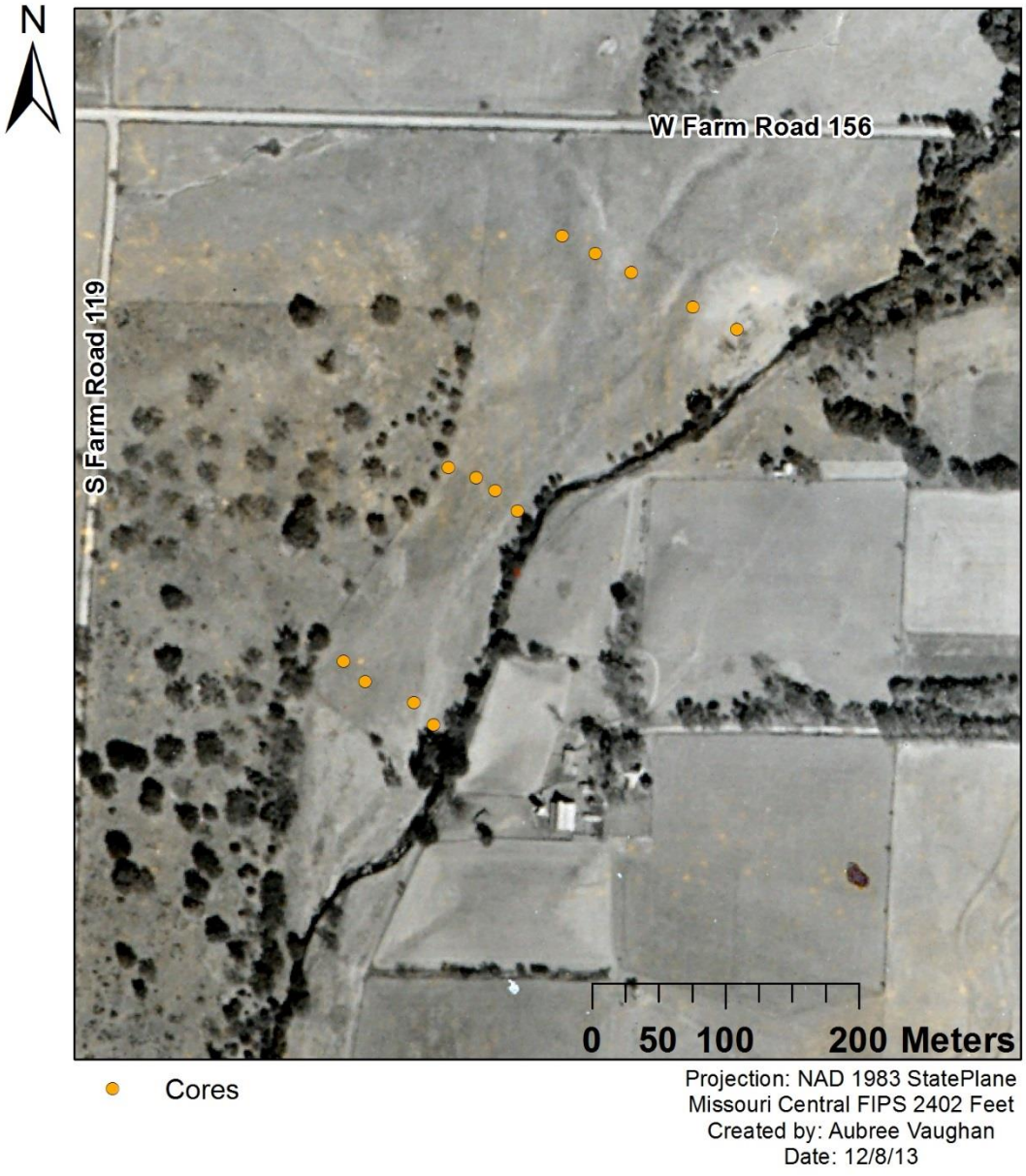

Figure 7. 1953 aerial photograph of study area and core sampling locations.

Figure 8. 1970 aerial photograph of study area and core sampling locations.

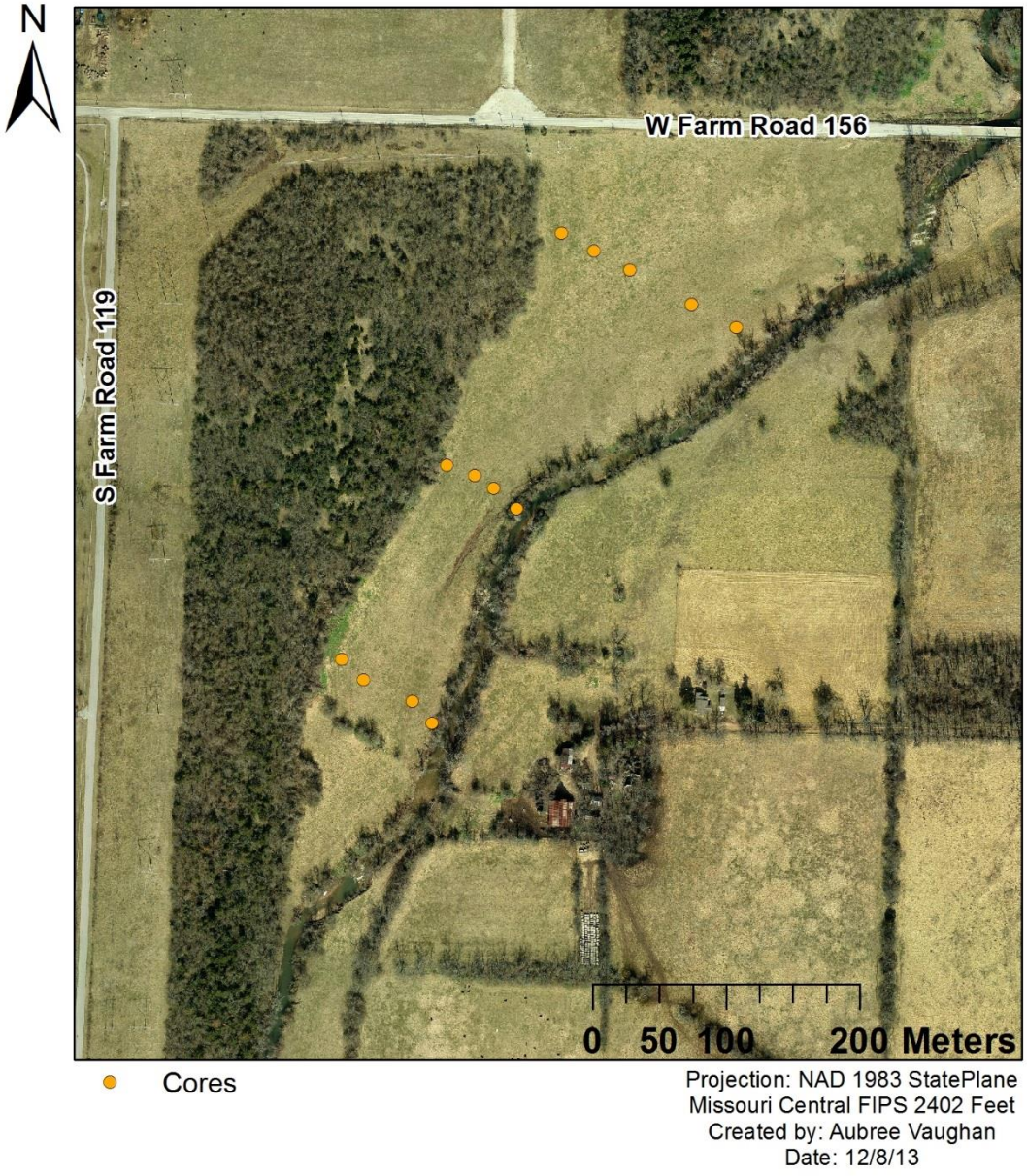

Figure 9. 2010 aerial photograph of study area and core sampling locations.

Since data collection for this study, efforts by the James River Basin Partnership (JRBP) have resulted in implementation of a riparian corridor easement as part of a Section 319 grant from the Missouri Department of Natural Resources and the Environmental Protections Agency Region VII. Barbed wire fencing and native seedlings have been planted within a 30.5 m buffer of the channel to reduce nonpoint source pollution and control cattle access to the channel (Figures 10 and 11). Even though environmental management practices have been implemented since this study began, this research seeks to better understand how flood inundation, proximity to the channel, and landform classification based on elevation influences the deposition of heavy metals throughout an urban floodplain.

Figure 10. Study area with recent seedling plants and new barbed wire fence.

Figure 11. Broader view of riparian easement project.

CHAPTER FOUR: METHODS

Field Methods

Survey of Study Area. To compute topographic surveys of the study area, including three Transect profiles and 13 soil core locations, a Trimble GeoExplorer 2005 series GeoXH handheld GPS with external Zepher antenna was used. This portable mapping-grade GPS unit is capable of providing sub-foot accuracy. The GeoXH handheld GPS uses H-Star technology with the external Zepher antenna to provide post-processed accuracy of 20 cm or better for static GPS positions (TNS, 2005). The Topcon GTS-225 Electronic Total Station and TDS Ranger Data Logger were used to perform channel morphology and stream habitat surveys with a range of 3,000 meters (TDS, 2000). The TDS Ranger data logger utilizes the Windows CE operating system and surveys are performed using Survey Pro. Data were referenced using ForeSight DXM software (TDS, 2004).

An approximately 70 m by 90 m sampling grid was also constructed for collection of surface samples across a section of study area floodplain. The sampling grid was positioned across the floodplain using tapelines and a straight fence line for reference to locate collection sites at 10 m intervals. The locations for collection were chosen to encompass Transect two and various topographical changes across the floodplain, including a chute feature. The Trimble GeoExplorer 2005 series GEOXH handheld GPS with external Zepher antenna was used to collect data for the sampling points throughout the grid, which were later displayed in ArcMap 10.2 with corresponding heavy metal concentrations (ppm).

A rapid geomorphic field assessment along Wilson Creek was performed by this author with Ozarks Environmental and Water Resources Institute (OEWRI) on 07/20/2012, and prepared for the James River Basin Partnership (Owen et al., 2012). Findings and results from the assessment are incorporated into this study to better describe channel characteristics such as channel size and shape, bed conditions, and bank stability. A modified rapid geomorphic assessment was performed every 91 to 122 m to identify basic indicators of geomorphic process (Rosgen, 1996; Fiztpatrick et al., 1998; Owen et al., 2012).

Sample Collection. A total of 13 soil cores were extracted along three Transects, producing 192 samples (Figure 12) (Appendix A and Appendix B-1). A Giddings coring machine was used to collect 11 soil cores and an Oakfield probe was used to collect 2 more soil cores. Sample sites were chosen for representation of different depositional environments. The Oakfield probe was used at floodplain locations where the ground was too soft to drive the truck with the Giddings coring machine. Transect 1 cores 2 through 5 were collected 08/29/2012 and the remaining cores were collected 02/12/2013. Core locations were chosen in an effort to collect data from various topographic features across the study area floodplain. Tube refusal with the Giddings was recorded for each of the coring locations, ranging from 45 cm to 210 cm. Refusal was considered to be the point at which the tube could no longer move down in the soil profile due to gravel or very tight clay. Samples were analyzed for depth following extraction and were promptly placed in Ziploc® freezer bags. Munsell color was determined for samples within core 1B-2 from Transect 1. The sample bags were labeled with the date, Transect, core, depth, and a site identification number.

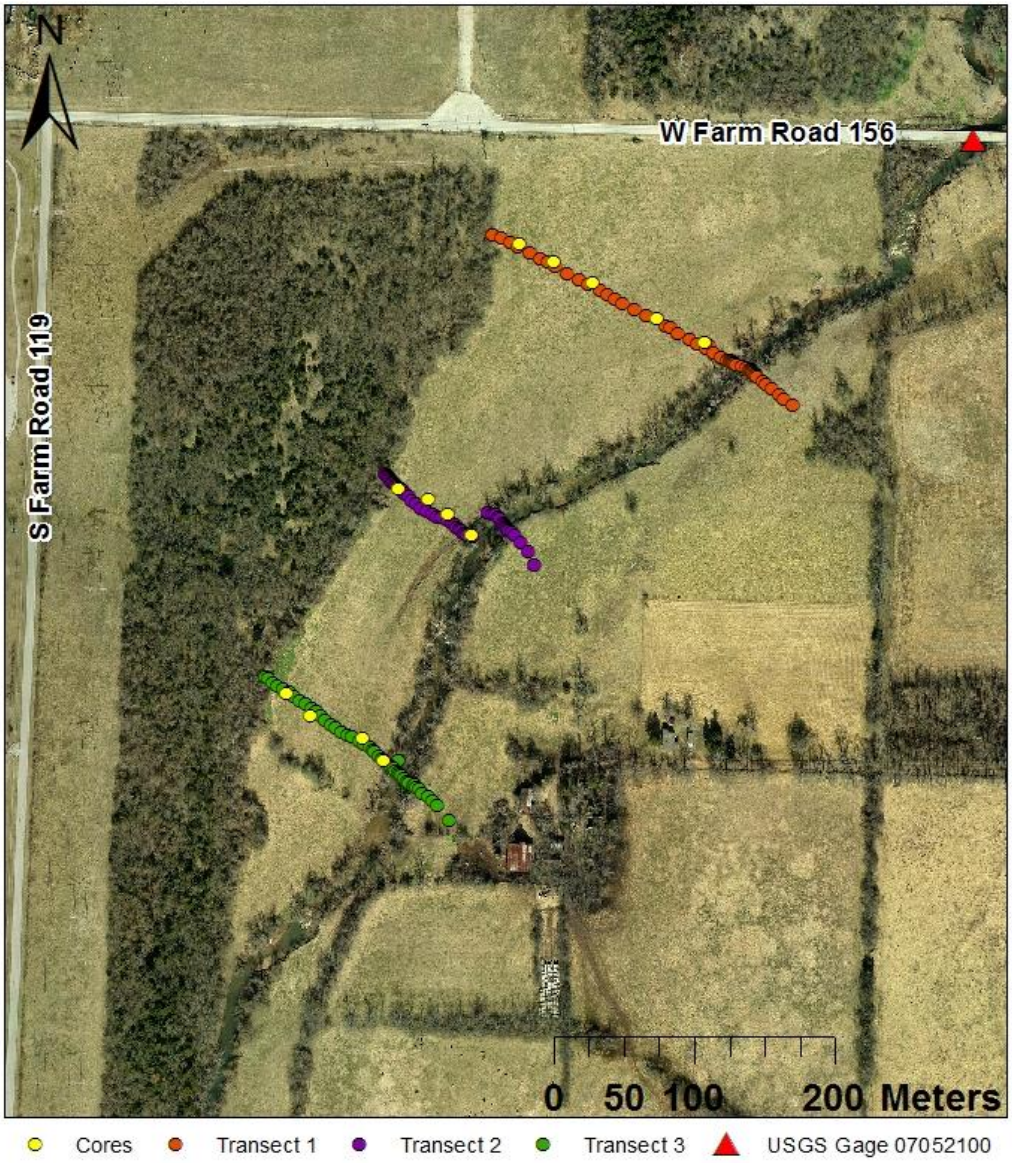

Figure 12. Transect and core locations.

A total of 96 surface samples were collected from the floodplain on 06/07/2013 (Figure 13) (Appendix B-2). A trowel was used to remove the top 10 cm of sediment, including any vegetation and roots. Samples from a depth of 20 cm to 30 cm were collected and placed in a metal free bag. Field duplicates were collected for future accuracy assessment. Sample bags were labeled with the date and grid coordinate, and then transported to the Missouri State University (MSU) sediment lab to dry for further analyses.

Laboratory Methods

Sample Preparation. All samples were taken directly from the study site to MSU. The original bags containing the samples were left open and placed in an oven to dry at 50-60^{o} C for 24 to 48 hours. After the drying process, samples were removed from the oven, disaggregated by mortar and pestle, and sieved to 2 mm or less with a stainless steel sieve. The sieved samples were then placed in clean, metal free bags for future analysis. Each bag was labeled with the same site identification number as used in the sample collection process. Any excess sediment (> 2 mm) was set aside and not used in analysis.

Chemical Composition. All < 2 mm sieved sample fractions were analyzed in the MSU geomorphology lab for metal concentrations with an X-MET3000TXS+ Handheld X-Ray Fluorescence Analyzer (XRF) (Hewett, 1995; "Biological Assessment," 2003; OEWRI, 2007b; Roberts et al., 2009). This instrument is classified as a portable hand-held open- beam X-ray tube based analytical X-ray device. The X-MET3000TXS+ handheld elemental analyzer is based on energy dispersive X-ray fluorescence technology

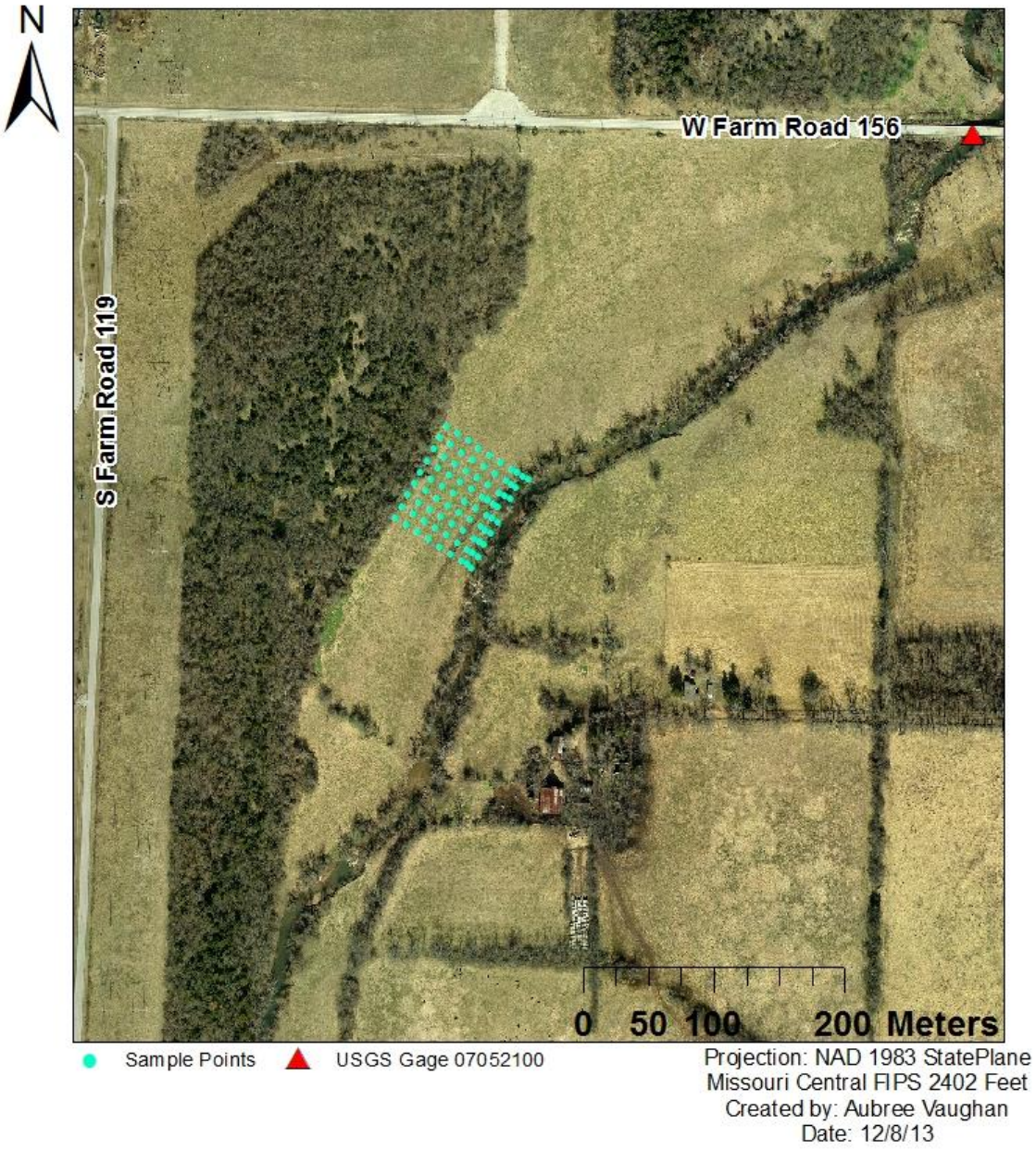

Figure 13. Floodplain surface sampling grid.

and uses an X-ray tube as the source of X-rays. The X-ray tube has a Ru target, 40kV HV supply, and a high-resolution, high count-rate PentaPIN® SiPIN detector system that allows for fast and accurate soil analyses. The instrument is operated by a HP iPAQ PDA with a Windows Mobil 5.0 operating system.

X-rays produced by the instrument bombard the atoms of the target sample. Photons collide with electron shells and electrons move. The movement of the electrons decreases the atom's energy and an X-ray photon is emitted. The energy of the photon being emitted is approximately equal to the decrease in the atom's energy and the X-rays fluoresce. Each element produces uniquely defined energy changes and the quantities of electrons in various shells are proportional to the number of atoms of the element in the sample.

The detector system measures the fluorescent X-rays and the energies that are produced from each X-ray. The net intensities of the X-rays are converted into element concentrations using empirical coefficients and linear and polynomial multi-parameter regressions derived from calibration standards. Each sample was measured for a time span of 90 seconds to detect 12 different metals (Appendix C). Each metal has a specific detection limit, and those samples returning "no detect" were designated a number equaling half of their detection limit for future graphing purposes. Analytical error for this method is ± 20 percent difference for sample duplicates.

Radiometric Dating. Radiometric data analysis using a GC4020 GE Co-Axial Detector and DSA 1000 Digital Spectrum Analyzer with 747 Series Lead Shield was performed in the MSU Geomorphology Lab (OEWRI, 2009). Results from the analysis were used to identify and quantify gamma-ray emitting radionuclides in soil samples.

The radionuclide Cs^{137} was used as a tracer to study erosion and sedimentation (Bernard and Laverdière, 2001; Matisoff and Bonniwell, 2002; Walling and He, 1993; Walling and He, 1997). Radioactive fallout from nuclear testing in the 1950s and 1960s resulted in the presence of Cs^{137} in the soil profile. Once deposited, Cs^{137} strongly adsorbs to soil particles and is then trapped in the sediment profile. The strong adsorption to surface sediment causes Cs^{137} to remain relatively stable in the soil profile, making the isotope a significant tracer for dating sediment throughout a floodplain. Gamma spectrometer analysis was used to identify the first Cs^{137} occurrence in a core and assign the layer a date of 1954 (Walling and He, 1993). Following, peak concentrations were identified and the layer containing the greatest Cs^{137} was dated 1963 (Shade, 2003; Rodgers, 2005). Core 1B-2 from Transect 1 and core 1 from both Transect 2 and 3 were analyzed for Cs^{137}.

Particle Size. Under the operation of an OEWRI research assistant, Adam Mulling, the LS 13 320 Multi-Wavelength Optical Bench Laser Diffraction Particle Size Analyzer with Liquid Module and Flow Cell Geospatial Analysis in the MSU Geomorphology Lab was used to measure the size distribution of particles suspended in liquid for core 1B-2 from Transect 1 (OEWRI, 2008; He and Walling, 1997; Eshel, Levy, Mingelgrin, and Singer, 2004; Rodríguez and Uriarte, 2009) (Appendix D). The aqueous liquid module is capable of suspending sediment samples in the size range of 0.04 μm to 2000 μm. The Polarization Intensity Differential Scattering (PIDS) assembly provides the primary size information for particles in the 0.04 μm to 0.4 μm range. The PIDS assembly also enhances the resolution of the particle size distributions up to 0.8 μm. This additional measurement is necessary, as it is very difficult to distinguish particles of

different sizes by diffraction patterns alone when the particles are smaller than 0.4 μm in diameter. The relative percent difference value for each sample should be ± 20 percent. After passing quality assurance and quality control, sediment size percentages were graphed to illustrate distribution throughout the core profile.

Organic Carbon. Sediment sample analysis for organic carbon matter was performed in the Geomorphology Laboratory at MSU using standard methods (OEWRI, 2007a). Total carbon content of samples was identified using a high-temperature combustion procedure with precision of ± 20 percent RPD. To determine inorganic carbon, samples were pretreated in a 450° C muffle furnace for three hours to remove the organic component. The inorganic carbon amount was subtracted from the total carbon to calculate organic carbon value of each sample (Owen et al., 2011) (Appendix E).

Geospatial Analysis. Watershed delineation was performed to identify the area influencing water and sediment load to the study site. Digital Elevation Model (DEM) files were downloaded from the Missouri Spatial Data Information Service (MSDIS) to create a mosaic of the study area in ArcMap10.2. Various hydrology tools in the ArcMap10.2 spatial analyst toolset such as Fill, Flow Direction, Flow Accumulation, Snap Pour Point, and Watershed tools were utilized to achieve the watershed for the study area. The new layer was then used to achieve information about geographic features within the watershed.

Aerial photography was used to compare channel location and land use changes from the years 1953, 1970, and 2010. The geoprocessing tool in ArcMAP allows the historical, scanned aerial photographs to be georeferenced to a more recent aerial with a defined projection and coordinate system. Aerial photographs from 1953, 1970, and

2010 were compared in this study. This study used eight hard-edged ground control points (GCPs) in combination with the second-order polynomial function to achieve the best spatial accuracy, resulting in a root-mean-square error (RMSE) of <2 (Hughes, McDowell, and Marcus, 2006). Georeferenced aerials were used to measure channel width changes of a 57-year period. A total of four locations were chosen to compare channel width changes. Recorded widths at the four locations were the average width of four measurements. This method was performed in order to report as accurate a representation of the channel widths as possible.

Light Detection and Ranging (LiDAR) data was utilized to create a topographic map that was then utilized to identify various valley floor landforms across the floodplain study area. This data was necessary for interpreting why sedimentation and contamination patterns occurred at various elevations across the floodplain. LiDAR data was downloaded from MSDIS with the aid of the LiDAR LAS Download tool. The LAS data set is a point cloud file, containing 7,955,314 points that each possess elevation data from the classifications of ground, low vegetation, medium vegetation, high vegetation, building, and water. The ground classification is used in this study.

The dataset was a product of a contracted project between USACE and Sanborn to provide LiDAR mapping services for Greene County Missouri (SMC, 2011). The project was set up to only provide elevation information for Greene County, which in return only provided classification information for ground and water. Project specifications for quality control included: bare earth vertical accuracy of 15cm, horizontal accuracy of 0.5m, a total of 17 check points, horizontal datum/vertical datum at NAD 83/NAVD 88, and the projection units in U.S. Survey Feet. Final product

deliveries were in both UTM Zone 15 (meters) and MO SPCS Central Zone (US Svy Feet). The project used the multi-return Leica ALS-60 LiDAR system. This system utilizes geodetic GPS positioning, orientation derived from high-end inertial sensors, and high-accuracy lasers (SMC, 2011).

In this study, acquired LiDAR data was processed to obtain both first and last return point data. Last return data was filtered in order to obtain a LiDAR surface representation of bare earth. The LAS dataset was then converted to a multipoint feature class, using the conversion tools in the ArcMAP 3D analyst toolbox. This data was displayed as a conglomerate of points in a map, and was then interpolated to triangular irregular networks (TIN). Although TINs have a disadvantage of slow processing due to their large file size, the high precision of this type of spatial interpolation is best fit for this study's analysis of elevation change across a valley floor. The TIN was converted to a raster in order to create a new Hillshade raster, displaying shaded relief of the surface raster by considering the illumination source angle and shadows. The new Hillshade raster allows map viewers to better see elevation changes. This raster was later used to display elevation surface and landform surface.

The 2008 Greene County Soil Survey acquired from the Center for Applied Research and Environmental Systems website was analyzed in combination with the developed elevation surface map in ArcMAP 10.2 to improve accuracy of soil series distribution across the study area. Each soil series has a corresponding slope (%) and landform association (NRCS, 2008). To improve accuracy of soil series locations across the study area, soil series data were edited in ArcMAP 10.2 to better match their corresponding slope (%) and landform. The resulting datasets were used to

create a map of the various valley floor landforms throughout the study area.

Hydrological Analysis. United States Geological Survey (USGS) gage data was collected for 7 different gages within the Wilson Creek watershed. Location, drainage area, period of record, average discharge (Q) for period of record, and max Q for period of record were gathered. PeakFQ software was then used to calculate discharge recurrence intervals (Q-RI) at USGS gage 07052100. Area (m^2), Q (m^3/s), velocity (m/s), and wetted perimeter (m) were quantified at bankfull and total channel levels for each surveyed cross-section using Hydraflow Express. Hydraflow Express is hydrologic software that is used to calculate various hydrologic equations (Owen et al., 2011). A flood frequency curve was also created for the 24 years of record at USGS gage 07052100 at FR 156 using the Log-Pearson III Analysis (Wallis and Wood, 1985; Stedinger and Cohn, 1986). USGS gage 07052100 has 24 years of records for annual peak discharge at the study area. This data was analyzed and calculated in Excel to create a flood frequency curve for the recorded years of 1933 to 2012.

GPS cross-section survey data was used to represent the channel and then Hydraflow Express was used to calculate the area (m^2) at different water level intervals to display various levels of floodplain inundation. The channel flood capacity was estimated using the Manning's equation and compared to flood frequency estimates based on USGS gage data (Knighton, 1998; Flynn, Kirby, and Hummel, 2006). The roughness coefficient, or Manning's "n", was selected from a table of n-values, but an on-site assessment aided in determining the appropriate n-values for bankfull and total channel calculations (Chow, 1959). Bankfull calculations used an n-value of 0.035,

while total channel capacity n-values ranged from 0.035 to 0.05 to incorporate dense brush near the

channel bank (Chow, 1959).

A longitudinal profile was created using LiDAR data, which was then used to determine slope of the channel and riffle slope of two sub-reaches (Rosgen and Dimension, 1996). Slope of the entire reach was calculated by finding the difference between the first (upstream) and last (downstream) elevation points, and dividing the resulting elevation change by the distance between the measured points. Two sub-reach slopes were calculated to identify any significant changes in slope throughout the study reach. Riffle slope was identified for Transect 1, and an average riffle slope between Transects 2 and 3 was used as the second sub-reach slope.

CHAPTER FIVE: RESULTS AND DISCUSSION

This section presents and discusses the findings from geomorphic and geochemical analysis of the Wilson Creek floodplain and channel in the following sections: (1) channel form and discharge capacity based on cross-section and flood frequency analysis; (2) historical site characteristics and disturbance based on evaluation of historical photography and land use history; (3) Surface soil distribution of trace metals; (4) landform characterization, including evaluation of spatial distribution and stratigraphy of valley landforms and flood prone areas; and (5) Core profile trends to evaluate floodplain contamination trends and depths.

Present-Day Channel Morphology

A 597 m channel reach within the Wilson Creek study site was analyzed using three cross-sections, a longitudinal profile to calculate channel slope, and geomorphic field assessment (Rosgen, 1996). The longitudinal profile for the entire Wilson Creek study reach has a slope of 0.0015 m/m and a typical concave longitudinal profile as measured from MSDIS LiDAR data (Figures 14 and 15). Further calculations of two sub-reach riffle slopes indicate that the slope increases in the downstream direction. The riffle slope for the Transect 1 sub-reach is 0.0012 m/m, while the average riffle slope of Transects 2 and 3 increases to 0.0016 m/m.

The bed of the study reach is approximately 30 % bedrock with most of the bedrock exposed along the upstream portion of the study reach near the bluff and

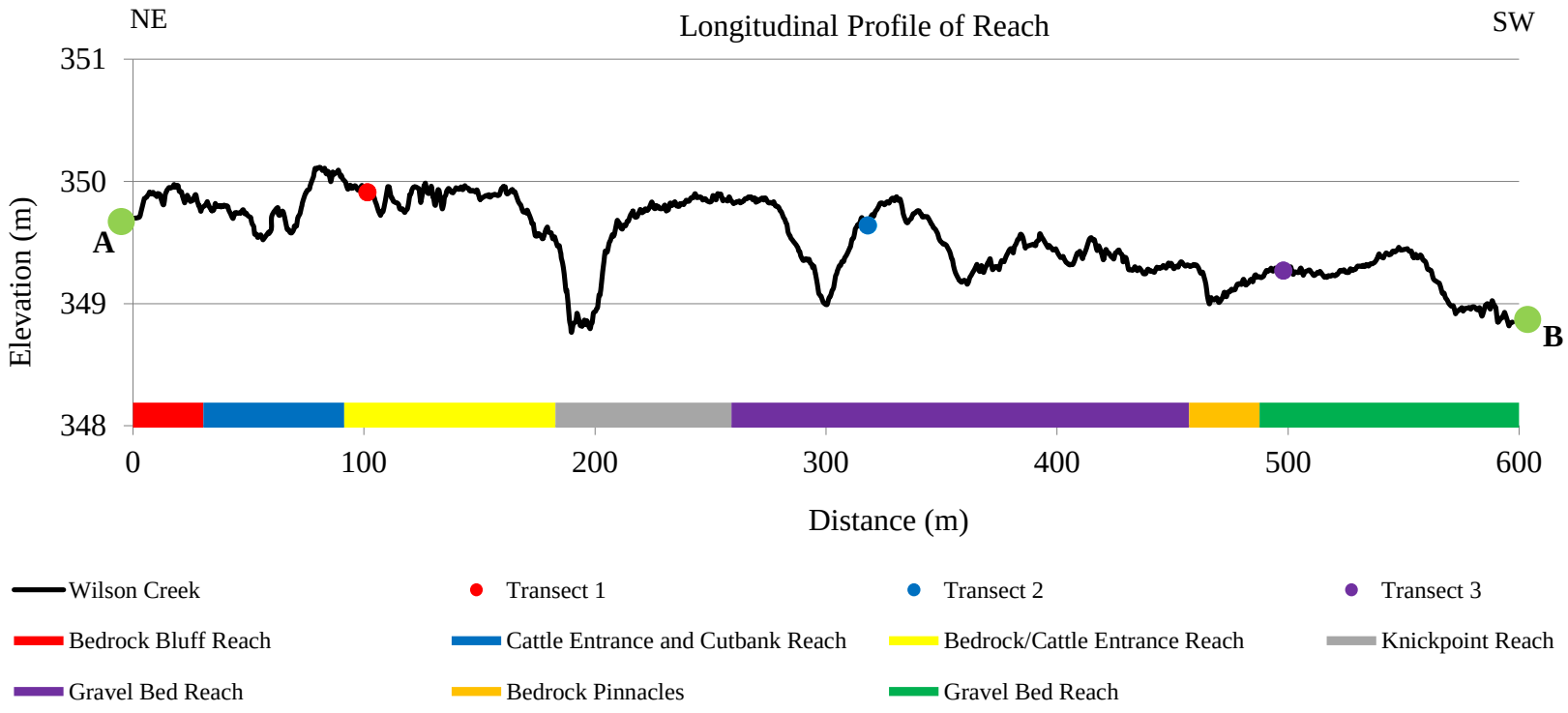

Figure 14. Longitudinal Profile of study area reach, reading Northeast (NE) to Southwest (SW). Points "A" and "B" correspond to the letters and points in Figure 9, marking the beginning and end of the reach.

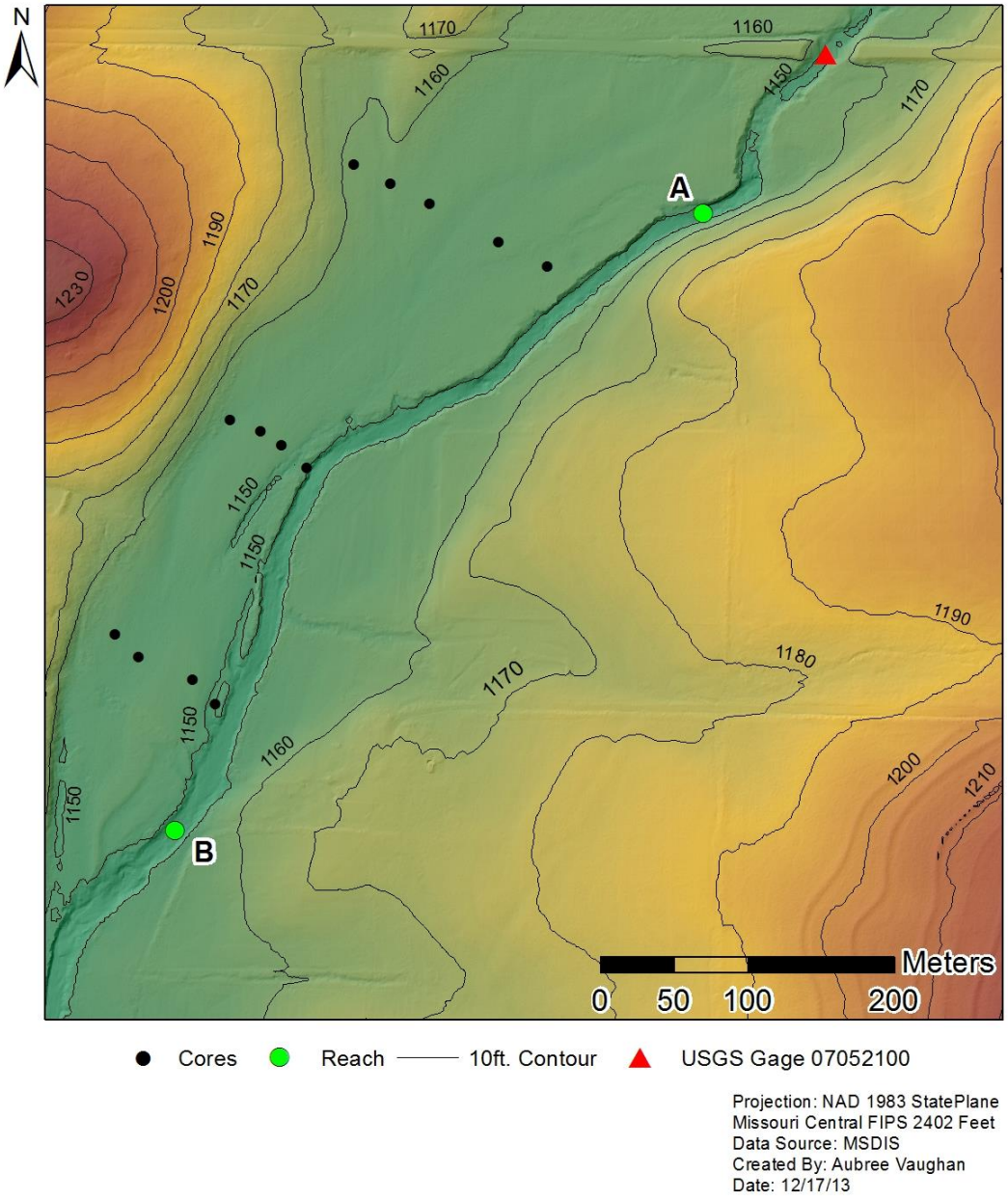

Figure 15. Topography of study area on Wilson Creek. Points "A" and "B" mark the beginning and end of the study reach.

terrace along the east bank of the channel (Figure 14) (Owen et al., 2012). Bedrock controlled streams tend to flow relatively straight for long distances along the bluff line and appear to be somewhat locked in place (Pavlowsky, 2004). As described by Owen et al., (2012), the longitudinal profile shows Transect 1 located within the bedrock/cattle entrance reach, Transect 2 within the gravel bed reach, and Transect 3 within a gravel bed reach (Figures 16 and 17). On-site field assessments and previous studies have recorded evidence of a bedrock knickpoint at stream distance 180 m (Figures 14 and 18) (Owen et al., 2012). Bedrock exposure in the channel bed occurs less frequently as the reach progresses downstream (Owen et al., 2012).

The distribution of bedrock and location of the knickpoint in the channel could also help explain the increase in slope at the second sub-reach. As seen in Figure 19, a knickpoint can result in greater channel erosion and degradation of terraces downstream (Bridge, 2003). Following, the floodplain of an incising channel should increase in width in the down-valley direction (Figure 19) (Bridge, 2003). In this study, the knickpoint might have been moving upstream until stalled by the bedrock obstruction in the bed near Transect 1. This bedrock stalling can cause slope to remain relatively low and result in a more "stable" sub-reach. (Bridge, 2003 and Owen et al., 2012). Bank heights also decrease downstream, following the knickpoint model (Bridge, 2003; Owen et al., 2012).

Analysis of the elevation surface and aerial photographs can aid in the explanation for the increasing slope at the downstream sub-reach. The topographic map shows narrowing of the valley floor as distance downstream increases towards Transect 3. This increased constriction of the valley floor can induce steeper channel slope, greater

Figure 16. Bedrock/Cattle Entrance Reach (90 m) looking downstream (Owen et al., 2012).

Figure 17. Gravel Bed Reach (457 m) looking downstream (Owen et al., 2012).

Figure 18. Bedrock Knickpoint (200m), looking at the left bank erosion (Owen et al., 2012).

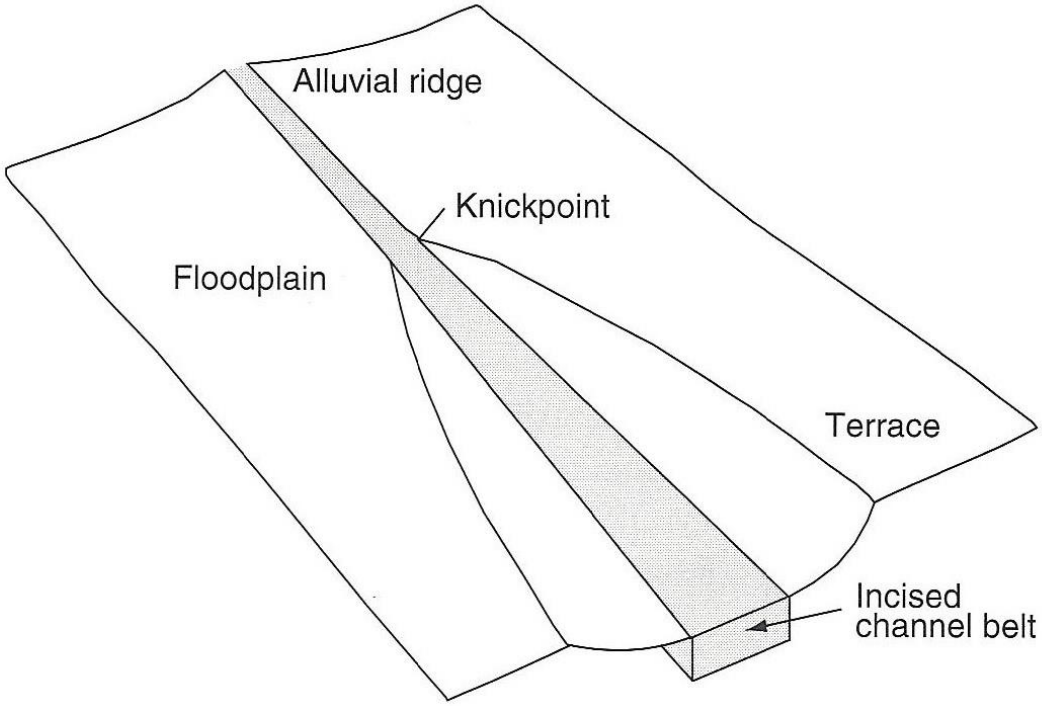

Figure 19. Conceptual model for knickpoint influence on channel incision, riverbank retreat, and terrace formation (Bridge, 2003).

erosion and incision, and greater scour (Bridge, 2003). Several chutes appear to be forming along the banks of Transects 2 and 3 (Figure 15). These chutes indicating floodplain scour could be a result of increased flood energy over the floodplain, as demonstrated by Bridge's (2003) knickpoint model. Even if the observed knickpoint and narrowing downstream valley are not related events, both combine to influence channel morphology. These findings enhance the concept that the downstream sub-reach of the study area is receptive to greater instability than the upper portion of the reach.

Channel cross-sections were surveyed to capture elevation changes and locate core sites. Based on cross-section profiles, Transect 1 appears to have a natural levee forming along the west bank, and Transects 2 and 3 both have a chute forming along the west of the bank (Figures 20 through 22). Bankfull is represented by the width of the water surface at the point where water would spill out into the adjacent floodplain if the natural levee was not in existence. A previous study at this segment of Wilson Creek also found bank height to decrease, and bankfull channel width to increase as distance downstream from the observed knickpoint increased (Figures 23 and 24) (Owen et al., 2012). These findings indicate a typical knickpoint model, and downstream channel widening, in response to flood energy and gravel and cobble deposition in the channel.

The Manning's roughness coefficient was set at 0.035 for bankfull calculations while the floodplain's roughness coefficient ranged from 0.035 to 0.05 for total channel calculations to incorporate dense brush near the channel bank. Calculated estimates of channel capacity for bankfull stage and the total channel are reported in Tables 4 and 5. The natural levee at Transect 1 was not included in the HydraFlow Express bankfull

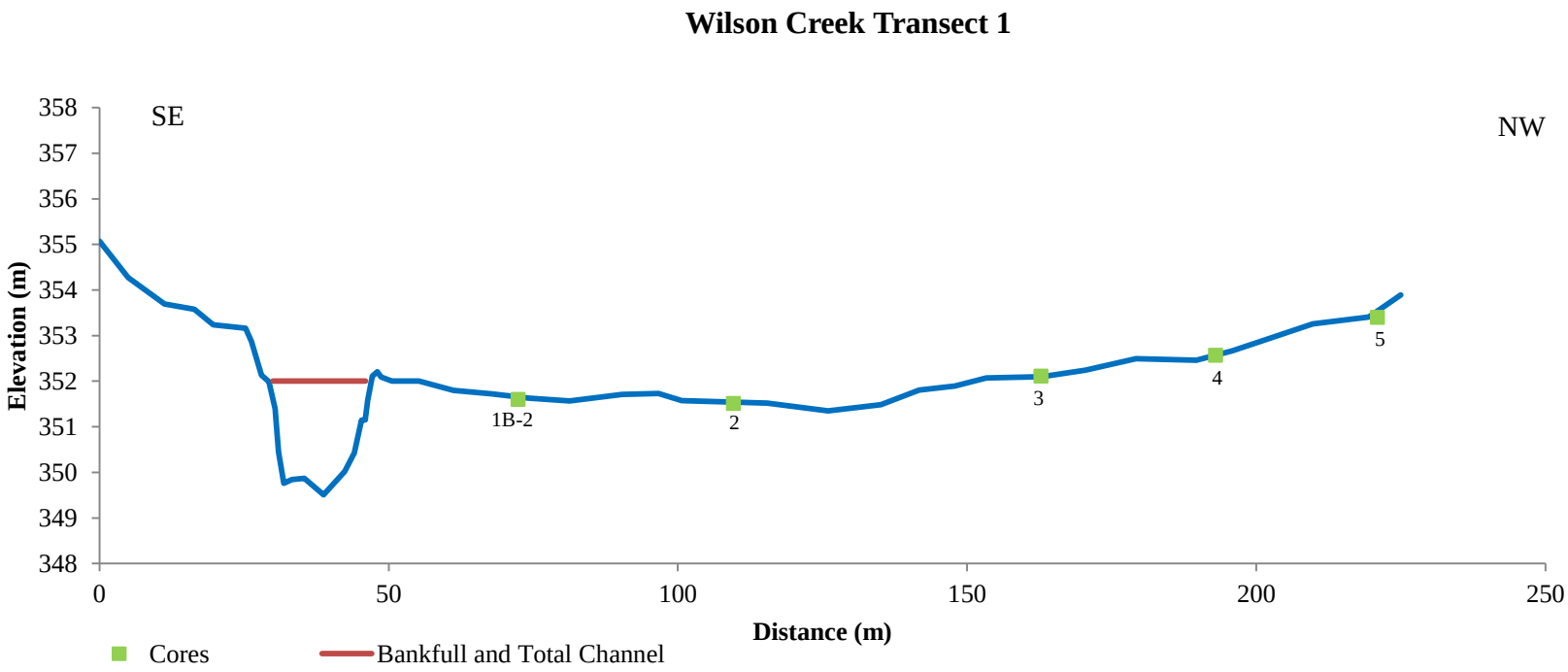

Figure 20. Transect 1 downstream cross-section profile reading southeast (SE) to northwest (NW), with core locations, bankfull level, and total channel level.

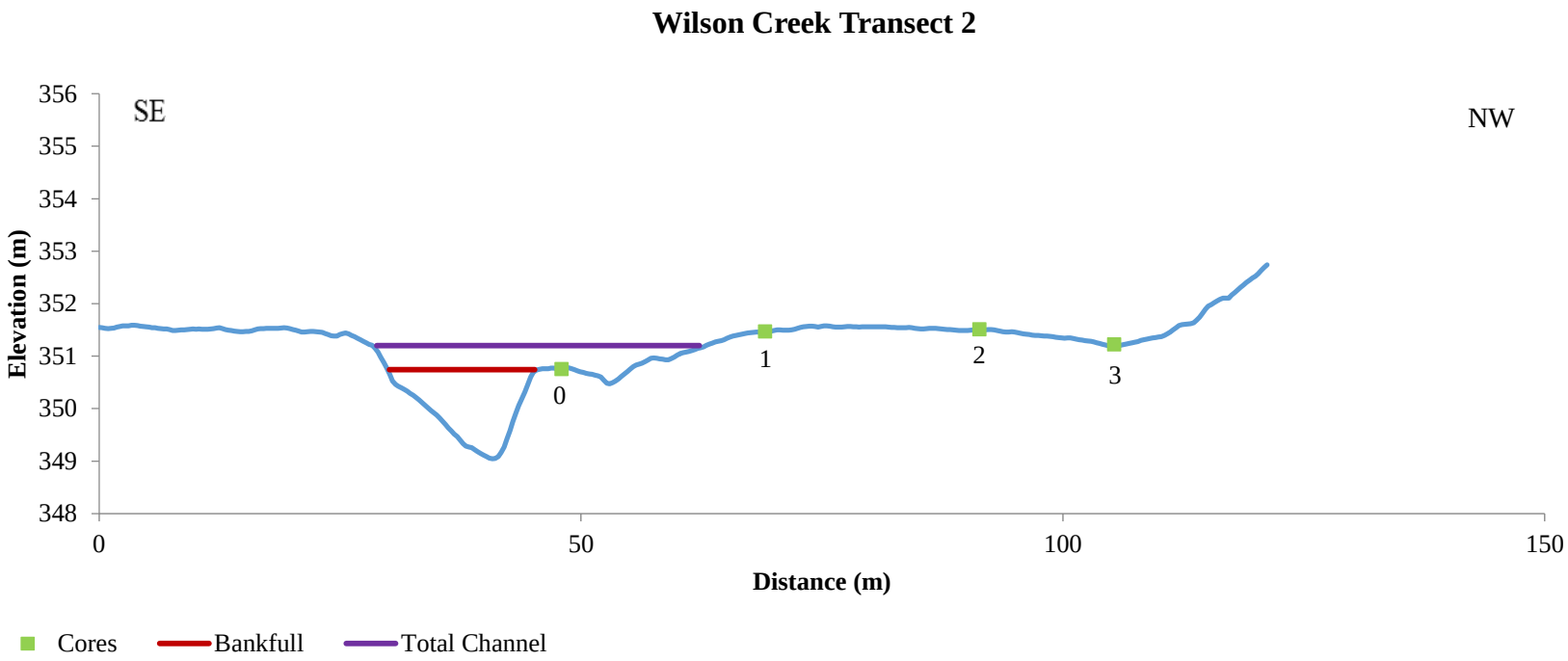

Figure 21. Transect 2 downstream cross-section profile, reading SE to NW, with core locations, bankfull level, and total channel level.

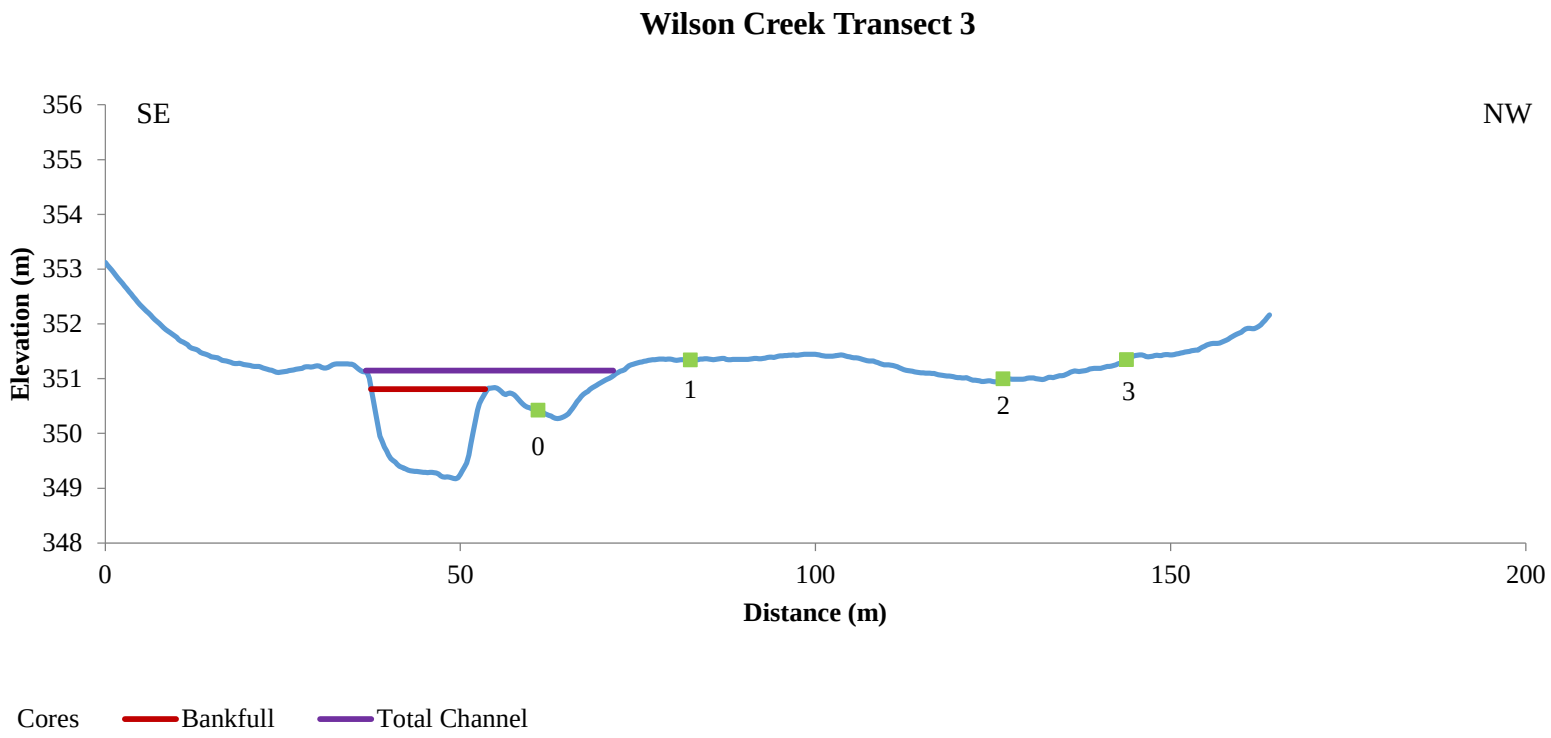

Figure 22. Transect 3 downstream cross-section profile, reading SE to NW, with core locations, bankfull level, and total channel level.

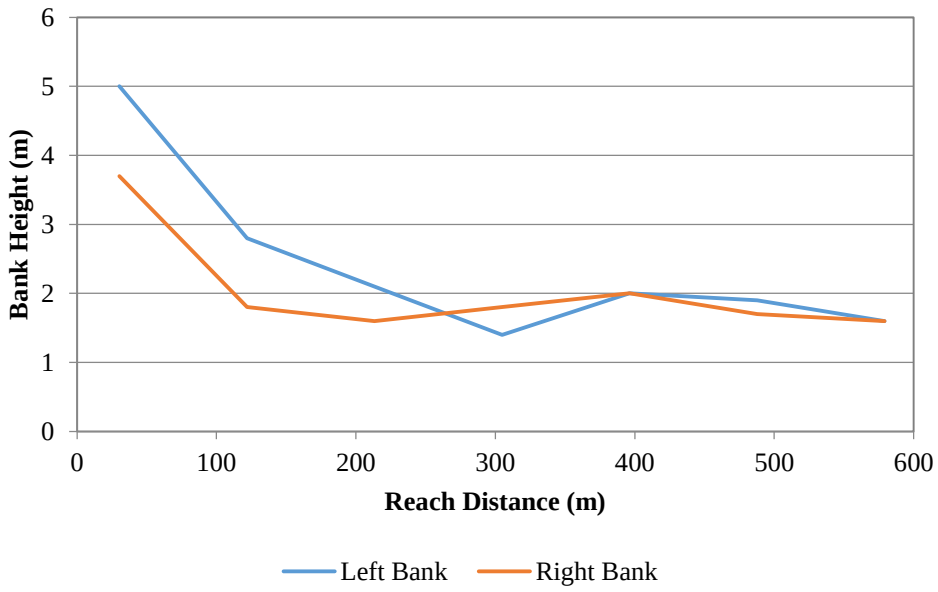

Figure 23. Bank Heights throughout study reach (Owen et al., 2012).

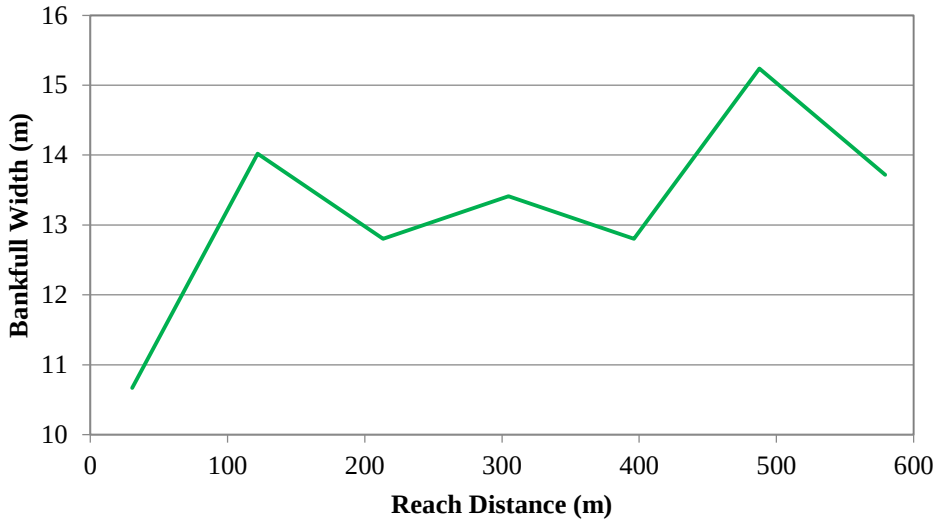

Figure 24. Bankfull widths throughout study reach (Owen et al., 2012).

Table 4. Bankfull capacity.

Transect	Width (m)	Max Depth (m)	Mean Depth (m)	Wetted Perimeter (m)	Area (m2)	Velocity (m/s)	Discharge (m3/s)	RI
T1	18.21	2.53	1.51	19.75	32.37	1.58	51.17	1.25
T2	18.13	1.73	1.06	18.62	14.95	0.99	14.98	<1
T3	16.7	1.49	1.09	17.36	19.26	1.94	37.38	1.05

Table 5. Total channel capacity.

Transect	Width (m)	Max Depth (m)	Mean Depth (m)	Wetted Perimeter (m)	Area (m2)	Velocity (m/s)	Discharge (m3/s)	RI
T1	18.21	2.53	1.51	19.75	32.37	1.58	51.17	1.25
T2	42.06	2.37	1.67	42.68	36.7	1.04	38.01	1.05
T3	45.43	2.1	1.67	46.24	43.32	1.73	75.1	2

calculation. Based on USGS gage data and HydraFlow Express calculations, the channel appears to be slightly undersized, with a capacity to convey the 1 to 1.25 year flood (Table 6; Figure 25). The typical bankfull channel is expected to contain the 1.5-year flood, suggesting that the channel could potentially widen in order to accommodate the 1.5-year flood capacity (Rosgen, 1996; Owen et al., 2012). Bankfull capacity at Transect 1 is just below the 1.5 Q-RI, while bankfull capacity at Transect 2 is less than the 1.005 Q-RI, and bankfull capacity at Transect 3 is just below the 1.25 Q-RI. Total channel capacity analysis demonstrates that the channel is widening at Transects 2 and 3 in an attempt to accommodate the 1.5-year flood. Total channel capacity at Transect 2 is 1.05 Q-RI, and total channel capacity at Transect 3 is 2-QR-I.

Analysis of the aerial photographs indicate that historical floodplain changes have occurred in the form of bank erosion and channel widening. Between Transects 2 and 3, the floodplain has likely been eroding due to channel widening. This trend should continue as an effort to accommodate the 1.5 year flood, or until dynamic equilibrium is achieved. Also, greater gravel and cobble deposition in the channel below the bedrock knickpoint reach will fill the channel, decreasing channel area, and cause the channel to respond by widening to accommodate floods and transport bed load.

Historical Channel Changes

Channel widths were measured at four locations along the study reach to determine how much widening had occurred between the years 1953 to 1970 and 1970 to 2010 (Figure 26 and 27; Table 7). Analysis of the three aerials, in combination with the three transect cross-section profiles, can help demonstrate a widening trend (Figures 7 through 9 and 20 through 22). With the exception of the most downstream width

Table 6. Flood recurrence intervals for USGS gaging station 07052100 at FR 156.

Q-RI	Discharge (m^3/s)
1.005	24.10
1.01	26.39
1.05	34.41
1.11	40.07
1.25	48.71
1.5	59.02
2	73.04
2.33	80.03
5	114.50
10	147.46
25	195.89
50	237.15
100	283.17

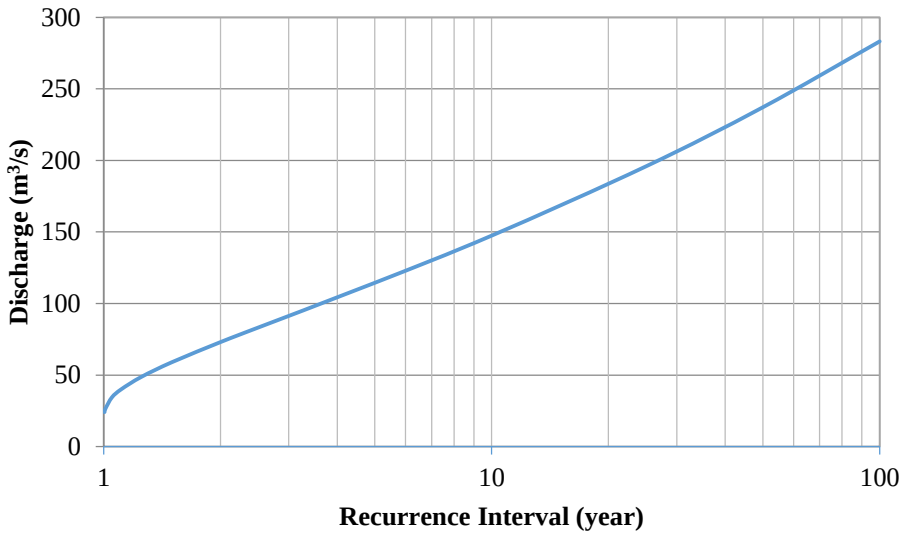

Figure 25. Flood frequency curve for USGS gaging station 07052100 at FR 156.

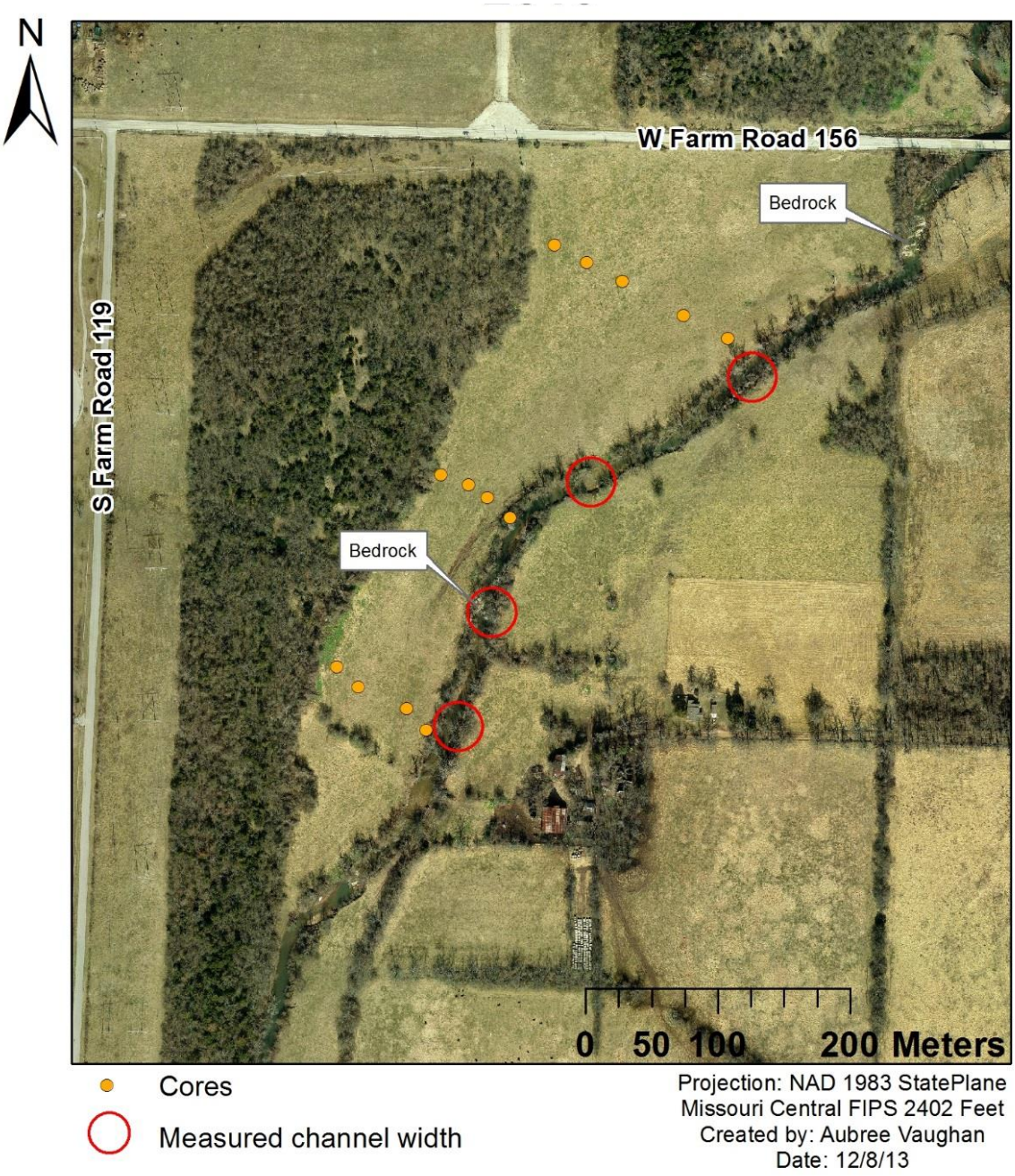

Figure 26. 2010 aerial with locations of channel width measurements in relation to core locations.

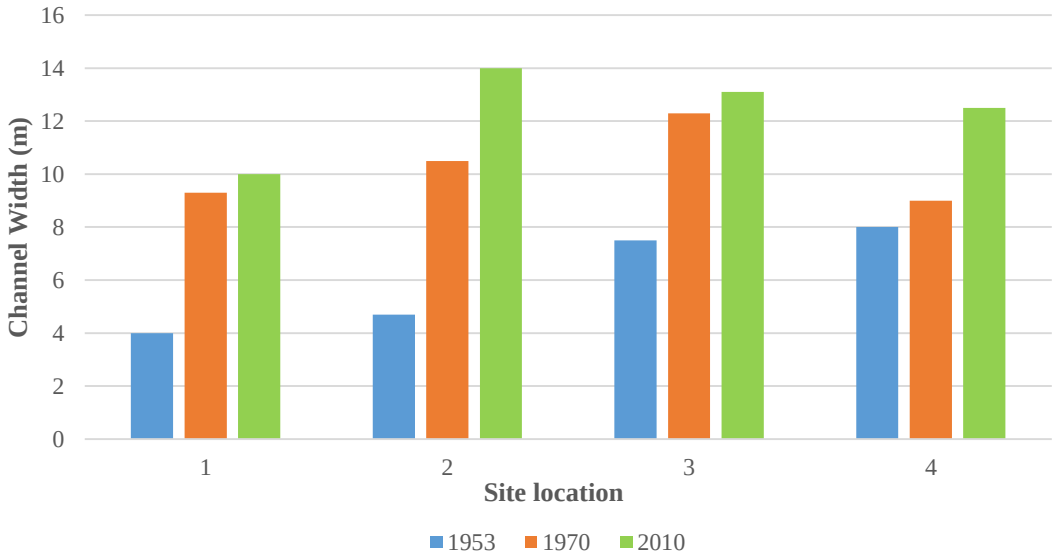

Figure 27. Changes in channel widths between 1953 and 2010, moving downstream.

Table 7. Channel width measurements from aerial photography.

Location (Reach meter)	Latitude (DD)	Longitude (DD)	1953 Width (m)	1970 Width (m)	2010 Width (m)
112	37.16695	93.37218	4	9.3	10
259	37.16621	93.37355	4.7	10.5	14
393	37.16533	93.37439	7.5	12.3	13.1
484	37.16455	93.37469	8	9	12.5

measurements that had likely already widened by 1953, channel widening occurred more rapidly between 1953 and 1970. The channel width at the most upstream measurement increased over 5 m from 1953 to 1970, but widened only 0.7 m over the next 40 years. Widening at this cross-section near Transect 1 could have been slowed, or even stalled, by bedrock control, gravel deposition in the channel, and tree root protection (Pavlowsky, 2004; Owen et al., 2012). Evidence of a knickpoint progression upstream and channel widening support this notion.

Based on the 2010 aerial, bedrock also appears to be present in the next to last downstream width measurement at stream distance 393 m (Figure 26). This channel width increased 4.5 m between 1953 and 1970, and only widened another 1.1 m in the following 40 years. The reduced rate of widening at this location may reflect bedrock control.

The greatest increase between 1970 and 2010 occurred at the most downstream measured channel width. This cross-section widened 3.5 m in the last 40 years, while an increase of only 1 m was measured between 1953 and 1970. A 1.8 to 2.1 m diameter legacy tree is located at approximately 550 m in the study reach on the left (east) bank, indicating that the channel has not shifted much at this location, but could have been widening (Figure 28) (Owen et al., 2012). Another legacy tree is located approximately 30-40 m downstream and on the opposite bank from the legacy tree in Figure 28, reiterating that the channel has not migrated across the valley much in the past 100-200 years. Once again, valley constriction, floodplain scour, greater return flows, and a steeper channel could have induced this increase in erosion and incision.

In summary, the key aspects of the study channel include bedrock control, a

knickpoint model, historical expansion of channel widths since as early as 1953, and near bankfull capacity (1.5 Q-RI) (Rosgen, 1996). Bedrock control in the channel is evident in the desktop and field investigations. The bedrock control created a knickpoint at 180 m in the study reach, following a typical knickpoint model as represented by Bridge (2003). Historical expansion of channel widths has occurred since as early as 1953. The expansion is an adjustment to meet the requirements of sediment load and discharge imposed upon the channel by the drainage basin. The current bankfull level is near the recommended 1.5 Q-RI.

Floodplain Landforms

LiDAR data displayed as triangular irregular networks (TIN) can help delineate floodplain landforms (Figure 29). This form of spatial interpolation uses high-precision modeling, making elevation changes easily recognizable. Variations in floodplain elevation are apparent in the LiDAR map, especially moving downstream. Floodplain scour appears to have formed chutes along the west bank near Transects 2 and 3 as was earlier demonstrated by their cross-section profiles (Figure 29).

To further channel and floodplain morphology analysis, the LiDAR and soils maps were combined to create a valley floor landform map (Figure 30). As documented by Hughes (1982) and the NRCS (2008), each soil series has a unique slope and landform association. These qualities were used in combination with LiDAR elevation data to identify boundaries for various landforms found throughout the study area (Figure 25). Starting roughly 50 m upstream from Transect 2, a bench with chutes has formed east of

Figure 28. Legacy tree (550 m) on left bank (Owen et al., 2012).

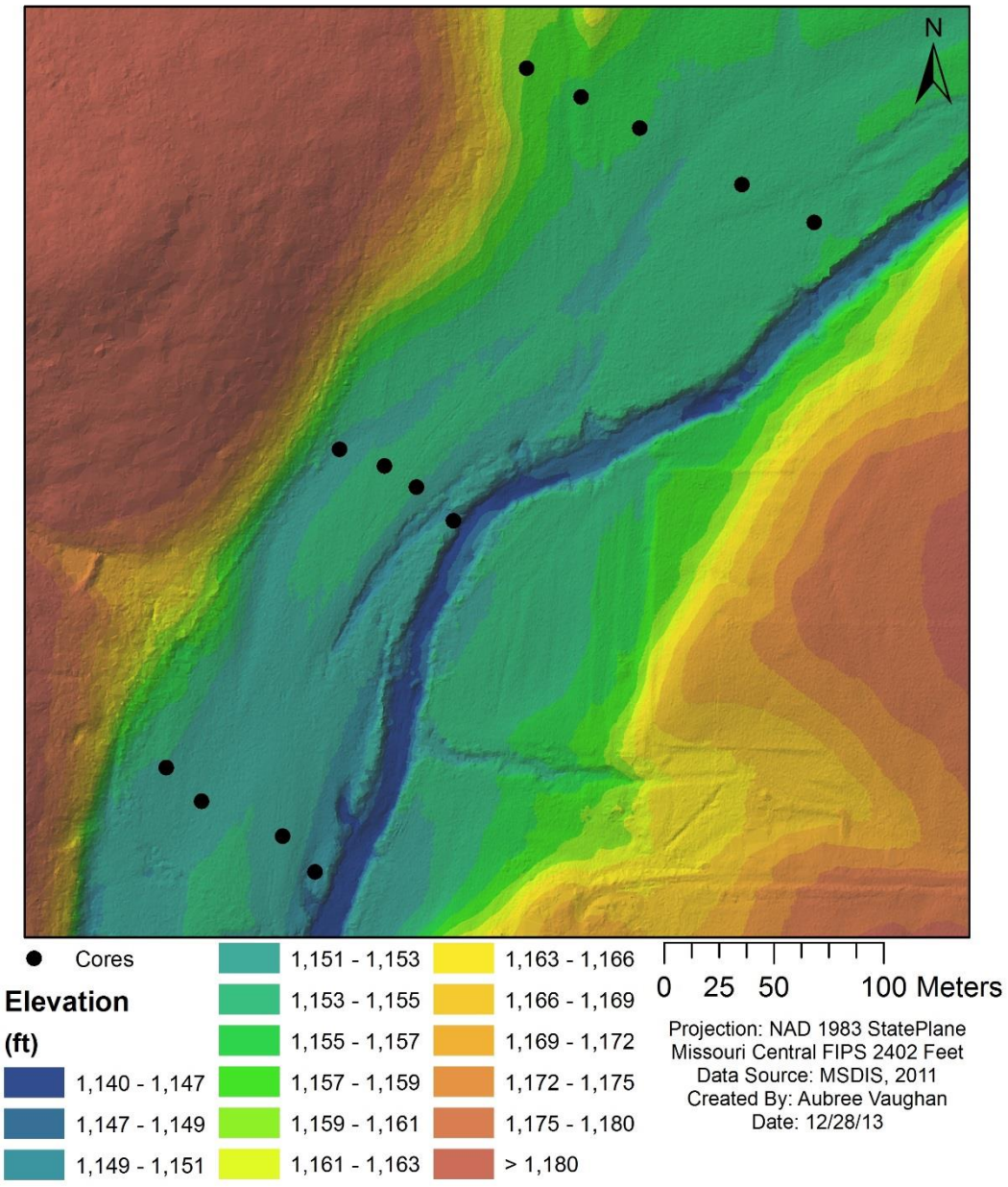

Figure 29. LiDAR map displayed with the hillshade effect.

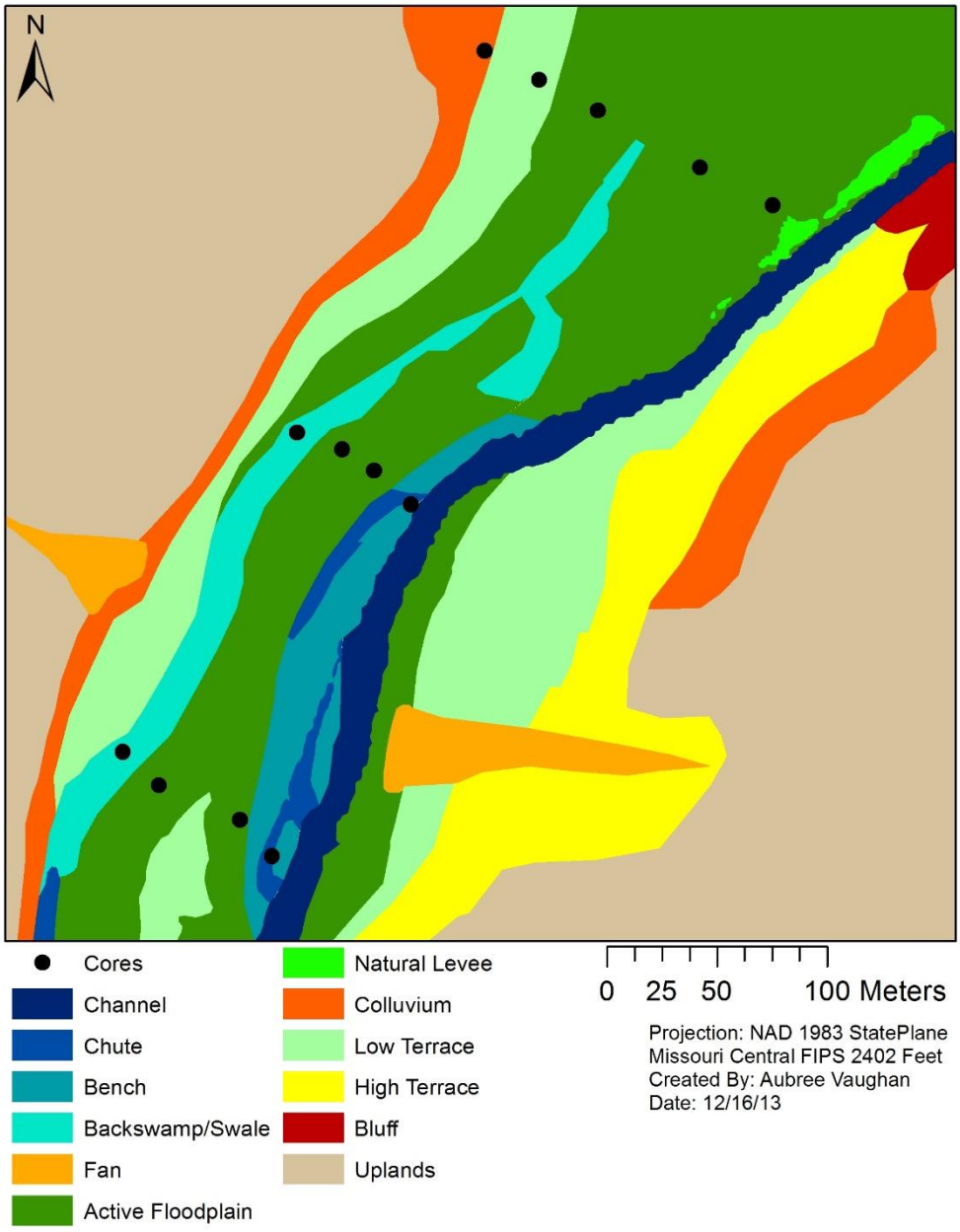

Figure 30. Landforms based on soil classifications and LiDAR (NRCS, 2008, SMC, 2011).

the channel. These landforms are an indicator of channel widening at this location. These landform features were included in total channel capacity at Transects 2 and 3, but should continue to scour in an effort to accommodate the 1.5-year flood (Rosgen, 1996).

A low terrace is located just before slope of the valley walls increase along both sides of the valley floor. These areas indicate the elevation of the historical floodplain prior to channel incision. An outcropping of low terrace in the southwest section of Figure 30 demonstrates how flood flow has rerouted around the section of low terrace, forming a chute at the base of the valley wall. This chute is likely a result of the narrow valley floor at this section of the study area. As the valley floor constricts, greater erosion and scour will occur across a floodplain. A depression in the floodplain was identified and mapped as "backswamp/swale" (Figure 29 and 30). This valley floor landform collects overbank flow and runoff from uplands that are then funneled across the floodplain in a confined elevation depression. The depression increases downstream of Transect 3, forming the chute that was previously pointed out at the base of the valley wall. Identifying and understanding the spatial distribution of these valley floor landforms can aid in the understanding of metal distribution in floodplain sediments.

The floodplain landforms for the study area can be summarized as follows: a 5-50 m wide low terrace, a 100-150 m wide active floodplain, well developed backswamp and swale to the west of the valley floor, and a chute system below the knickpoint and at valley constriction. These floodplain landforms can influence sedimentation patterns across the valley floor.

Metal Concentrations in Floodplain Deposits

Surface Soil Trends. A sampling grid was constructed across a section of the floodplain near Transect 2 for collection of surface sediment samples (Figure 13). A total of 96 samples were collected and analyzed for concentrations of Ca, Cu, Fe, Pb, and Zn (Appendix C-2). These five elements were selected for analysis because they displayed the greatest variation throughout the samples. The heavy metals Fe, and to a slightly lesser extent, Ca, tend to be naturally occurring, while elevated concentrations of Cu, Pb, and Zn are typically associated with anthropogenic sources in urban areas (Sutherland, 2000; Bilos, Colombo, Skorupka, and Rodriguez, 2001). The grid was intentionally constructed to include samples ranging from the top of the bank, along a chute, and extend laterally across the floodplain.

Regression analysis was performed for three different metal associations based on the identified landform the surface samples were collected from. Figures 31 through 33 display results for regression analysis of samples collected from a bench, floodplain, and all samples combined. Little to no correlation is found between either Fe and Ca or Fe and Cu. No correlation exists between Zn and Pb across the bench landform, but a high correlation of nearly 0.9 is exhibited by the Zn and Pb relationship in floodplain samples. The lack of correlation among Fe, Ca, and Cu suggest that each metal is unique in its upstream sources. The positive correlation between Zn and Pb indicate that parent sources within the floodplain landform are similar, or possibly the same.

The distributions of metals in surface soils are mapped in Figures 34 through 38. Calcium concentrations in surface soils are consistently the highest within 15 m of the

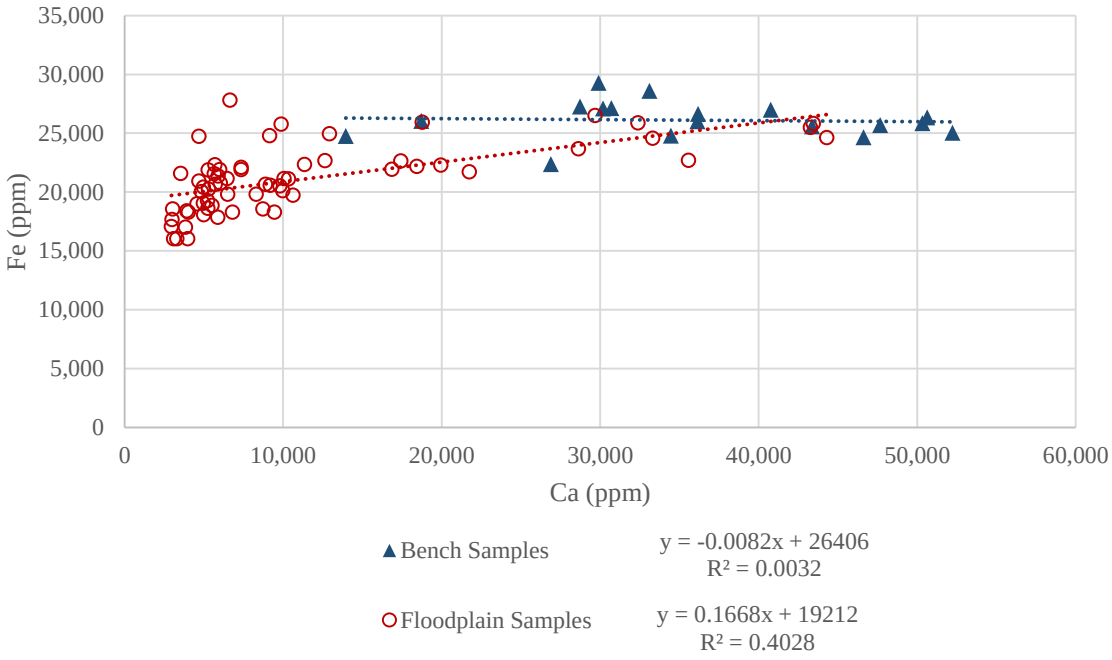

Figure 31. Fe x Ca correlations of floodplain and bench samples.

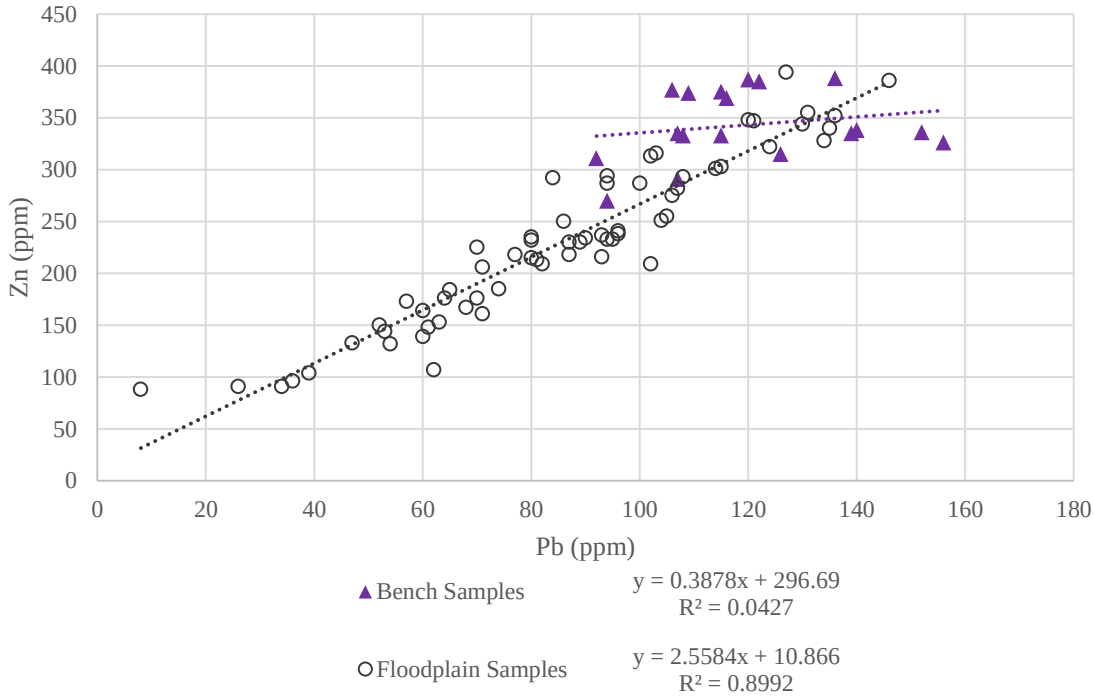

Figure 32. Zn x Pb correlations of floodplain and bench samples.

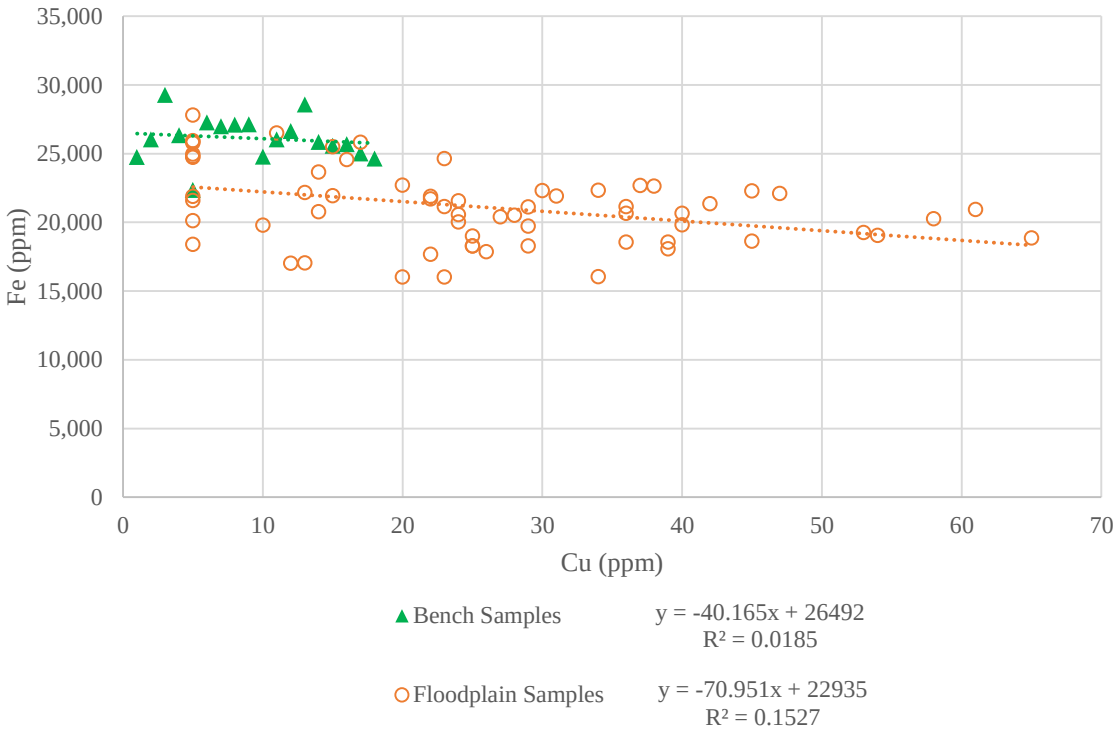

Figure 33. Fe x Ca correlations of floodplain and bench samples.

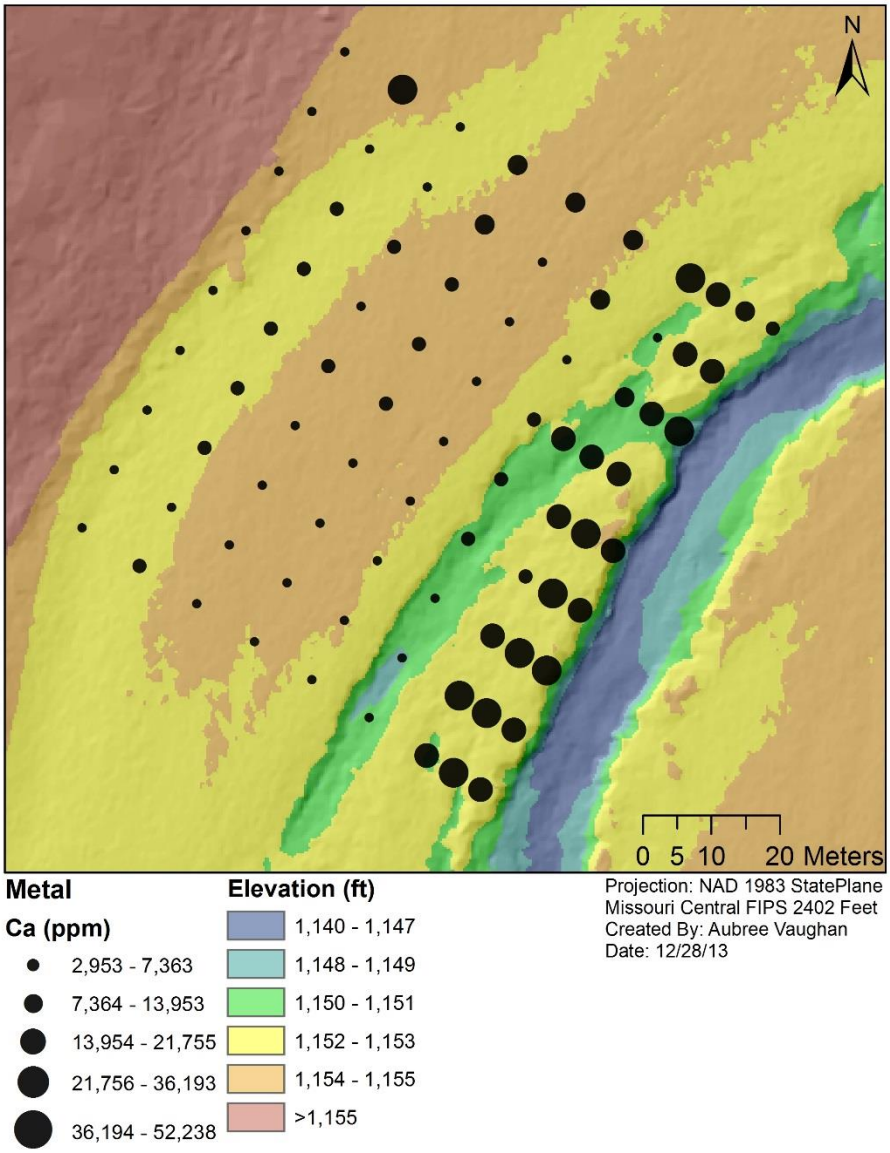

Figure 34. Ca concentration in valley floor surface sediment.

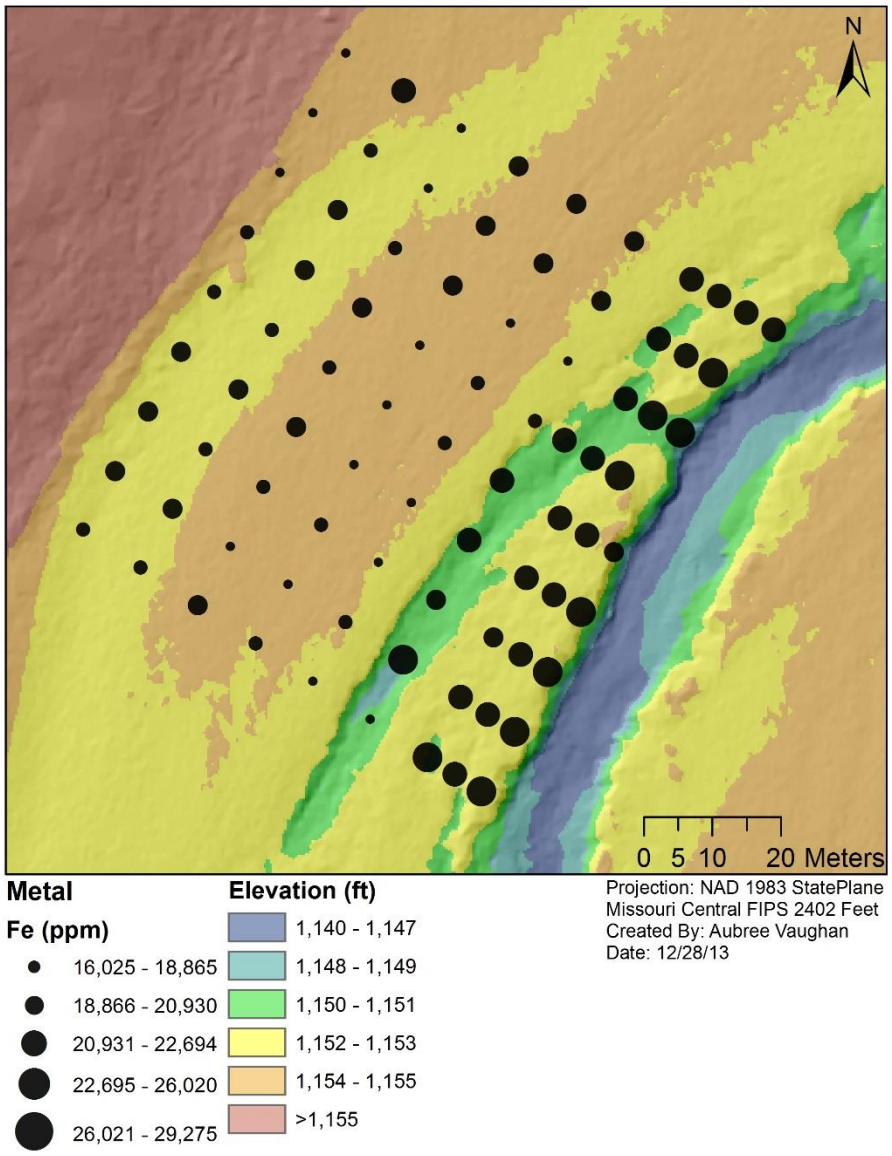

Figure 35. Fe concentration in valley floor surface sediment.

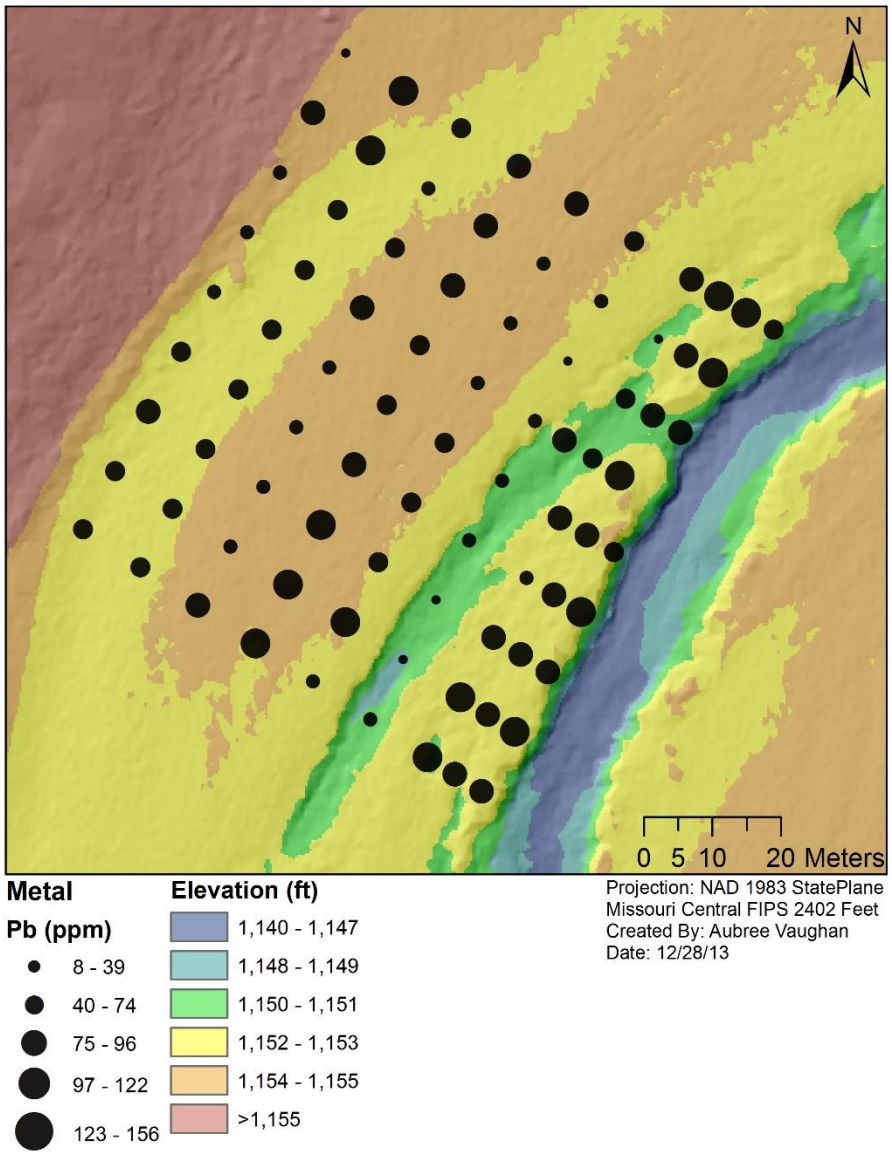

Figure 36. Pb concentration in valley floor surface sediment.

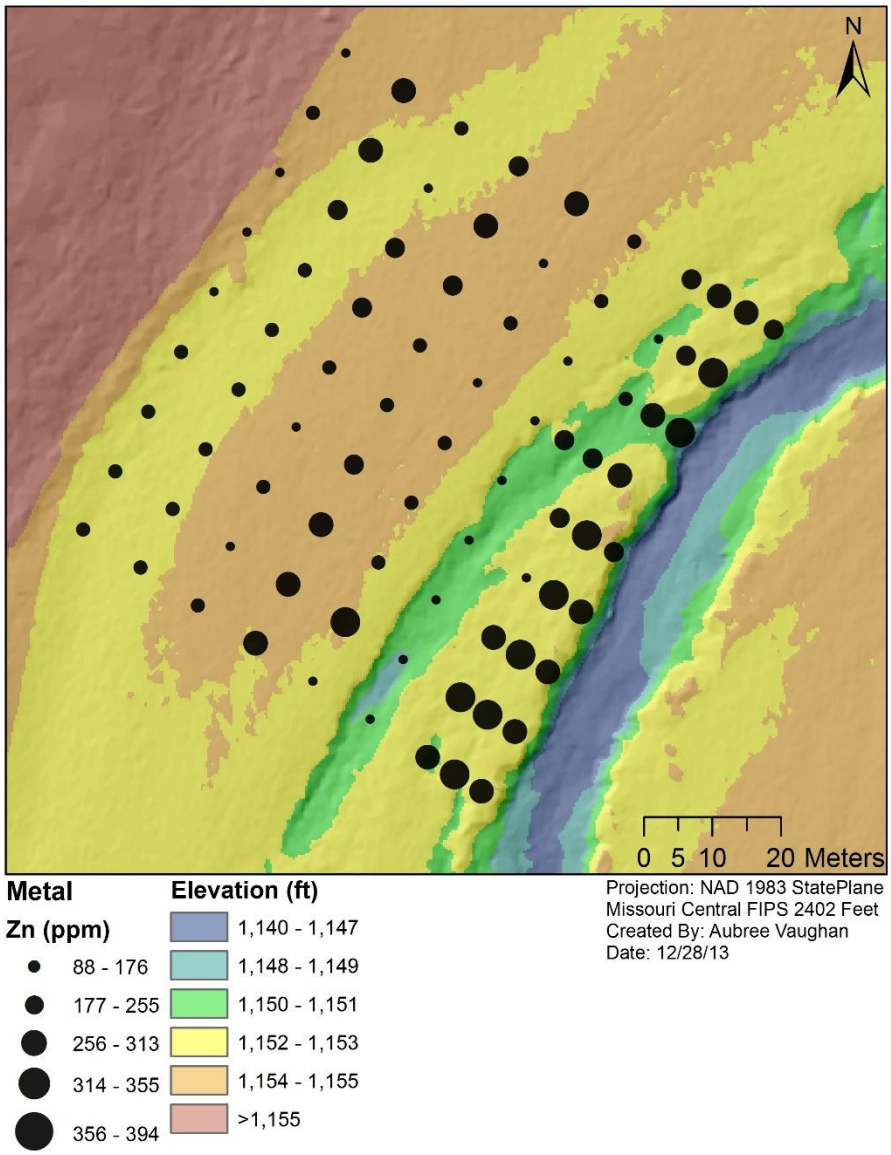

Figure 37. Zn concentration in valley floor surface sediment.

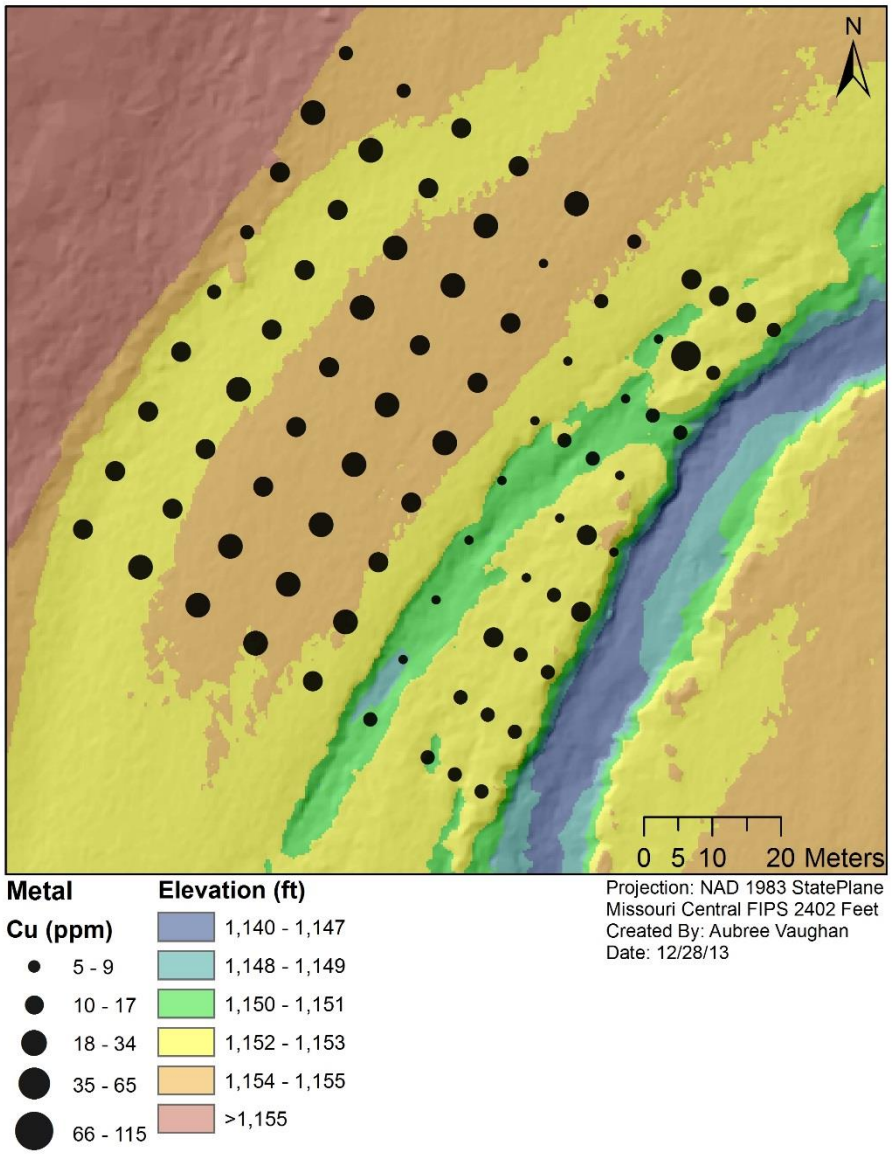

Figure 38. Cu concentrations in valley floor surface sediment.

channel and decrease as floodplain elevation increases (Figure 34). Based on the landform map, this 15 m area of highest Ca is a bench that was recently formed due to channel widening (Figure 30). The proximity to the channel, elevation, and frequency of inundation within the 15 m section can help explain the higher concentrations of Ca. This area is frequently inundated by flood waters as described earlier due to the channels inability to withhold the 1 to 1.25 year flood. High Ca concentrations can be supplied from the erosion of karst limestone bedrock ($CaCO_3$) or Ca-rich urban sources, which helps explain why the highest values of Ca within the area are located where the most frequent inundation and recent sedimentation occurs.

The high Ca along the active floodplain could be a result of recent sedimentation from loess topsoil and/or carbonate bedrock scour containing high levels of natural Ca (Goddard, Mikhailova, Post, Schlautman, and Galbraith, 2009). Loess-derived soil particles, particularly from alfisols and mollisols in the central Midwest-Great Plains region, are known to be Ca-rich (Berner and Berner, 1996; Goddard et al., 2009). Further, the major source of Ca has long been assumed to be dust in the air from soil erosion, but recent studies and patterns of concentrations in the air and precipitation suggest that urban and industrial sources also produce significant emissions of Ca (Soloman and Natusch, 1977). Therefore, weathering of urban surfaces and input by runoff from the city of Springfield could also be a source of anthropogenic Ca.

Iron concentrations are highest within 15 m of the channel, and are also discovered at high levels in several samples collected in the chute (Figure 35). This could be an indicator of recent deposition in the chute, or perhaps erosion of the chute is

exposing high levels of Fe that occur at greater depths below the surface. Higher concentrations of Fe are common in Ozark regions with deep, cherty, clayey soils (Allgood and Persinger, 1979). Linear regression analysis indicates little correlation between Fe and the other metals in surface soils. Erosion of residuum from soil erosion upstream and bank and bed erosion could be a source of higher residual Fe concentrations derived from weathered sediment.

Similar trends of higher metal concentrations near the channel are displayed for Pb and Zn (Figures 36 and 37). Concentrations for both Pb and Zn are high along the active floodplain, and lower for samples collected within the chute. Average concentrations within 15 m of the channel are 109 ppm for Pb and 315 ppm for Zn. This similar trend between Pb and Zn explains that the source of these metal deposits within 15 m of the channel is possibly the same.

Distribution of Cu appears to be opposite of Fe throughout the floodplain surface sampling grid (Figure 38). Concentrations of Cu are lowest within 15 m of the channel and the chute, but increase with distance and elevation from the channel. The area with higher concentrations of Cu is identified as active floodplain in the landform map, but a backswamp forming between the historic floodplain and active floodplain could be reducing inundation of the active floodplain. If this area of higher Cu concentration is not frequently inundated by floodwaters, sources of Cu could be a result of aerial fallout or possibly a result of local runoff, rather than inundation of floodwaters.

Subsurface Floodplain Geochemical Profiles. Concentrations of 12 heavy metals were identified throughout all 13 cores to analyze geochemical profiles, but only Ca, Cu, Fe, Pb, and Zn were used to analyze profile trends and their spatial distribution

throughout the study area (Figures 39 through 44). Floodplain core properties are displayed in Table 8. Once again, Ca and Fe are recognized as more naturally-occurring metals, while Cu, Pb, and Zn are recognized as anthropogenic metals.

Concentrations for anthropogenic metals tend to be highest near the channel and slightly below the surface, decreasing with distance from the channel and with depth (Martin, 2000; Martin, 2004). This trend was seen throughout Transect 1 (Figure 45). Concentrations for these three elements were highest at the surface for cores 3, 4, and 5, just below the surface for core 2, and exceptionally high in the bottom 20 cm of core 1B-2 (Figure 45). One possible cause of the high metal concentrations at deep depths could be that this location was at one time the old channel bed and detritus fill that has since been buried by floodplain sediment. Another cause could be that an old house or barn used to reside in this location, and the sample core just happened to hit contaminated, buried waste material. A more likely cause of this finding is that an area of natural Zn and Pb sulfide mineralization was encountered. The historic Brookline Mine was located just west of the study area watershed, indicating that these deposits of highly concentrated Pb and Zn are common for the area (Thompson, 1986).

Average surface concentrations within the top 30 cm of sample for each of the three elements did decrease with distance from the channel with the exception of core 5, which increased in concentration for both Pb and Zn (Figure 46). Concentrations for Pb and Zn in Transect 1 core 5 are most likely results of local runoff rather than floodwaters. Concentrations of Ca and Fe were graphed separate from Cu, Pb, and Zn as they are expected to be more naturally occurring than the anthropogenic metals, and should

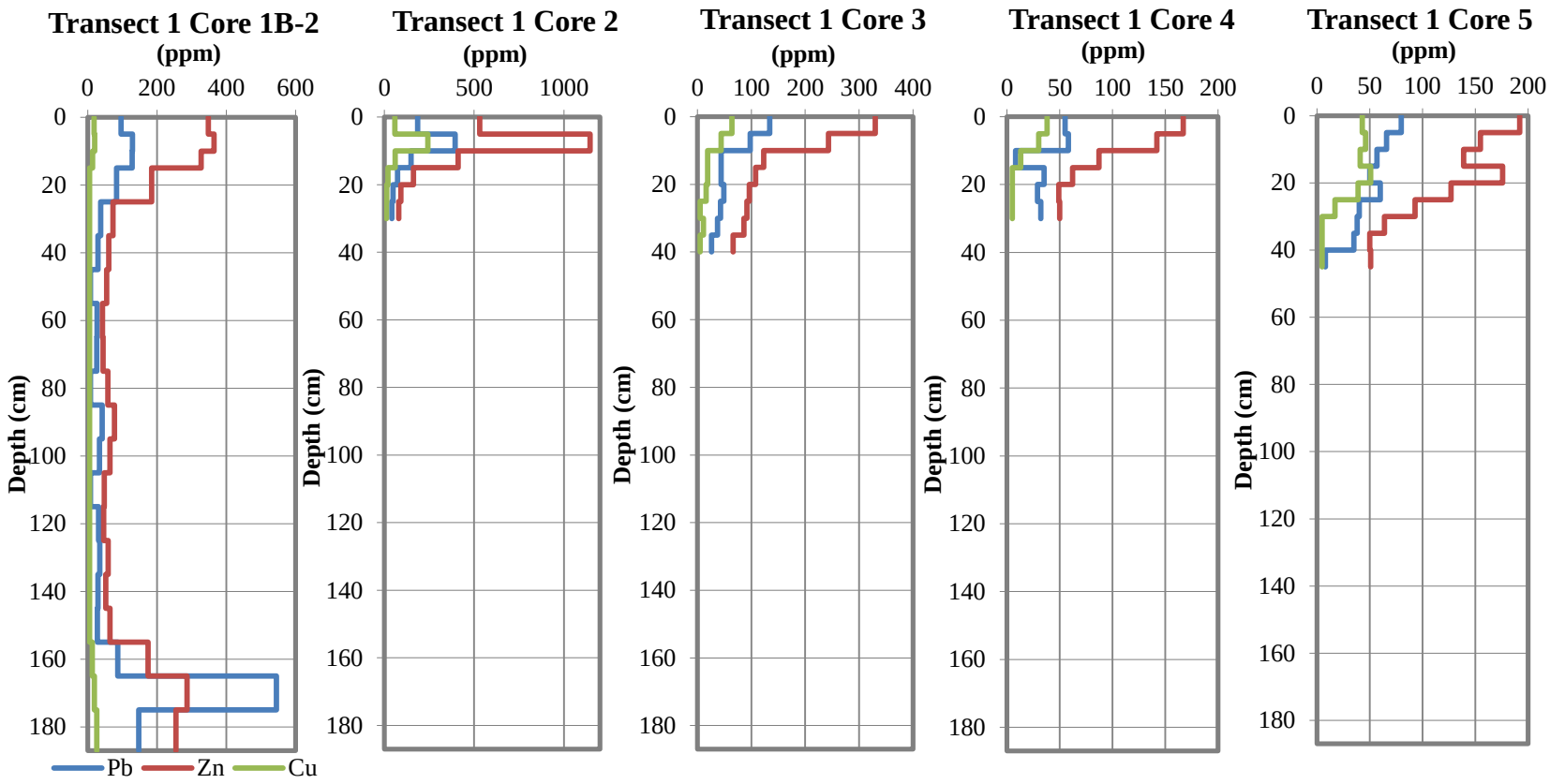

Figure 39. Pb, Zn, and Cu concentrations for cores in Transect 1.

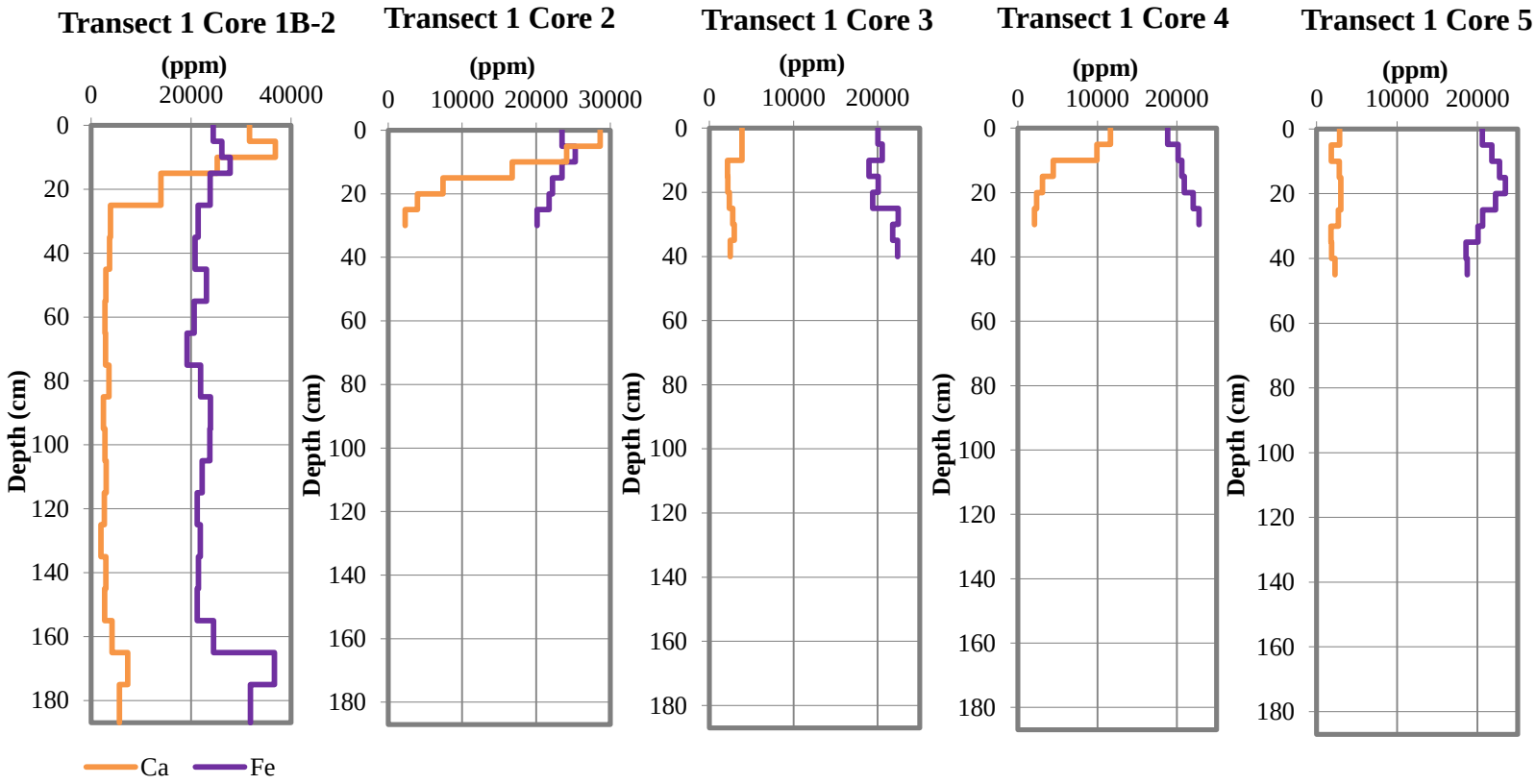

Figure 40. Ca and Fe concentrations for cores in Transect 1.

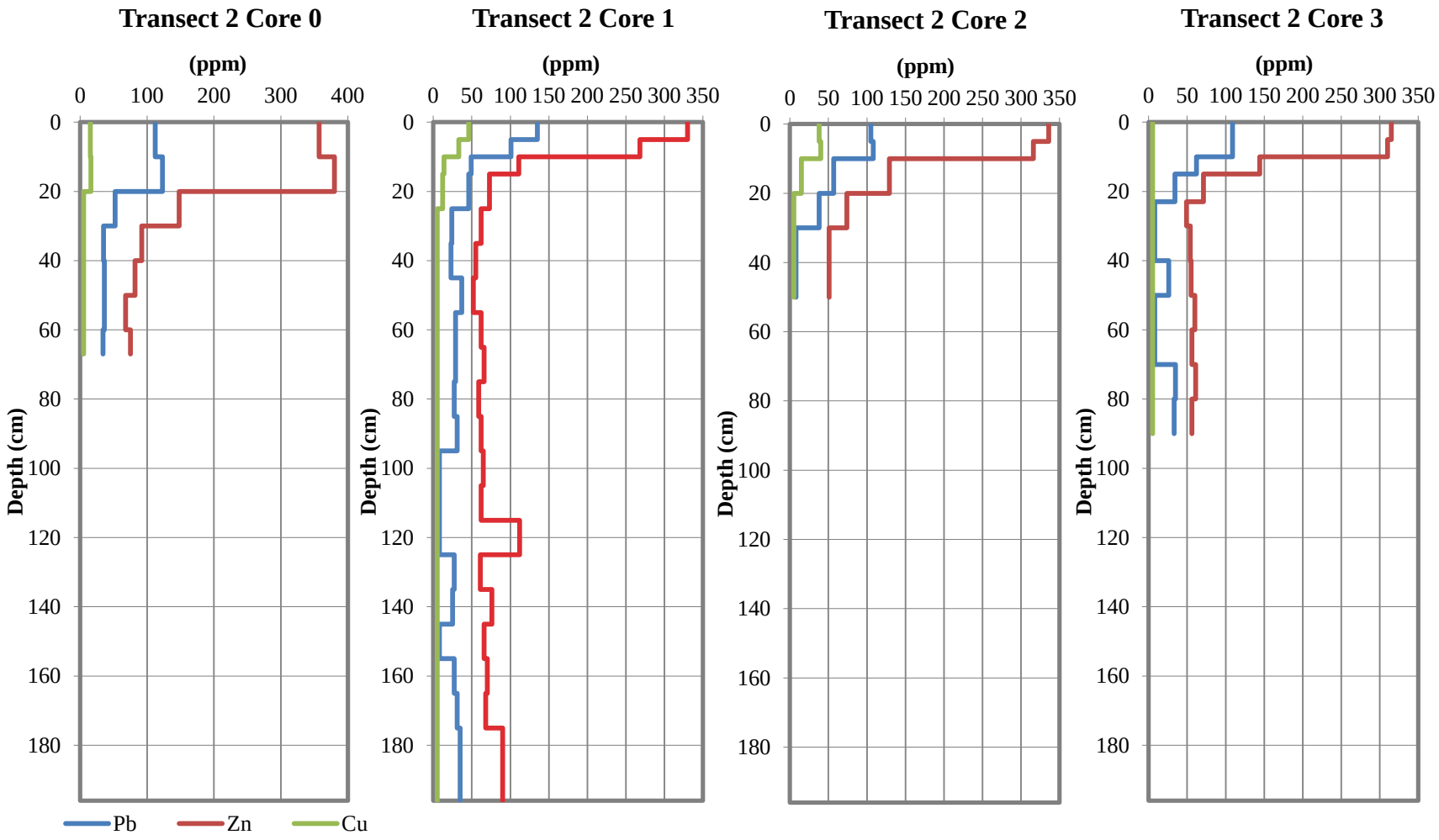

Figure 41. Pb, Zn, and Cu concentrations for cores in Transect 2.

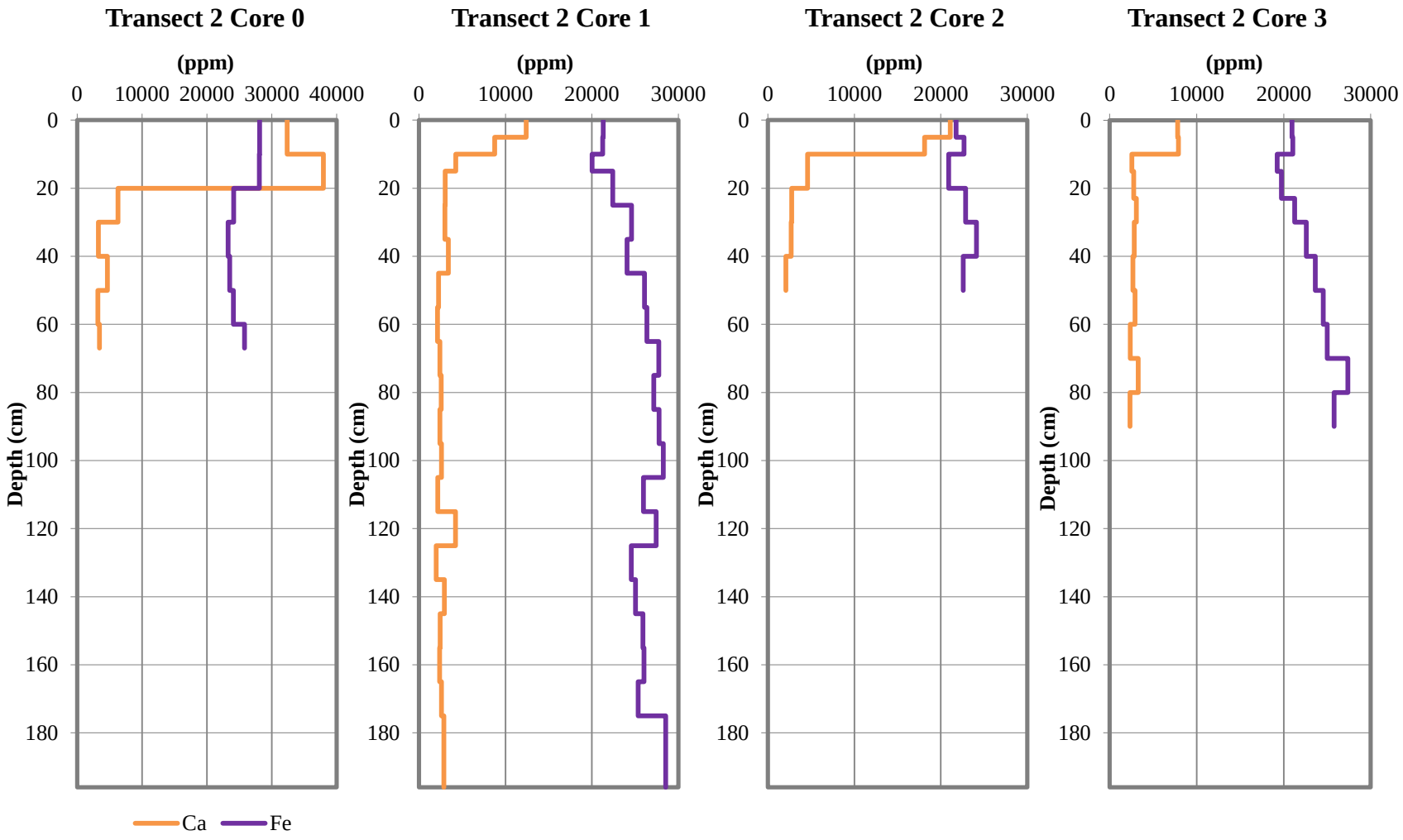

Figure 42. Ca and Fe concentrations for cores in Transect 2.

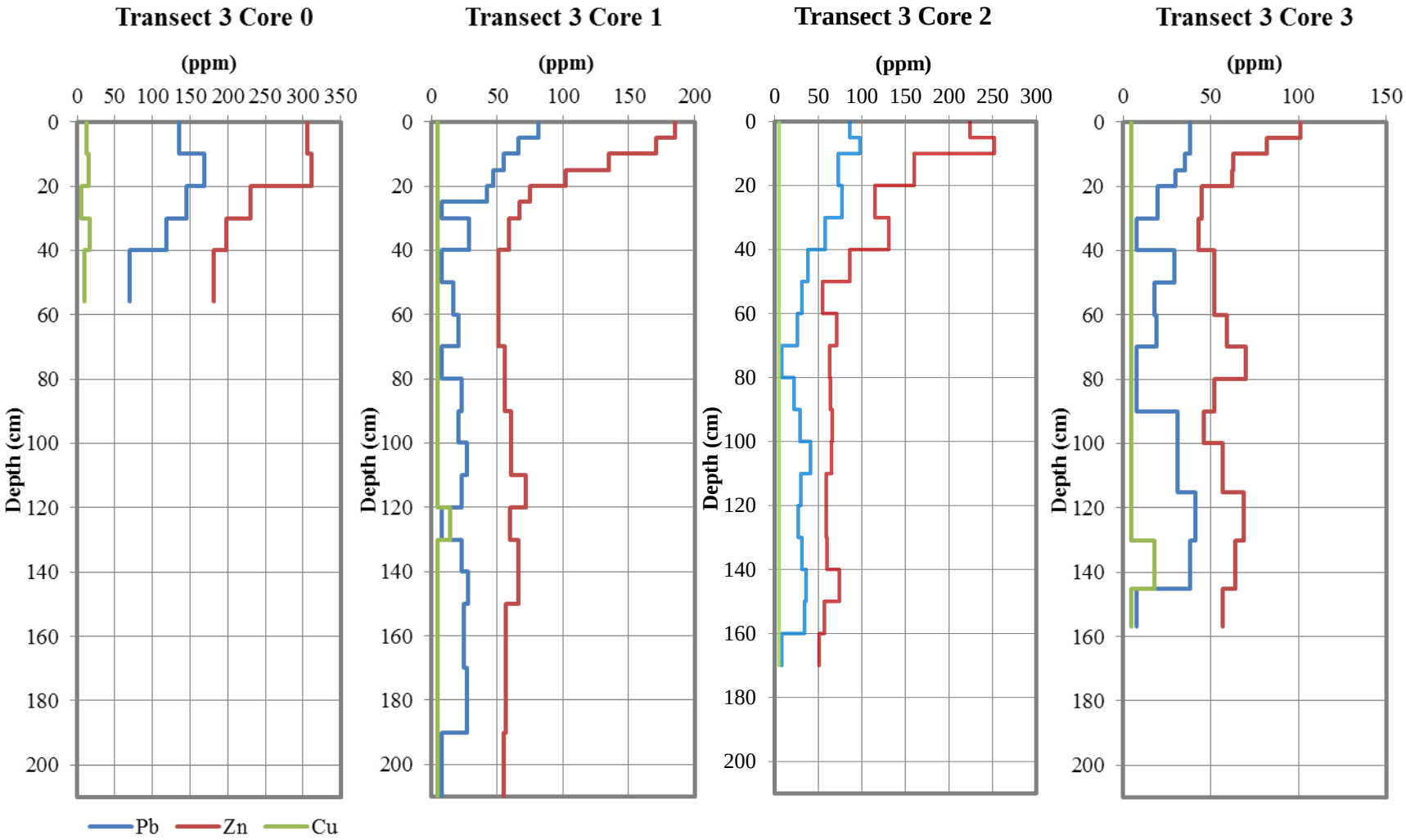

Figure 43. Pb, Zn, and Cu concentrations for cores in Transect 3.

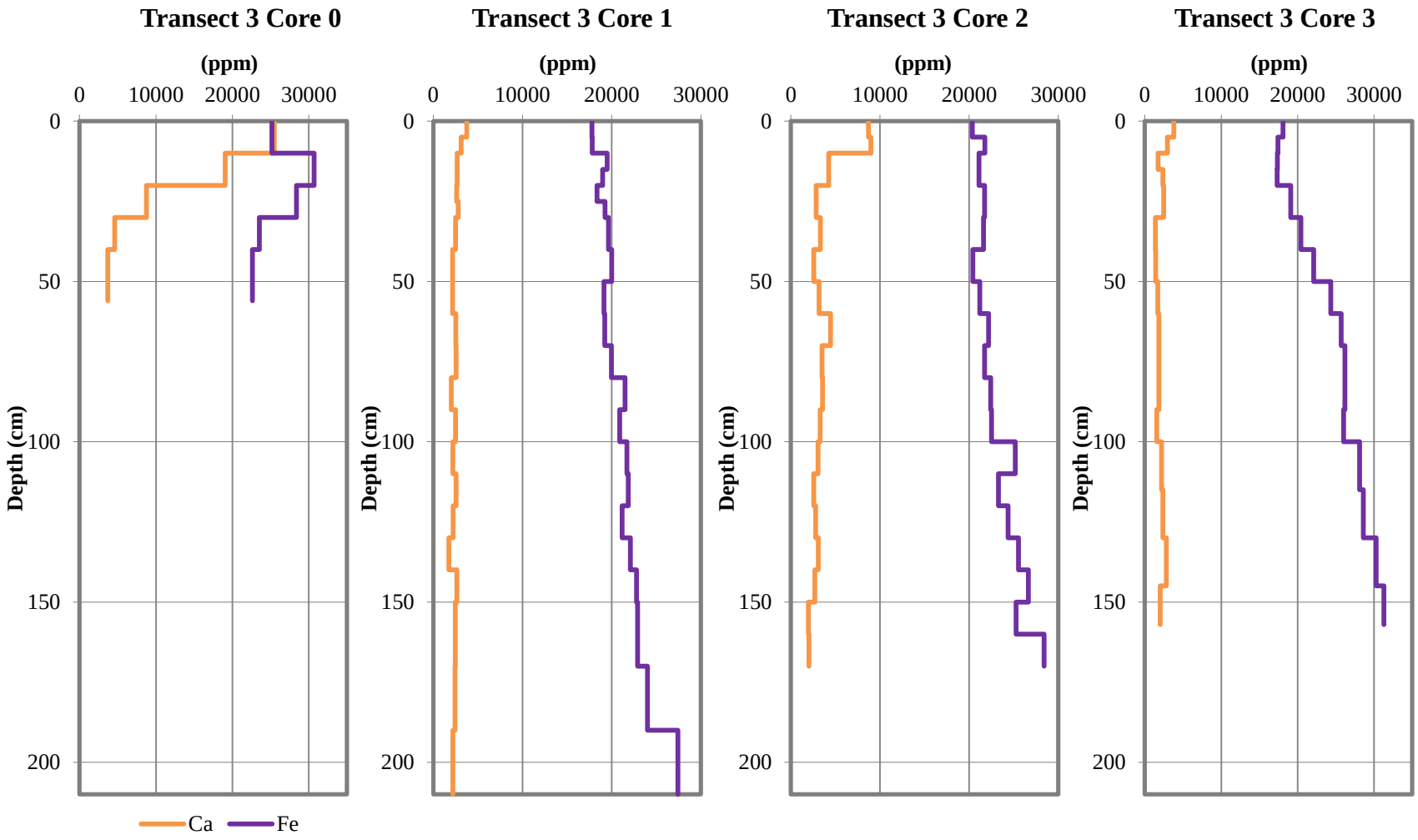

Figure 44. Ca and Fe concentrations for cores in Transect 3.

Table 8. Floodplain core descriptions.

Transect	Core	Latitude DD	Longitude DD	Elevation (m)	Landform*	Depth (cm)	Distance from Channel (m)
1	1B-2	37.1672	-93.3724	351.8	AF	187	25.8
1	2	37.1674	-93.3728	351.8	AF	30	63
1	3	37.1676	-93.3733	352.1	AF	40	116.2
1	4	37.1677	-93.3736	352.6	HF	35	146.4
1	5	37.1678	-93.3739	353.2	CV	45	174.4
2	0	37.166	-93.3743	350.7	C	67	1.5
2	1	37.1661	-93.3744	351.5	AF	196	23.8
2	2	37.1662	-93.3746	351.5	AF	50	41.3
2	3	37.1663	-93.3748	351.2	B	90	62.5
3	0	37.1645	-93.3749	350.4	C	56	7.8
3	1	37.1647	-93.3751	351.4	AF	210	29.4
3	2	37.1648	-93.3755	351.0	AF	170	68.7
3	3	37.165	-93.3757	351.3	B	157	90.5

* AF = Active Floodplain, B = Backswamp, C = Chute, CV = Colluvium, HF = Historical Floodplain

A.

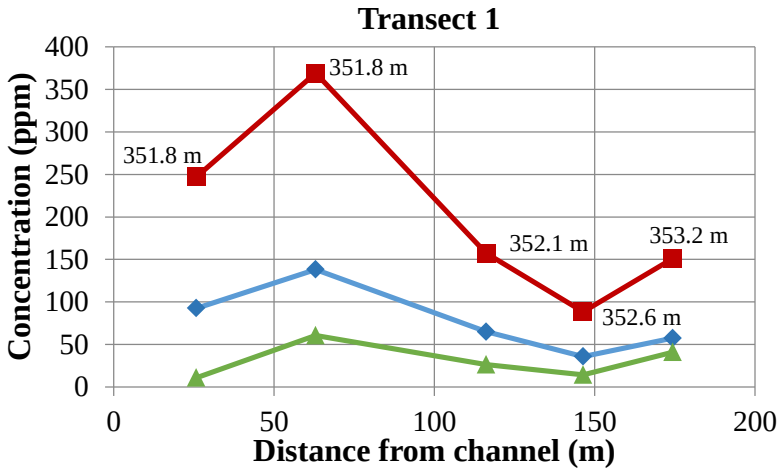

B.

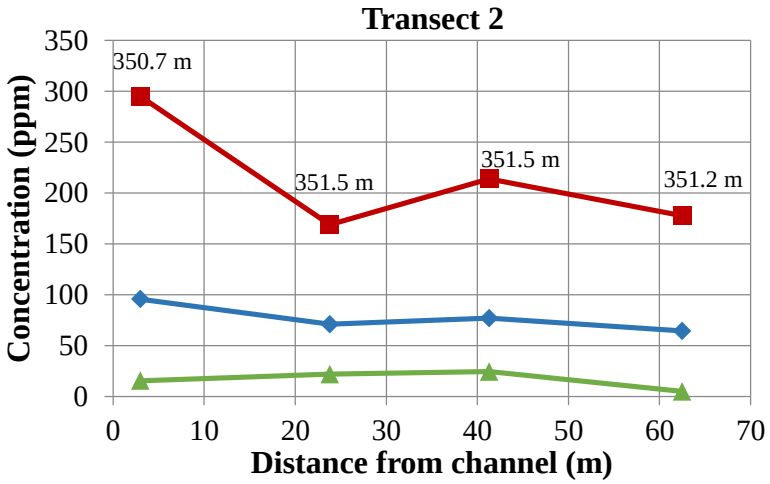

C.

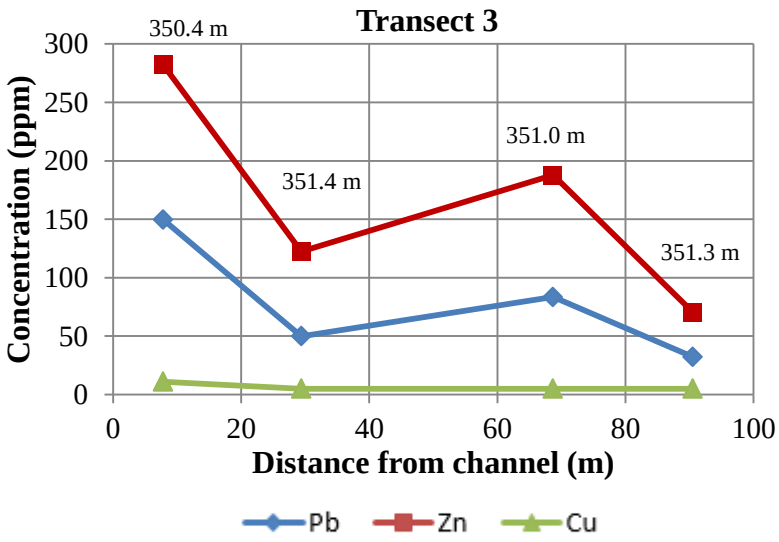

Figure 45. Average concentrations of Cu, Pb, and Zn and proximity to the channel for the top 30 cm of all Transect core samples. Elevation displayed above sample location.

A.

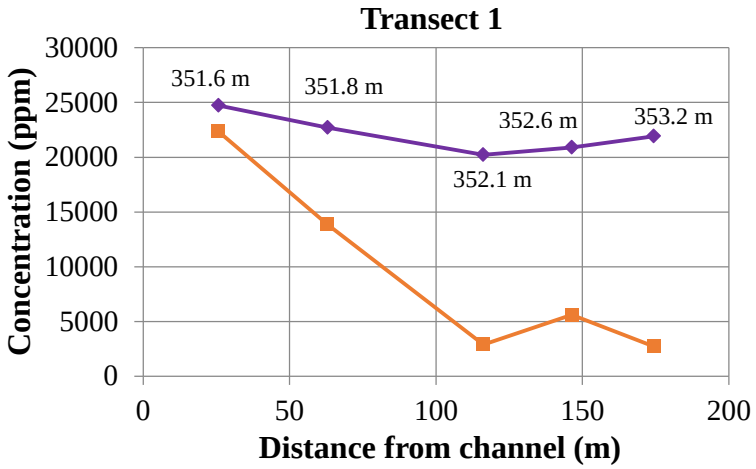

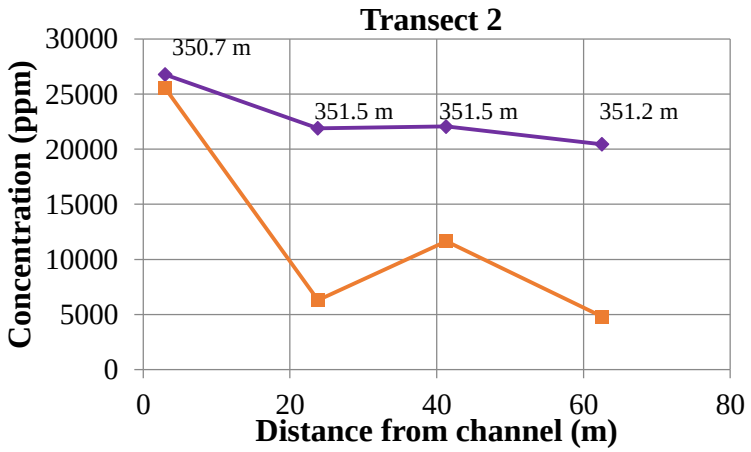

C.

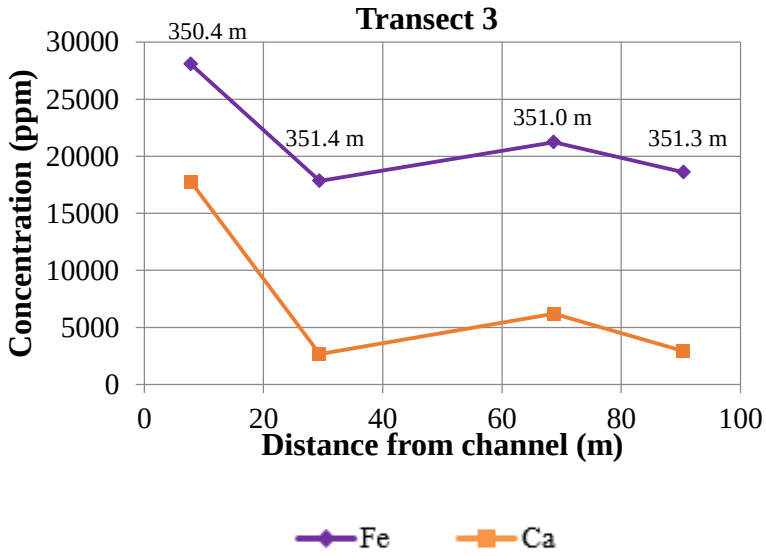

Figure 46. Average concentrations of Ca and Fe and proximity to the channel for the top 30 cm of all Transect core samples. Elevation displayed above sample location.

indicate sediment source and landform association more than contamination source. Results for Ca were consistently highest at the surface for cores 2 through 5, while core 1B-2 contains the more expected trend of the highest Ca at depths just below the surface (Figure 46). As discussed previously, Transect 1 appears to be fairly stable because of its ability to almost accommodate the 1.5-year flood. This suggests that high discharge events are more frequently contained within the channel banks at Transect 1, resulting in less floodplain inundation and sedimentation. Based on topographic analysis and flow accumulation, Transect 1 is often inundated by runoff from uplands. Surface deposition of Ca across Transect 1 is likely a combination of urban runoff from the channel and floodplain inundation. Core profiles for Fe in Transect 1 display the highest values of Fe to be within 5-30 cm, while once again core 1B-2 contains the highest Fe at the bottom 20 cm (Figure 39). At 165 cm in core 1B-2 Ca, Fe, Pb, and Zn all showed a significant increase in concentration.

The greatest depths of concentration occurred in cores closest to the channel. Concentrations of Pb, Zn, and Cu in Transect 2 were consistent through the top 30 cm and decreased with depth and distance from the channel. (Figures 41 and 45). The greatest depth of anthropogenic metals is found in Core 0, located within 2 m of the channel. A similar trend is seen with Ca throughout Transect 2. The proximity to the channel indicates that these cores are exposed to greater inundation and sedimentation. Therefore, concentrations of anthropogenic metals and Ca are found at a greater depths due to proximity to the channel and indundation frequency. Similar to the anthropogenic metals, Ca is highest near the channel and decreases with depth and distance from the channel with the exception of core 1, which is located 23.8 m from the channel (Figures

42 and 46). High Ca along the bank is likely a result of sedimentation from weathered bedrock or loess soil. The low value of Ca at core 1 could be caused by its relatively high elevation. This section is mapped as active floodplain, but the cross-section profile and LiDAR map of this Transect suggests that this core is located at an area in transition to becoming historical floodplain or low terrace (Figures 21, 29, and 30). If this transition is occurring, the elevation of core 1 is not inundated by floodwaters as regularly as lower elevations along the Transect. Concentrations of Fe are highest at the core closest to the channel, but follow a similar trend of increasing concentrations with depth in the remaining cores for Transect 2. Transect 2 displays evidence of topographic control across the floodplain. Lower elevated floodplain landforms contain greater depths and concentrations of metals, while floodplain landforms with higher elevation contain less metal concentrations.

Anthropogenic metals Cu, Pb, and Zn throughout Transect 3 are highest within the top 30 cm of each core with the exception of Pb in core 3, which is located farthest from the channel (Figures 38 and 41). A resurgence of both Pb and Zn in core 3 occurs between 115 and 130 cm, where the highest concentration of Pb for the entire core sample is located. This common trend between Pb and Zn is not unexpected as demonstrated by the previously explained correlation between the two metals, but concentration levels at such deep depths could indicate that this layer was previously at the surface and then covered by significant deposition, or that these metals are naturally occurring at higher than background concentration in this location. More than likely, this was an encounter with natural mineralization as previously described in the discussion of Transect 1 core 1B-2. Examination of Ca and Fe concentrations shows that Fe is

relatively constant throughout the three cores furthest from the channel, while Ca has greater than expected presence at the surface of core 2 when comparing the other cores in the Transect (Figures 39 and 41). Core 0 is once again located closest to the channel and contains the highest surface values for both Ca and Fe in Transect 3, suggesting that recent deposition at this near channel location has been relatively high.

Topographic control was tested by identifying metal concentrations and their relation to sample elevation above thalweg elevation (Lambert and Walling 1987; Walling et al., 1992). The same metal concentrations from Figures 45 and 46 were plotted with their height above the corresponding cross-section thalweg elevation (m) (Figure 47 and 48). Transect 1 concentrations for the anthropogenic metals generally declined with height above the thalweg, with the exception of Core 5. This core's proximity to FR 156 and the upland section of the valley floor is possibly influencing sedimentation more by runoff or hillslope erosion than by flood inundation. This same trend was scene for Fe across Transect 1, with Cu generally declining as elevation above the thalweg increased. All metal concentrations throughout Transect 2 and Transect 3 demonstrated a reduction trend as the elevation above the thalweg increased (Figures 42 and 43). The overall trend is expected, with metal concentrations decreasing with increased elevation from the thalweg and channel.

Core Stratigraphy. Heavy metal concentrations for all 192 overbank core samples are displayed in Appendix C, but a more in depth analysis was performed on the three deepest cores (Figure 49 through Figure 51). All three cores display concentrations of Pb and Zn above background levels from surface depths to 20-30 cm. Background

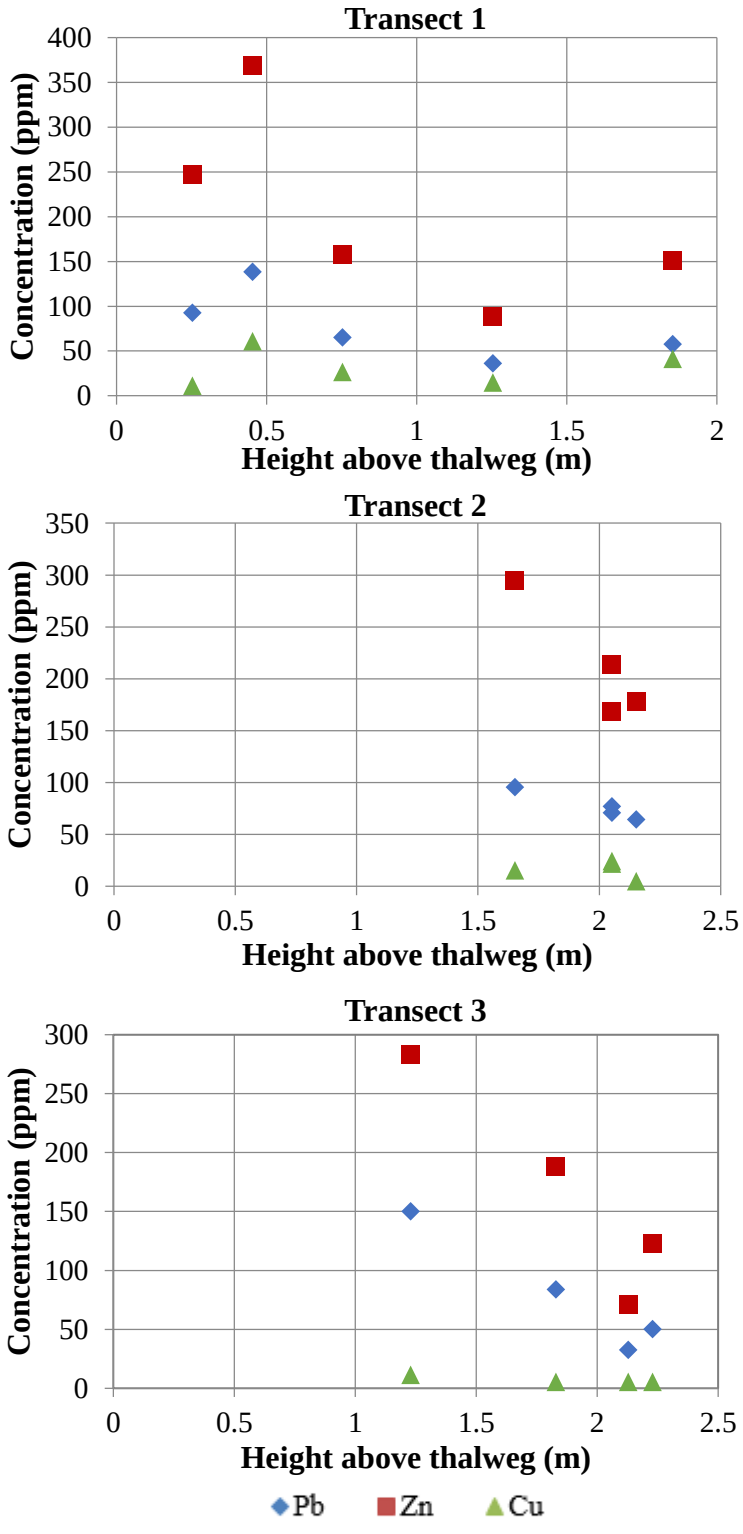

Figure 47. Average concentrations Ca and Fe and proximity to the channel for the top 30 cm of all Transect core samples.

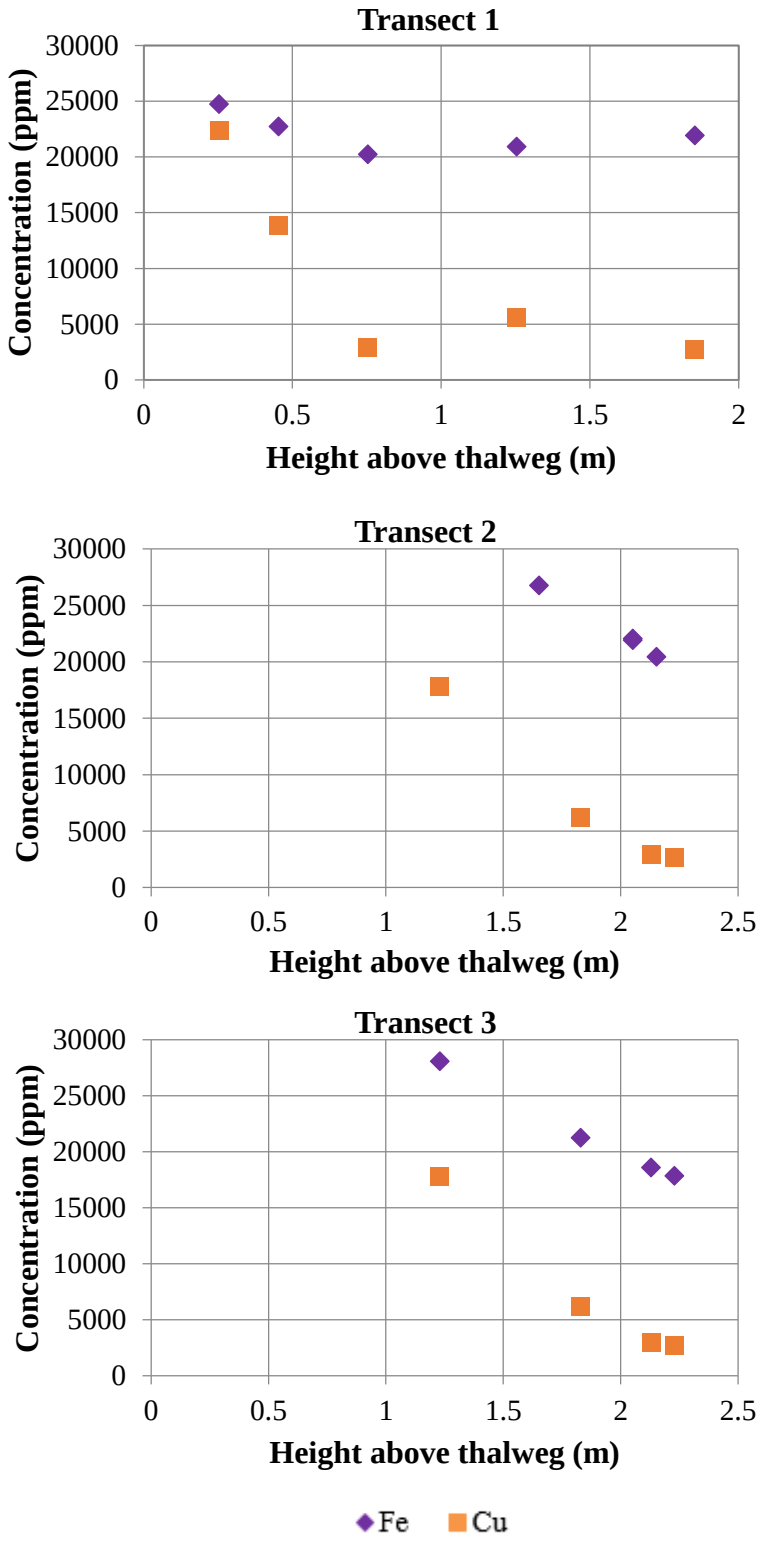

Figure 48. Average Pb, Zn, and Cu concentrations (ppm) for top 30 cm of sediment sample compared to elevation (m) above each corresponding cross-section thalweg elevation (m).

Wilson's Creek Floodplain

Transect 1 Core 1B-2
Core Location: 152 m
Total Depth: 187 cm
Elevation: 351.8 m
Sample Date: 2/12/13

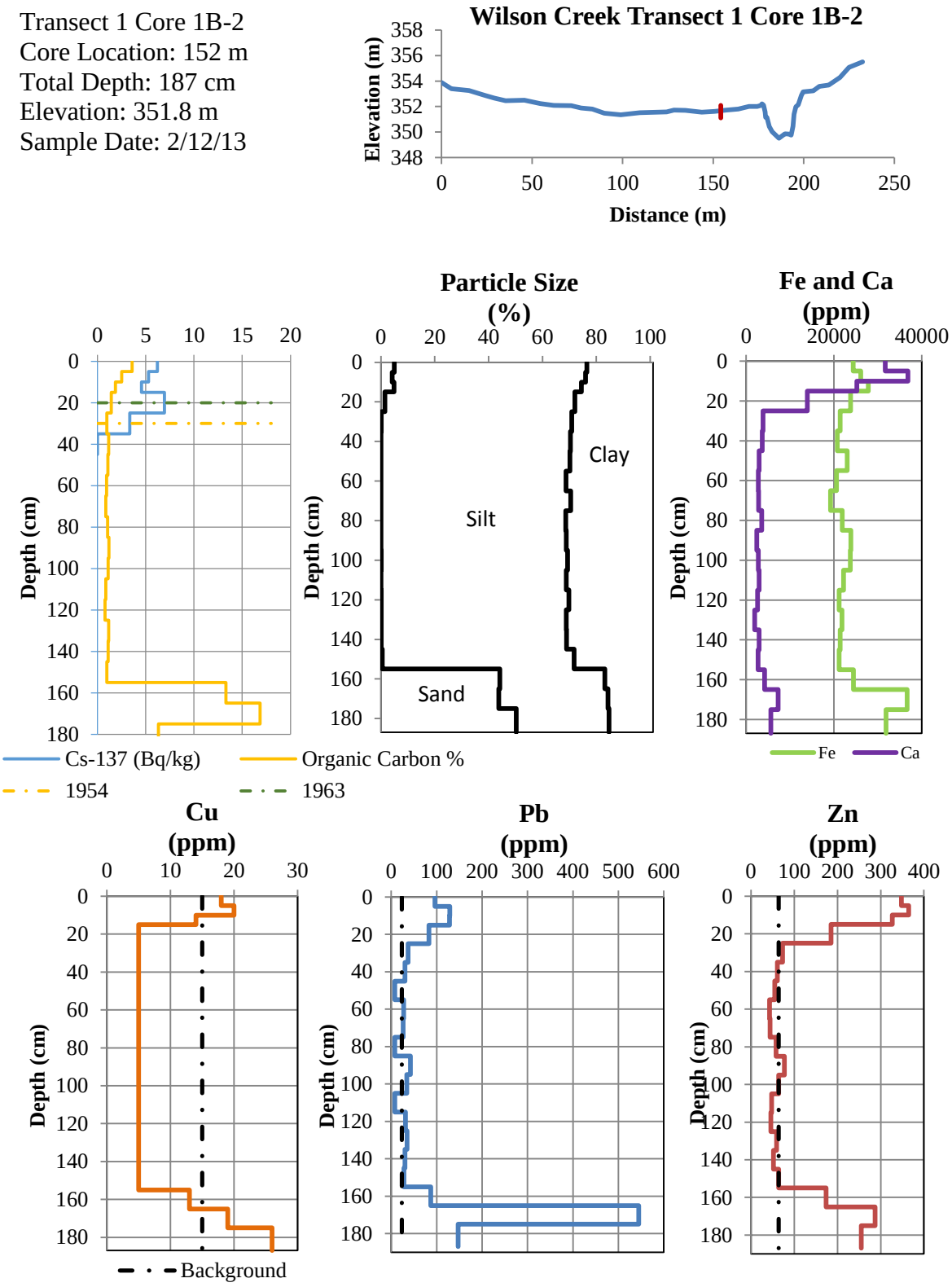

Figure 49. Cs-137, particle size, Fe, Ca, Cu, Pb, and Zn concentrations with select background levels. Source of background levels: Rogers (2005) and Shade (2003).

Wilson's Creek Floodplain

Transect 2 Core 1
Core Location: 52.1 m
Total Depth: 196 cm
Elevation: 351.5 m
Sample Date: 2/12/13

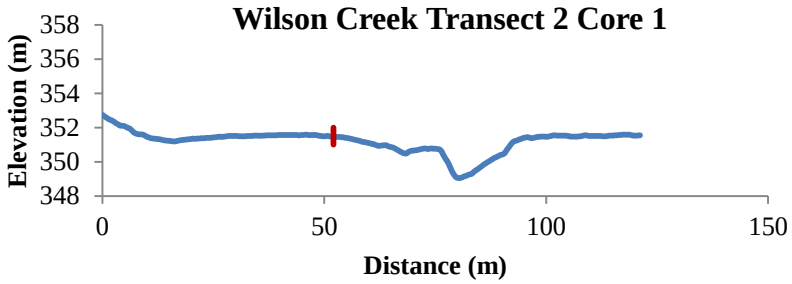

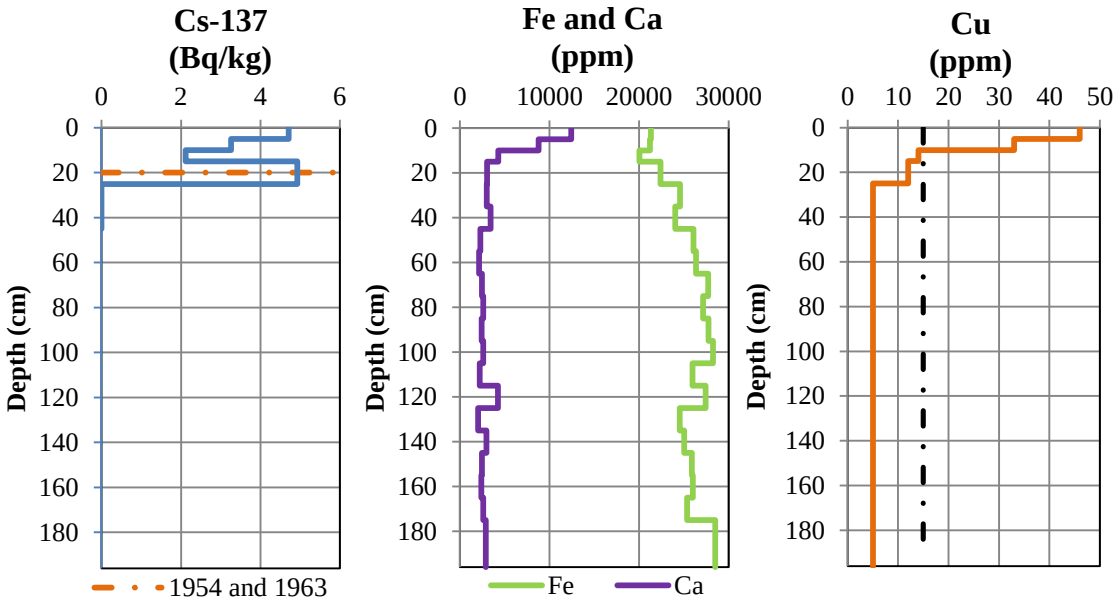

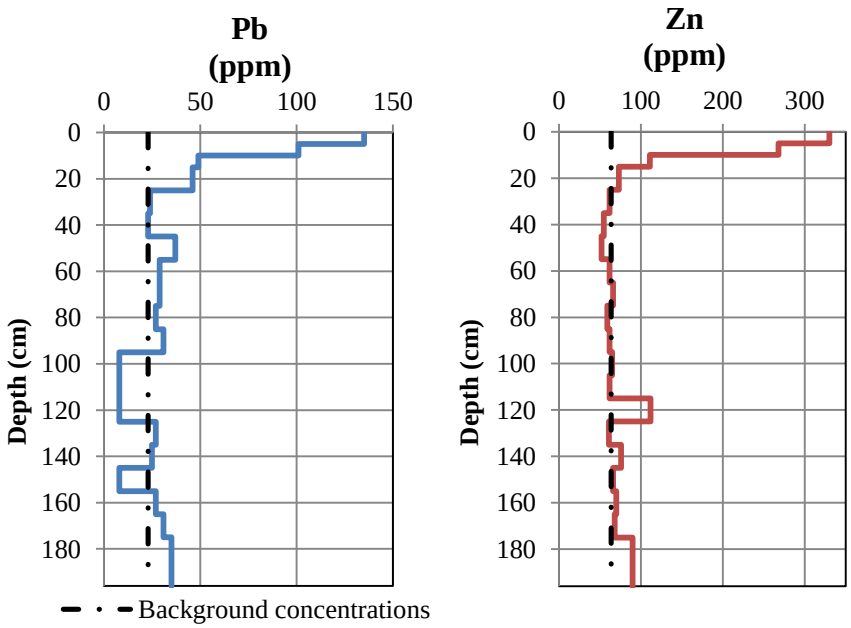

Figure 50. Fe, Ca, Cu, Pb, and Zinc concentrations with select background levels. Source of background levels: Rogers (2005) and Shade (2003).

Wilson's Creek Floodplain

Transect 3 Core 1
Core Location: 57.9 m
Total Depth: 146 cm
Elevation: 351.4 m
Sample Date: 2/12/13

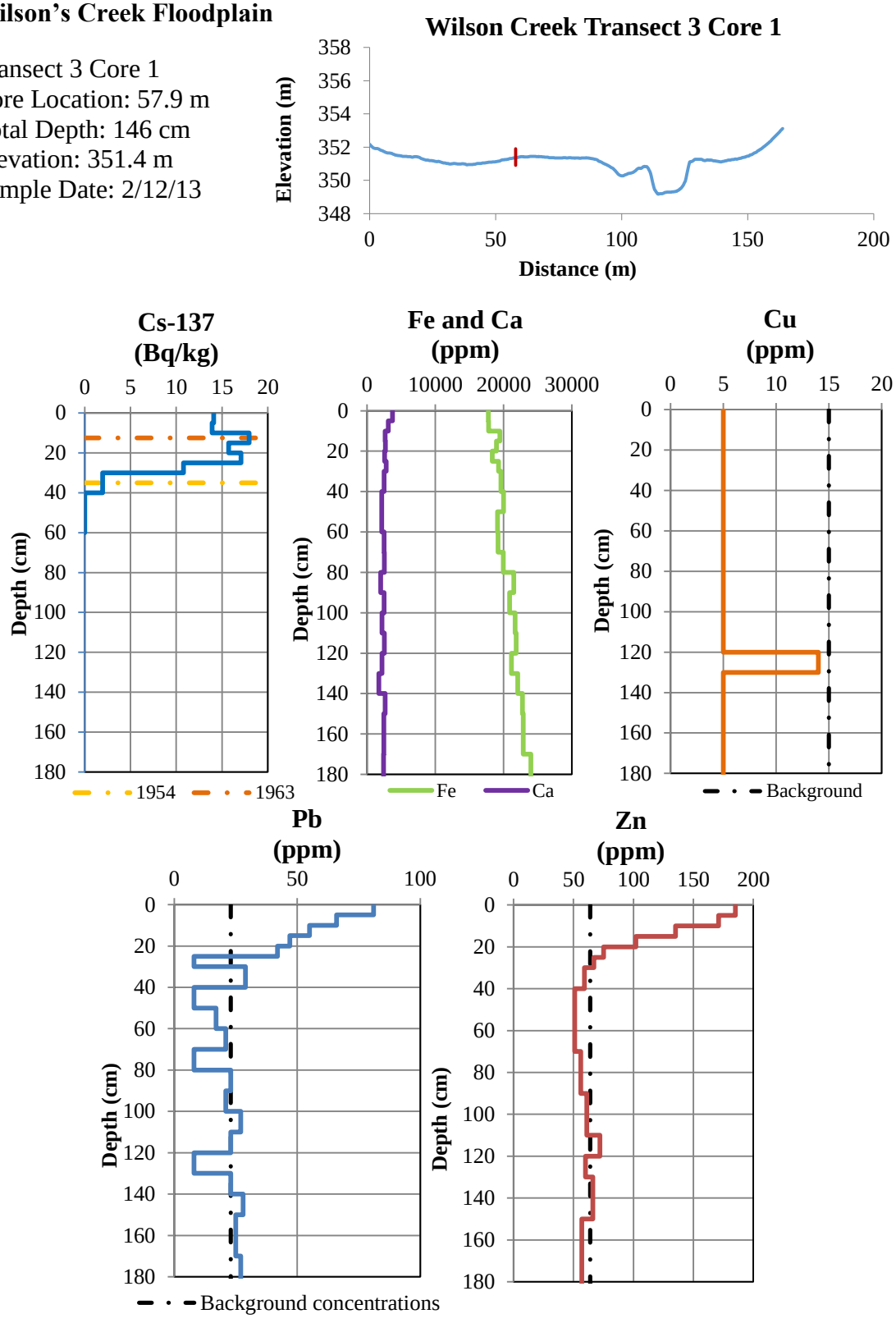

Figure 51. Fe, Ca, Cu, Pb, and Zn concentrations with select background levels. Source of background levels: Rogers (2005) and Shade (2003).

levels of Cu, Pb, and Zn were acquired from previous studies in the watershed (Rodger, 2003; Shade, 2005). The background concentration for Cu is 15 ppm, for Pb is 23 ppm, and for Zn is 64 ppm (Rodger, 2003; Shade, 2005). Core 1B-2 from Transect 1 also has high levels of Pb and Zn from 155-187 cm. Levels of Pb at the bottom 20c m of core 1B-2 are 15-20 times greater than the Pb levels at the last 20 cm of the other two cores. These increased concentrations at depth could indicate contamination from the industrial era of downtown Springfield, MO, or a possible encounter with mineralization.

An in depth analysis on Transect 1 core 1B-2 contains profile information for Cs^{137}, particle size, organic carbon, and select heavy metals (Figure 49). Munsell color for this core was primarily 10YR 3/2 (very dark grayish brown) with the bottom 155-187 cm being 7.5YR 2.5/1(black). Transect 1 core 1B-2 was used as representative data for all other cores in the study because particle size and organic carbon data were analyzed for this core only. The particle size data for core 1B-2 shows that silt is the most prominent sediment size comprising 69-72% of the core from depths of 0-155 cm and 34-41% of the remaining samples at 155-187 cm (Figure 44). Particle size for the top 80 cm of the core is fairly typical for the Dapue silt loam, which is mapped in that area by NRCS (NRCS, 2008). Sand is relatively low at 0-5% of the core from 0-155 cm, but makes up 44-50% of the bottom 155-187 cm. Sand percentages in this soil class usually decline with depth, indicating that core 1B-2 and surrounding areas were possibly exposed to altering fluvial processes, or natural mineralization (Howoritz, 1991). Percentage of clay is lowest at the bottom 27 cm of the core and maintains a fairly constant percentage throughout the rest of the samples in the core.

These particle size results are fairly consistent with the upward fining trend expected as a result of hydraulic sorting in the fluvial environment (Knighton, 1998), but sand increases in the top 25 cm of the core. The higher sand percentage could be a result of splay that is formed when overbank flows break through natural levees, typically resulting in local accumulations of predominantly sandy material (Knighton, 1998). This coarsening trend could also be a result of erosion from the surrounding area's loess-dominated soils and the exposure of sandier parent materials, which has been observed in most recent historical deposits (Magilligan, 1992; Lecce and Pavlowsky, 2001). Further, as flooding increased due to urbanization, higher flow energy would be available to transport more sand onto the floodplain.

Organic carbon percentage ranged from 0.86 to 2.08 % in the first 20 cm of the soil core. This averages at the representative value of 1.5 % for the Dapue silt loam soil class, and values remain relatively stable until 155 cm (Figure 44). Similar results of initially high organic matter were discovered in previous studies within the watershed (Shade, 2003; Rodgers, 2005). The bottom 20 cm of core 1B-2 reaches an organic carbon value of 17 %. This spike in organic carbon is located at the same depth as the high concentrations of anthropogenic metals as discussed earlier for the geochemical properties of this core, strengthening the idea that this location was possibly a site of buried organic-rich channel fill deposits. Horowitz and Elrick (1987) found that concentrations of various trace elements, as well as organic carbon, increase as surface area increases. This helps to relate the high sand content at the same depths where the highest organic carbon was detected (Figure 44).

Table 9. Cesium-137 activity in representative sample cores.

Location			Depth (cm)		Cs-137		Sedimentation Rate
Transect	Core	Landform*	from	to	(Bq/kg)	Soil Surface Year	(cm/yr)
1	1B-2	AF	0	5	6.20		
			5	10	5.30		
			10	15	4.57		
			15	25	6.93	1963	0.40
			25	35	3.34	1954	0.51
			35	45	0.00		
			45	55	0.00		
2	1	AF	0	5	4.71		
			5	10	3.26		
			10	15	2.12		
			15	25	4.94	1954 and 1963	0.34
			25	35	0.00		
			35	45	0.00		
3	1	AF	0	5	14.07		
			5	10	13.90		
			10	15	17.95	1963	0.25
			15	20	15.72		
			20	25	17.07		
			25	30	10.80		
			30	40	1.97	1954	0.59
			40	50	0.00		
			50	60	0.00		

* Active Floodplain

Cesium Profiles. The analysis of Cs^{137} provides a basis for dating the soil profile. Peak levels of Cs^{137} indicate the surface sediment for 1963, with first release at 1954 (Walling and Woodward, 1992; Walling and He, 1993; Owen et al., 1999; Bernard et al., 2001; Sekabira et al., 2001; Matisoff et al., 2002; Ritchie et al., 2004). After identification of peak Cs^{137} in the core, sedimentation rates can be estimated for the years ranging from 1954-present day (2013) and from 1963-present day (2013). Results for Cs^{137} analysis of all three representative cores are displayed in Table 9. Core 1B-2 from Transect 1 contains peak Cs137 at a depth of 20 cm and the initial deposition beginning in 1954 at a depth of 30 cm (Figure 44). This data demonstrates an average sedimentation rate between the years 1954-2013 at 0.51 cm/yr. Sedimentation rates between 1963-2013 ranged from 4.57 to 6.93 Bq/kg, resulting in an average sedimentation rate from 1963-2013 at 0.4 cm/yr.

Transect 2 core 1 was also analyzed for Cs137 (Figure 45). Initial deposition (1954) and peak deposition (1963) are both located at 20 cm. The lack of division between the identifying years indicates that significant land use changes or erosion might have altered the soil surface near the time of deposition for either year 1954 or 1963. By identifying 20 cm as the surface soil in 1963, sedimentation for the past 59 years has been 0.4 cm/yr.

Initial deposition of Cs137 in Transect 3 core 1 was identified at 35 cm and peak deposition at 12.5 cm (Figure 46). Sedimentation rates from 1954-2013 were 0.59 cm/yr while sedimentation rates between 1963-2013 were reduced to 0.25 cm/yr. This decrease in sedimentation rate is possibly due to the Cs^{137} being mixed at deeper depths.

Post-1963 sedimentation rates are similar to those found in the nearby Pearson Creek watershed (Owen et al., 2011). The average sedimentation rate for 1963-2013 at this study area was 0.33 cm/yr, whereas the average sedimentation rate for 1963-2009 in the Pearson Creek watershed was 0.34 cm/yr (Owen et al., 2011). Shade (2003) also analyzed Cs^{137} from samples within the Wilson Creek watershed, but those samples were collected at downstream locations. Shade (2003) determined the average sedimentation rate from 1954-2002 was 0.8 cm/yr, and between 1963-2002 was 0.4 cm/yr. In comparing Owen et al. (2011) and Shade's (2003) findings to this study, results are similar. Although Shade (2003) found higher 1954-2002 sedimentation rates at the downstream locations, these higher rates were possibly a trend throughout the watershed. In the 24 years of record at the FR 156 USGS gage, no recorded floods have exceeded the 25 year reoccurrence interval, indicating that floodplain deposition might have been more controlled by smaller annual floods rather than the notable, larger flood events (Shade, 2003).

The overall stratigraphy of the study area floodplain can be summarized by a combination of variables; valley landform type, sediment texture, organic matter, Cs^{137} levels, and metal concentrations. The age of a floodplain landform can be identified in a fairly accurate manor based on its elevation and proximity to the channel. Higher landform elevation and greater distance from the channel typically indicate an older landform. At this study area along Wilson Creek, the channel is attempting to widen and create new landforms within the active floodplain. With these changes, noticeable textural difference will occur. Once again, elevation and proximity to channel influence sediment texture throughout floodplain landforms. Lower elevations will collect larger

grain sizes, while smaller grain sizes are spread across the floodplain with dissipating floodwaters. Grain sizes were generally larger towards the bottom of core samples, becoming smaller as elevation increased. Grain size was found to correlate with organic matter in this study.

Increased levels of organic matter were recorded within the first 20 cm as identified by previous studies at Wilson Creek (Shade, 2003; Rodgers, 2005). Larger grain sizes were found to correlate with greater organic matter. As found by Horowitz and Elrick (1987), concentrations of various trace elements, as well as organic carbon, increase as surface area increases. Based on nearby watershed history, there is reason to believe that the high organic matter discovered at depths within Transect 1 are a result of an encounter with natural mineralization.

Concentrations of Cs^{137} and heavy metals throughout a floodplain can also help identify sedimentation trends and floodplain landform age. Based on Cs^{137} analysis, the average sedimentation rate for the study area is 0.4 cm/yr. Floodplain sediment dating is further supported by the concentrations and types of metals found in samples. Certain heavy metal deposits reflect land use changes within the watershed. At this study area, Transects 1 and 2 displayed an increase in metal concentrations after 1963, while Transect 3 displayed an increase after 1953. In 1945 a residential construction boom hit the city of Springfield. Land was excavated and impervious surfaces were added. Based on aerial photograph analysis, trees around the study area were removed between 1953 and 1970. All of these factors resulted in greater population, less infiltration, and the introduction and remobilization of heavy metals into Wilson Creek.

CHAPTER SIX: CONCLUSION

This study describes the geomorphology, sedimentology, and pollution storage potential for a floodplain area along Wilson Creek. The floodplain has been affected by urbanization and other land use changes. Pollutants resulting from industrial uses and urbanization are found within the top 30 cm of the floodplain deposited since 1954, making potential remobilization and bioavailability a concern. Although bedrock control seems to be stabilizing the cross-section and area surrounding Transect 1, cross-sections further downstream in the study reach may be expected to widen in order to accommodate the 1.5-year flood. Results from floodplain and channel morphology indicate that this widening is already occurring and may continue in the future. Bank erosion and channel widening creates greater potential for remobilization of contaminants stored in the floodplain. Although these concentrations are much higher than those found in deeper deposits, concentrations will likely be diluted by uncontaminated floodplain material and therefore may not pose a threat to the stream ecology. Implemented protective action regarding the 319 project should help reduce erosion of sediment and contaminants into the Wilson Creek, but future development in the watershed may have additional hydrological and geomorphic impacts that need to be monitored and possibly controlled by environmental management.

Geomorphological Implications

Urban streams adjust to increased water and sediment supply. The floodplain at Wilson Creek has also been subject to alterations due to urban land use changes. Key findings of this study regarding the geomorphology of the study area are:

(1) The channel appears to be slightly undersized, and has the capacity to contain the 1-1.25 yr flood. Bankfull capacity should be able to withhold the 1.5 yr flood, suggesting that the observed widening is occurring as an attempt to accommodate the 1.5 yr flood capacity;

(2) Aerial photographs indicate channel widening and floodplain erosion have occurred since the earliest aerial in 1953. Widening trends are influenced by bedrock control at various locations throughout the study reach, but are expected to continue into the future;

(3) Cross-section profiles display a possible shift from an active floodplain to a historical floodplain, or low terrace, due to incision at Transect 3. A bedrock knickpoint located near Transect 1 is causing the channel incision, riverbank retreat, and terrace formation at Transect 3;

(4) The valley floor becomes narrower downstream. Constriction at this location has caused channel slope to increase, greater erosion and incision, and greater scour along Transects 2 and 3. A multi-threaded chute system has developed across the floodplain surface, most likely because of increased flood energy over the floodplain.

(5) Surface soil (to 30 cm) trends exhibit a strong correlation between Pb and Zn across the floodplain, indicating a similar parent source material. No correlations exist among the other analyzed surface metals.

(6) Lateral trends throughout core samples demonstrate a decline in surface contamination (top 30 cm) as distance from the channel increases. Core 5 from Transect 1 was an exception, and likely a result of greater exposure to urban runoff and hillslope erosion.

(7) Topographic control influenced sedimentation patterns. Metal concentrations typically decreased on higher elevation landforms;

(8) The floodplain remains depositional in nature. Using Cs^{137} dating, overbank sedimentation rates averaged approximately 0.48 cm/yr from 1954 to2013 and 0.33 cm/yr from 1963 to 2013.

This study reach of Wilson Creek is similar to most Ozark streams for being relatively straight and primarily controlled by overbank deposition and not channel migration. Bedrock control is evident in the most upstream section of the reach, but due

to increasing impervious surfaces and excess surface water, the remaining channel within the reach could be subject to widening.

Pollution Control Implications

The ability of floodplains to act as a sink or storage unit for pollutants transported from upstream has been well documented. This study confirms that the urban floodplain along Wilson Creek is also acting as a sink for pollutants coming from upstream point and non-point sources of pollution. Key findings of this study regarding pollution control implications are:

(1) The urban floodplain stores pollutants from both floodwater inundation and local runoff from nearby neighborhoods and roads. Surface samples suggest that anthropogenic metals are more closely linked to floodwater inundation than local runoff or aerial deposition along the Wilson Creek study reach.

(2) Surface levels of anthropogenic metals do not appear to be of major environmental concern, with the exception of core 2 from Transect 1. This core has Pb levels above 400 ppm, which the EPA considers toxic for residential sediment, at depths from 5-10 cm. Although dilution would most likely reduce concentrations of concern, erosion in this area could remobilize potentially hazardous levels of Pb;

(3) Floodplain cores exhibit fairly typical heavy metal trends as values tend to decrease with increased depth and distance from the channel, but core 1B-2 from Transect 1 possessed exceptionally higher than expected values for Fe, Pb, and Zn at depths from 165-187 cm. The correlation of these high values with particle size and organic carbon has been documented to occur in areas of natural mineralization.

(4) Although the floodplain is acting as a sink for metal pollution, remobilization of pollutants and excess sediment into the channel is possible. Widening trends at the study area will continue to erode channel banks and parts of the floodplain, releasing sediment and any stored pollutants. However, widening will be limited by hydraulic geometry to contain the dominant discharge, possibly the 1.5 yr flood.

This research provides support for future studies related to metal analysis of floodplain surface samples, particularly with the use of LiDAR data. Once converted to a TIN, this high-precision data allowed for simple and accurate identification of

topographic changes across a valley floor. Incorporating this data with metal distribution proved that distribution patterns of anthropogenic metals Cu, Pb, and Zn and the naturally occurring metals Ca and Fe are influenced by elevation change and proximity to the channel. Future studies can use the methods utilized in this research. By combining aerial photographs, cross-sectional data, flood reoccurrence intervals, and a map of valley landforms, patterns in the distribution of heavy metals are more easily identifiable and explainable.

REFERENCES

Allgood, F. P. and Persinger, I. D. (1979). Missouri general soil map and soil association descriptions. USDA-SCS, Columbia, Missouri, 75.

Anderson, W. I. (1998). *Iowas Geological Past: Three Billion Years of Change*. Iowa City: University of Iowa Press.

Arnold, C. L. Boison P. J., and Patton, P. C. (1982). Sawmill Brook: an example of rapid geomorphic change related to urbanization. *J. Geol.*, 90, 155-166.

Arnold, C. L. and Gibbons, C. J. (1996). Impervious surface coverage: the emergence of a key environmental indicator. *American Planners Association J.* 62, 243-258.

Bagnold, R.A. (1966). An approach to the sediment transport problem from general physics: U.S. Geological Survey Professional Paper 422-I, p. I1–I37.

Bernard, C. and Laverdière, M. R. (2001). Assessment of soil erosion and sediment sources in an Ohio watershed using Beryllium-7, Cesium—137, and Lead-210. *Journal of Environmental Quality*, 31(1), 54-61.

Berner, E.K., and R.A. Berner. (1996). Global environment: Water, air, and geochemical cycles. Prentice Hall, Upper Saddle River, NJ.

Biological Assessment and Fine Sediment Study: Big River (lower): Irondale to Washington State Park, St. Francois, Washington, and Jefferson Counties, Missouri (2003). Missouri Department of Natural Resources (MDNR). Prepared by the Water Quality Monitoring Section, Environmental Services Program, Air and Land Protection Division of the Missouri Department of Natural Resources.

Bilos, C., Colombo, J. C., Skorupka, C. N., Rodriguez Presa, M. J. (2001). Sources, distribution and variability of airborne trace metals in La Plata City area, Argentina. *Environmental Pollution*, 111(1), 149-158).

Bloom, A. L., (1998). *Geomorphology: A Systemic Analysis of Late Cenozoic Landforms* (3rd ed.). Long Grove, IL: Waveland Press, Inc.

Booth, D. B. and Jackson, C. R. (1997). Urbanization of aquatic systems: degradation thresholds, stormwater detection, and the limits of mitigation. *J. Am. Water Resour. Assoc.*, 33, 1077-1090.

Boyle, S. and March, J., and History Museum for Springfield-Greene County (Springfield, MO.). (1997). *Crossroads at the spring:A pictorial history of Springfield, Missouri.* Virginia Beach, VA: Donning.

Brewer, P.A., Taylor, M.P. (1997). The spatial distribution of heavy metal contaminated sediment across terraced floodplains. Catena 30, 229-249.

Bridge, J. A. (2003). Rivers and floodplain forms, processes, and sedimentary record: Malden, Blackwell Scientific Publications.

Bridge, J. S. and Leeder, M. R. (1979). A simulation model of alluvial stratigraphy. *Sedimentology* 26, 617-644.

Carlson, J. (1999). Zinc Mining Contamination and Sedimentation Rates of Historical Overbank Deposits, Honey Creek Watershed, Southwest Missouri. Master of Science Thesis, Southwest Missouri State University, Springfield, MO, 163 pp.

Chin, A. (2006). Urban transformation of river landscapes in a global context. *Geomorphology*, 79, 460-487.

Chow, V.T. (1959). Open-channel Hydraulics. McGraw-Hill Book Company, New York.

Cotton, C. A. (1940). Classification and correlation of river terraces. *J. Geomorphology*, 3(1), 26-37.

Dark, H. E. (1981). *Springfield of the Ozarks: An Illustrated History.* Windsor Publications, 1.

Dark, H. E. (1984). *Springfield, Missouri. Forty Years of Growth and Progress, 1945-1985.* Dolandark Graphics.

Delina, A., Babre, A., Popovs, K., Sennikovs, J., & Grinberga, B. (2012). Effects of karst processes on surface water and groundwater hydrology at Skaistkalne Vicinity, Latvia. *Hydrology Research*, *43*(4), 445-459.

Dunne, T. and Leopold, L. B. (1978). *Water in Environmental Planning.* New York: Freeman. 818 pp.

Ellis, E., Church, M., and Rosenau, M. (2004). Characterization of Four Secondary Channels of the Lower Fraser River. Habitat Conservation Trust Fund. Final Report. Retrieved 9 September 2013 from <http://www.geog.ubc.ca/fraserriver/reports/hctffinalreport_schan.pdf>.

Eshel, G., Levy, G.J., Mingelgrin, U., and Singer, M.J. (2004). Critical evaluation of the use of laser diffraction for particle-size distribution analysis. *Soil Science Society of America Journal*, 68, 736-743.

Espey, W. H. Jr., Morgan, C. W., and Mash, F. D. (1965). *A study of some effects of urbanization on storm runoff from a small watershed. Tech. Rep.*44D 07-6501 CRWR-2, Center for Research in Water Resources, University of Texas, Austin.

Fairbanks, J. and Tuck, C.E. (1915). Past and Present of Greene County: Early and Recent History and Genealogical Recores of Many of the Representative Citizens. Bowen, Indianapolis, IN, 1, 1933.

Fitzpatrick, F.A., I.R. Waite, P.J. D'Arconte, M.R. Meador, M.A. Maupin, and M.E. Gurtz, 1998. Revised Methods for Characterizing Stream Habitat in the National Water-Quality Assessment Program. Water-Resources Investigations Report 98-4052, United States Geological Survey.

Flynn, K.M., W.H. Kirby, and Hummel, P.R. (2006). User's Manuel for Program PeakFQ, Annual Flood-Frequency Analysis Using Bulletin 17B Guidelines. Reston, VA: United States Geological Survey Techniques and Methods 4-B4.

Forstall, R. L. (1995). Missouri Population of Counties by Decennial Cennial Census: 199 to 1990. U.S. Bureau of the Census, Washington DC. <http://www.census.gov/population/cencounts/mo190090.txt>.

Förstner, U. (1990). Inorganic Sediment Chemistry and Elemental Speciation. In: R. Baudo, J. P. Giesy, and Muntau, H. (Editors). *Sediments: Chemistry and Toxicity of In-Place Pollutants*, 61-105.

Förstner, U. and Whitman, G. T. W. (1981). Metal Pollution in the Environment, 2nd Revised Edition, Springer – Verlag, Berlin, Germany.

Frissell, C. A., Liss, W. J., Warren, C. E., and Hurley, M. C. (1986). A hierarchical framework for stream habitat classification: viewing streams in a watershed context. *Environmental Management*, 10, 199-214.

Gale, Nord L., Craig D. Adams, Bobby G. Wixson, Keith A. Loftin, and Huang Yue-Wern. (2002). Lead concentrations in fish and river sediments in the Old Lead Belt of Missouri. *Environmental Science & Technology* 36, no. 20: 4262-4268.

Galloway, W. E. and Hobday, D. K. (1996). Terrigenous Clastic Depositional Systems: Fluvial Systems, Springer – Verlag Berlin Heidelberg, 60-90.

Galster, J. C, Pazzaglis, F. J., Hargreaves, B. R., Morris, D. P. Peters, S. C., and Weisman, R. N. (2006). Effects of urbanization on watershed hydrology: The scaling of discharge with drainage area. *Geology*, 34(9), 713-716.

Goddard, M. A., Mikhailova, E. A., Post, C. J., Schlautman, M. A., & Galbraith, J. M. (2009). Continental United States atmospheric wet calcium deposition and soil inorganic carbon stocks. *Soil Science Society of America Journal*, *73*(3), 989-994.

Graf, W.L. (1975). The impact of suburbanization on fluvial geomorphology. *Water Resources Research*, 11, 690–692.

Gregory, S. V., Lamberti, G. A., and Moor, K. M. S. (1989). Influence of Valley Floor Landforms on Stream Ecosystems. USDA Forest Service Gen. Tech. Rep. PSW-110.

Gregory, S. V., Swanson, F. J., McKee, W. A., and Cummins, K. W. (1991). An Ecosystem Perspective of Riparian Zones. *Bioscience,* 41(8), 540-551.

Harbor, J., (1999). Engineering geomorphology at the cutting edge of land disturbance: erosion and sediment control. *Geomorphology*, 31, 247–263.

He, Q., & Walling, D. E. (1997). Spatial variability of the particle size composition of overbank floodplain deposits. *Water, Air, and Soil Pollution*, *99*(1-4), 71-80.

Hirsch, R. M, Walker, J. F., Day, J. C., and Kallio, R. (1990). The influence of man on hydrologic systems. *Surface Water Hydrology (The Geology of America, Vol0-1),* ed. Wolman, M. G. and Riggs, H. C., 329-359. Boulder, CO: Geol. Soc. Am.

Holcombe, R. I., ed. (1883). History of Greene County, Missouri.

Horowitz, A. J. (1991). A primer on sediment-trace element chemistry (2nd edition). Lewis Publishers, Chelsea, MI, 136 pp.

Horowitz, A. J., & Elrick, K. A. (1987). The relation of stream sediment surface area, grain size and composition to trace element chemistry. *Applied Geochemistry*, 2(4), 437-451.

Howard, A. D., Fairbridge, R. W., and Quinn, J. H. (1968). Terraces, fluvial introduction. In *The Encyclopedia of Geomorphology*, (R. Fairgridge, ed.), 1117-1123. Reinhold, New York.

Hughes, H. E. (1982). Soil Survey of Greene and Lawrence Counties, Missouri. U.S. Department of Agriculture, Soil Conservation Service.

Hughes, M. L., McDowell, P. F., and Marcus, W. A. (2006). Accuracy assessment of georectified aerial photographs: Implications for measuring lateral channel movement in a GIS. *Geomorphology*, 74: 1-16.

Huntington, T.G. (2006). Evidence of Intensification of the Global Water Cycle: Review and Synthesis. Journal of Hydrology 319:83-95.

Jain, V., Fryier, K., and Brierly, G. (2008). Where do floodplains begin? The role of total stream power and longitudinal profile form on floodplain initiation processes. *Geological Society of America Bulletin*, 120(1/2), 127-141.

Kiner, L. K. and Vitello, C. (1997). James River Basin Inventory and Management Plan, Missouri Department of Conservation, Springfield.

Knighton, D. (1998). Fluvial forms and processes, a new perspective. Arnold, Hodder Headline Group, London, UK.

Knox, J. C. (1977). HUMAN IMPACTS ON WISCONSIN STREAM CHANNELS. *Annals of the Association of American Geographers*, 67(3), 323-342.

Knox, J. C. (2006). Floodplain sedimentation in the Upper Mississippi Valley: Natural versus human accelerated. *Geomorphology*, 79(3/4), 286-310.

Laforce, S., Simard, M., Leconte, R., & Brissette, F. (2011). Climate Change and Floodplain Delineation in Two Southern Quebec River Basins. *Journal of the American Water Resources Association*, *47*(4), 785-799. doi:10.1111/j.1752-1688.2011.00560.x

Lambert, C. P. and Walling, D. E. (1987). Floodplain sedimentation: a preliminary investigation of contemporary deposition within the lower reaches of the River Culm, Devon, UK. *Geografiska Annaler. Series A. Physical Geography*, 393-404.

Lecce, S. A. and Pavlowsky, R. T. (1997). Storage of mining-related zinc in floodplain sediments, Blue River, Wisconsin. *Physical Geography*, 18, 424-439.

Lecce, S. A. and Pavlowsky, R. T. (2001). Use of mining-contaminated sediment tracers to investigate the timing and rates of historical floodplain sedimentation. *Geomorphology* 38, 85-108.

Lecce, S. A. and Pavlowsky, R. T. (2004). Spatial and temporal variations in the grain-size characteristics of historical flood plain deposits, Blue River, Wisconsin, USA. *Geomorphology* 61, 361-371.

Lenat. D. R. and Crawford, J. K. (1994). Effects of land use on water quality and aquatic biota of three North Carolina Piedmont streams. *Hydrobiologia,* 294, 185-99.

Leopold, L.B. (1968). Hydrology for urban land planning — a guidebook on the hydrologic effects of urban land use. *USGS Circular* 554.

Lewin, J., Davies, B.E., Wolfenden, P.J., (1977). Interactions between channel change and historic mining sediments. In: Gregory, K.J. (Ed.), River Channel Changes. Wiley, Chichester, UK, 353-367.

Lóczy, D. (2011). Floodplains - Links between Countries and Landscapes. *Forum Geografic*, *10*(2), 5-9. doi:10.5775/fg.2067-4635.2011.001.

Magilligan, F. J. (1985). Historical Floodplain Sedimentation in the Galena River Basin, Wisconsin and Illinois. *Annals of the Association of American Geographers*, 75(4), 583-594.

Magilligan, F. J. (1992). Sedimentology of a fine-grained aggrading floodplain. *Geomorphology*, 4, 393-408.

Martin, C. W. (2000). Heavy metal trends in floodplain sediments and valley fill, River Lahn, Germany. *Catena*, *39*(1), 53-68.

Martin, C. W. (2004). Heavy metal storage in the near channel sediments of the Lahn River, Germany. *Geomorphology*, 61, 275-285.

Mason, J.A. and Knox, J.C. (1997). Age of colluvium indicates accelerated Late Wisconsin hillslope erosion in the Upper Mississippi Valley. Geology 25, 267–270.

Matisoff, G., Bonniwell, E. C., and Whiting, P. J. (2002). Soil Erosion and Sediment Sources in an Ohio Watershed using Beryllium-7, Cesium-137, and Lead-210. *Journal of Environmental Quality*, 31(1), 54-61.

Mertes, L. A. K. (1994) Rates of floodplain sedimentation on the central Amazon River. *Geology,* 22, 171-174.

Missouri Lead Mining History by County (n.d.). Missouri Department of Natural Resources (MDNR). Retrieved from <http://www.dnr.mo.gov/env/hwp/sfund/lead-mo-history-more.htm>.

Natural Resources Conservation Services (NRCS) (2008). Soil Survey Geographic (SSURGO) database for Greene County, Missouri. U.S. Department of Agriculture, Natural Resources Conservation Services.

Owen, M. R., Pavlowsky, R. T., and Olson, L. M. (2012). Channel Stability and Riparian Corridor Assessment to Identify Nonpoint Source Pollution, Wilson Creek, Springfield, Missouri.

Owen, M. R., Pavlowsky, R. T., and Womble, P. T. (2011). Historical Disturbance and Contemporary Floodplains Development along an Ozark River, Southwest Missouri. *Physical Geography*, 32(5), 423-444.

Owen, P.N., Walling, D.E., Leeks, G. J. L. (1999). Use of floodplain sediment cores to investigate recent historical change in overbank sedimentation rates and sediment sources in the catchment of the River Ouse, Yorkshire, UK. *Catena*, 36(1/2), 21-47.

Ozarks Environmental and Water Resources Institute (OEWRI). (2007a). *Standard Operating Procedure for: Vario EL III CHNOS Elemental Analyzer Operation*. Springfield, MO: Missouri State University.

Ozarks Environmental and Water Resources Institute (OEWRI). (2007b). *Standard Operating Procedure for: X-MET3000TXS+ Handheld XRF Analyzer*. Springfield, MO: Missouri State University.

Ozarks Environmental and Water Resources Institute (OEWRI). (2008). *Standard Operating Procedure for: LS 13 320 Laser Diffraction Particle Size Analyzer Operation*. Springfield, MO: Missouri State University.

Ozarks Environmental and Water Resources Institute (OEWRI). (2009). *Standard Operating Procedure for: GC4020 GE Co-Axial Detector and DSA 1000 Digital Spectrum Analyzer with 747 Series Lead Shield*. Springfield, MO: Missouri State University.

Paul, M. J., & Meyer, J. L. (2001). Streams in the urban landscape. *Annual Review of Ecology and Systematics*, 333-365.

Pavlowsky, R. T. (2004). Urban Impacts on Stream Morphology in the Ozark Plateaus Region. *Self-Sustaining Solutions for Streams, Wetlands, and Watersheds,* 60-68.

Pavlowsky, Robert T., Marc R. Owen, and Derek J. Martin. (2010). Distribution, geochemistry, and storage of mining sediment in channel and floodplain deposits if the Big River system in St. Francois, Washington, and Jefferson Counties, Missouri. *Big River Mining Sediment Assessment Project Final Report*: 1-40.

Pielke, R.A., M.W. Downton, and Miller, J.Z.B. (2002). Flood Damage in the United States, 1926-2000: A Reanalysis of National Weather Service Estimates. UCAR, Boulder, Colorado, 86 pp.

Rafferty, M. D. (2001). The Ozarks land and life. Second Edition. University of Arkansas Press. pp. 148-177.

Roberts, A.D., Mosby, D.E., Weber, J.S., Besser, J., Hundley, J., McMurray, S., and Faiman, S. (2009). An assessment of freshwater mussel (Bivalvia Margaritiferidae and Unionidae) populations and heavy metal sediment contamination in the Big River Missouri. Report prepared for U.S. Department of the Interior, Washington D.C.

Rodgers, W. (2003). Personal communication with Kathy Shade.

Rodgers II, W. E. (2005). Mercury contamination of channel and floodplain sediments in Wilson Creek Watershed, Southwest Missouri. Masters of Science Thesis, Department of Geography Geology, and Planning, Southwest Missouri State University, Springfield, Missouri.

Rodríguez, J. G., & Uriarte, A. (2009). Laser diffraction and dry-sieving grain size analyses undertaken on fine-and medium-grained sandy marine sediments: A note. *Journal of Coastal Research*, 257-264.

Rosgen, D. (1996). Applied River Morphology. Wildland Hydrology, Pagosa Springs, Colorado.

Rosgen, D. L., & Dimension, A. (1996). Field survey procedures for characterization of river morphology.

Ritchie, J. C., Finney, V. L., Oster, K. J., and Ritchie, C. A. (2004). Sediment deposition in the flood plain of Stemple Creek Watershed, northern California. *Geomorphology*, 61, 347-360.

Sanborn Map Company (SMC) (2011). Greene County, Missouri 2011 Digital Mapping Project. LiDAR and Survey Report. Sanborn Map Company, Inc.

Sauer, C. O. (1920). *The Geography of the Ozark Highland of Missouri.* New Youk NY: Greenwood Press.

Searburn, G. E. (1969). *Effects of urban development on direct runoff to East Meadow Brook, Nassau County, New York.* USGS Prof. Paper 627-B.

Schmudde, T. H. (1968). Flood Plain. In *The Encyclopedia of Geomorphology.* (Vol. 3, pp. 359-362). United States of America: Reinhold Book Corporation.

Schumm, S. A. (1977). *The fluvial system.* New York: Wiley-Interscience.

Sekabira, K., Origa, H. O., Basamba, T. A., Mutumba, G., Kakudidi, E. (2010). Assessment of heavy metal pollution in the urban stream sediments and its tributaries. *International Journal of Environmental Science and Technology,* 7(3), 435-446.

Shade, K.A. (2003). Temporal analysis of floodplain deposition using urban pollution stratigraphy, Wilson Creek, SW Missouri. Masters of Science Thesis, Department of Geography Geology, and Planning, Southwest Missouri State University, Springfield, Missouri.

Solomon, R.L., and Natusch, D.F.S.. (1977). *Vo1:lll: Distribution and characterization of urban dists. In: Environmental Contamination by Lead and Other Heavy Metals. G.* L. Rolfe and K. G. Reinbold, eds.Institute for Environmental Studies. Univ. of Illinois. Urbana-Champaign, IL.

Stedinger, J. R., & Cohn, T. A. (1986). Flood frequency analysis with historical and paleoflood information. *Water Resources Research, 22*(5), 785-793.

Stuiver, M.,Reimer, P.J.,Braziunas, T.F. (1998). High-precision radiocarbon age calibration for terrestrial and marine samples. Radiocarbon 40 (3), 1127–1151.

Sutherland, R. A. (2000). Bed sediment-associated trace metals in an urban stream, Oahu, Hawaii. *Environmental Geology*, 39(6), 611-627.

Thompson, T. L. (1986). Paleozoic Succession in Missouri: Part 4 Mississippian System, Missouri Department of Natural Resources, Division of Geology and Land Survey, Rolla, MO, 1986.

Thomson, K. C. (1987). Development in sinkhole areas and related drainage and stability problems, First Annual Watershed Conference. Watershed Committee of the Ozarks, Springfield, MO.

Trimble, W. W. (1993). Erosional effects of cattle on streambanks in Tennessee, U.S.A. *Earth Surface Processes and Landforms*, 19, 451-464.

Tripod Data Systems (TDS) (2000). Survey Pro for Windows CE User's Manual. Tripod Data Systems, Inc.

Tripod Data Systems (TDS) (2004). ForeSight DXM Reference Manual. Tripod Data Systems, Inc.

Trimble Navigation Limited (TNS) (2005). GeoExplorer 2005 Series Getting Started Guide. Trimble Navigation Limited.

United States Average Monthly or Annual Precipitation, 1971-2000. (2006). The PRISM Group at Oregon State University. Corvallis, Oregon, USA. \\ORION\F$\Metadata\meta_30sec\us_ppt01_30.

U.S. Army Corps of Engineers (1968). Flood Plain Information: Wilson Creek and Tributaries, Springfield, Missouri – Part I, U.S. Army Corps of Engineers, Little Rock, Arkansas District, Little Rock.

Vineyard, J.D. and Feder, G.L. (1982). Springs of Missouri. Divison of Geology and Land Survey, Missouri Department of Natural Resources in cooperation with the United States Geological Survey and Missouri Department of Conservation.

Walling, D. E. and He, Q. (1993). Use of cesium-137 as a tracer in the study of rates and patterns of floodplain sedimentation. *Tracers in Hydrology*. IAHS Publ. 215, 319-328.

Walling, D. E., & He, Q. (1997). Use of fallout Cs^{137} in investigations of overbank sediment deposition on river floodplains. *Catena*, *29*(3), 263-282.

Walling, D. E. and He, Q. (1999). Improved Models for Estimating Soil Erosion Rates from Cesium-137 Measurements. *Journal of Environmental Quality*, 28(2), 611-622.

Walling, D. E., Quine, T. A., and He, Q. (1992). Investigating contemporary rates of floodplain sedimentation. In Carling, P. A. and Petts, G. E. (eds), *Lowland floodplain rivers.* Chichester: Wiley, 165-184.

Walling, D. E. & Woodward, J. C. (1992). Use of radiometric fingerprints to derive information on suspended sediment sources. *Erosion and Sediment Transport Monitoring Programmes in River Basins,* J. Bogey, D. E. Walling & T. Day (eds.), IAHS Publ. 210, 153-164.

Wallis, J. R., & Wood, E. F. (1985). Relative accuracy of log Pearson III procedures. *Journal of Hydraulic Engineering*, 111(7), 1043-1056.

Wang, Q., Kim, D., Dionysiou, D. D., Sorial, G. A., and Timberlake, D. (2004). Sources and remediation for mercury contamination in aquatic systems—a literature review. *Environmental Pollution*, 131, 323-336.

Webb, T.I., Bartlein, P.J., Harrison, S.P., Anderson, K.H. (1993). Vegetation, lake levels, and climate in eastern North America for the past 18,000 years. In: Wright, H.E.J., et al. (Eds.), Global Climates since the Last Glacial Maximum. University of Minnesota Press, Minneapolis, pp. 415–467.

White, W. B. (2002). Karst hydrology: recent developments and open questions. *Engineering geology*, *65*(2), 85-105.

Wilby, R.L., K.J. Beven, and N.S. Reynard (2008). Climate Change and Fluvial Flood Risk in the UK: More of the Same? Hydrological Processes 22:2511-2523.

Wilson and Jordan Creeks Total Maximum Daily Load (TMDL) (2011). United States Environmental Protection Agency Region 7.

Wolman, M. G. and Leopold, L. B. (1957). River flood plains: some observations on their formation. *United States Geological Survey Professional Paper* 282C, 87-109.

APPENDICES

Appendix A. Core Properties

Appendix A. Floodplain core properties.

Transect	Core	Latitude DD	Longitude DD	Elevation (m)	Depth (cm)	Distance from Channel (m)
1	1B-2	37.16722	-93.37241	351.8	187	25.8
1	2	37.16737	-93.37278	351.8	30	63.0
1	3	37.16760	-93.37331	352.1	40	116.2
1	4	37.16773	-93.37361	352.6	35	146.4
1	5	37.16784	-93.37389	353.2	45	174.4
2	0	37.16598	-93.37425	350.7	67	1.5
2	1	37.16612	-93.37444	351.5	196	23.8
2	2	37.16621	-93.37460	351.5	50	41.3
2	3	37.16627	-93.37483	351.2	90	62.5
3	0	37.16453	-93.37494	350.4	56	7.8
3	1	37.16468	-93.37511	351.4	210	29.4
3	2	37.16482	-93.37553	351.0	170	68.7
3	3	37.16496	-93.37571	351.3	157	90.5

Appendix B. Sample Properties

Appendix B-1. Floodplain cores sample properties.

Collection Date	Code	Sample in Core	Transect	Core	Depth (cm) (min-max)	Munsell Color
8/29/2012	WFN-1*	1	1	1	0-5	
8/29/2012	WFN-2*	2	1	1	5-10	
8/29/2012	WFN-3*	3	1	1	10-15	
8/29/2012	WFN-4*	4	1	1	15-20	
8/29/2012	WFN-5*	5	1	1	20-25	
8/29/2012	WFN-6*	6	1	1	25-30	
8/29/2012	WFN-7*	7	1	1	30-35	
8/29/2012	WFN-8*	8	1	1	35-40	
8/29/2012	WFN-9*	9	1	1	40-45	
8/29/2012	WFN-10*	10	1	1	45-50	
8/29/2012	WFN-11*	11	1	1	50-55	
8/29/2012	WFN-12*	12	1	1	55-60	
8/29/2012	WFN-13*	13	1	1	60-65	
8/29/2012	WFN-14*	14	1	1	65-70	
8/29/2012	WFN-15*	15	1	1	70-75	
8/29/2012	WFN-16*	16	1	1	75-80	
8/29/2012	WFN-17*	17	1	1	80-85	
8/29/2012	WFN-18*	18	1	1	85-90	
8/29/2012	WFN-19*	19	1	1	90-95	
8/29/2012	WFN-20*	20	1	1	95-100	
8/29/2012	WFN-21*	21	1	1	100-105	
8/29/2012	WFN-22*	22	1	1	105-110	
8/29/2012	WFN-23*	23	1	1B	110-115	
8/29/2012	WFN-24*	24	1	1B	115-120	
8/29/2012	WFN-25*	25	1	1B	120-125	
8/29/2012	WFN-26*	26	1	1B	125-130	
8/29/2012	WFN-27*	27	1	1B	130-135	
8/29/2012	WFN-28*	28	1	1B	135-140	
8/29/2012	WFN-29*	29	1	1B	140-145	
8/29/2012	WFN-30*	30	1	1B	145-150	
8/29/2012	WFN-31*	31	1	1B	150-155	
8/29/2012	WFN-32*	32	1	1B	155-160	
8/29/2012	WFN-33*	33	1	1B	160-165	
8/29/2012	WFN-34*	34	1	1B	165-170	
8/29/2012	WFN-35*	35	1	1B	170-175	

* Not used in study.

Appendix B-1 continued. Floodplain cores sample properties.

Collection Date	Code	Sample in Core	Transect	Core	Depth (cm) (min-max)	Munsell Color
8/29/2012	WFN-36*	36	1	1B	175-180	
8/29/2012	WFN-37*	37	1	1B	180-185	
8/29/2012	WFN-38*	38	1	1B	185-190	
8/29/2012	WFN-39	1	1	2	0-5	
8/29/2012	WFN-40	2	1	2	5-10	
8/29/2012	WFN-41	3	1	2	10-15	
8/29/2012	WFN-42	4	1	2	15-20	
8/29/2012	WFN-43	5	1	2	20-25	
8/29/2012	WFN-44	6	1	2	25-30	
8/29/2012	WFN-45	1	1	3	0-5	
8/29/2012	WFN-46	2	1	3	5-10	
8/29/2012	WFN-47	3	1	3	10-15	
8/29/2012	WFN-48	4	1	3	15-20	
8/29/2012	WFN-49	5	1	3	20-25	
8/29/2012	WFN-50	6	1	3	25-30	
8/29/2012	WFN-51	7	1	3	30-35	
8/29/2012	WFN-52	8	1	3	35-40	
8/29/2012	WFN-53	1	1	4	0-5	
8/29/2012	WFN-54	2	1	4	5-10	
8/29/2012	WFN-55	3	1	4	10-15	
8/29/2012	WFN-56	4	1	4	15-20	
8/29/2012	WFN-57	5	1	4	20-25	
8/29/2012	WFN-58	6	1	4	25-30	
8/29/2012	WFN-59	7	1	4	30-35	
8/29/2012	WFN-60	1	1	5	0-5	
8/29/2012	WFN-61	2	1	5	5-10	
8/29/2012	WFN-62	3	1	5	10-15	
8/29/2012	WFN-63	4	1	5	15-20	
8/29/2012	WFN-64	5	1	5	20-25	
8/29/2012	WFN-65	6	1	5	25-30	
8/29/2012	WFN-66	7	1	5	30-35	
8/29/2012	WFN-67	8	1	5	35-40	
8/29/2012	WFN-68	9	1	5	40-45	
2/12/2013	WFN-69	1	1	1B-2	0-5	10YR 3/2
2/12/2013	WFN-70	2	1	1B-2	5-10	10YR 3/2
2/12/2013	WFN-71	3	1	1B-2	10-15	10YR 3/2

* Not used in study.

Appendix B-1 continued. Floodplain cores sample properties.

Collection Date	Code	Sample in Core	Transect	Core	Depth (cm) (min-max)	Munsell Color
2/12/2013	WFN-72	4	1	1B-2	15-25	10YR 3/2
2/12/2013	WFN-73	5	1	1B-2	25-35	10YR 3/2
2/12/2013	WFN-74	6	1	1B-2	35-45	10YR 3/2
2/12/2013	WFN-75	7	1	1B-2	45-55	10YR 3/2
2/12/2013	WFN-76	8	1	1B-2	55-65	10YR 3/2
2/12/2013	WFN-77	9	1	1B-2	65-75	10YR 3/2
2/12/2013	WFN-78	10	1	1B-2	75-85	10YR 3/2
2/12/2013	WFN-79	11	1	1B-2	85-95	10YR 3/2
2/12/2013	WFN-80	12	1	1B-2	95-105	10YR 3/2
2/12/2013	WFN-81	13	1	1B-2	105-115	10YR 3/2
2/12/2013	WFN-82	14	1	1B-2	115-125	10YR 3/2
2/12/2013	WFN-83	15	1	1B-2	125-135	10YR 3/2
2/12/2013	WFN-84	16	1	1B-2	135-145	10YR 3/2
2/12/2013	WFN-85	17	1	1B-2	145-155	10YR 3/2
2/12/2013	WFN-86	18	1	1B-2	155-165	7.5YR 2.5/1
2/12/2013	WFN-87	19	1	1B-2	165-175	7.5YR 2.5/1
2/12/2013	WFN-88	20	1	1B-2	175-187	7.5YR 2.5/1
2/12/2013	WFN-89	1	2	1	0-5	
2/12/2013	WFN-90	2	2	1	5-10	
2/12/2013	WFN-91	3	2	1	10-15	
2/12/2013	WFN-92	4	2	1	15-25	
2/12/2013	WFN-93	5	2	1	25-35	
2/12/2013	WFN-94	6	2	1	35-45	
2/12/2013	WFN-95	7	2	1	45-55	
2/12/2013	WFN-96	8	2	1	55-65	
2/12/2013	WFN-97	9	2	1	65-75	
2/12/2013	WFN-98	10	2	1	75-85	
2/12/2013	WFN-99	11	2	1	85-95	
2/12/2013	WFN-100	12	2	1	95-105	
2/12/2013	WFN-101	13	2	1	105-115	
2/12/2013	WFN-102	14	2	1	115-125	
2/12/2013	WFN-103	15	2	1	125-135	
2/12/2013	WFN-104	16	2	1	135-145	
2/12/2013	WFN-105	17	2	1	145-155	
2/12/2013	WFN-106	18	2	1	155-165	
2/12/2013	WFN-107	19	2	1	165-175	
2/12/2013	WFN-108	20	2	1	175-196	

Appendix B-1 continued. Floodplain cores sample properties.

Collection Date	Code	Sample in Core	Transect	Core	Depth cm (min-max)	Munsell Color
2/12/2013	WFN-103	15	2	1	125-135	
2/12/2013	WFN-104	16	2	1	135-145	
2/12/2013	WFN-105	17	2	1	145-155	
2/12/2013	WFN-106	18	2	1	155-165	
2/12/2013	WFN-107	19	2	1	165-175	
2/12/2013	WFN-108	20	2	1	175-196	
2/12/2013	WFN-109	1	2	2	0-5	
2/12/2013	WFN-110	2	2	2	5-10	
2/12/2013	WFN-111	3	2	2	10-20	
2/12/2013	WFN-112	4	2	2	20-30	
2/12/2013	WFN-113	5	2	2	30-40	
2/12/2013	WFN-114	6	2	2	40-50	
2/12/2013	WFN-115	1	2	3	0-5	
2/12/2013	WFN-116	2	2	3	5-10	
2/12/2013	WFN-117	3	2	3	10-15	
2/12/2013	WFN-118	4	2	3	15-23	
2/12/2013	WFN-119	5	2	3	23-30	
2/12/2013	WFN-120	6	2	3	30-40	
2/12/2013	WFN-121	7	2	3	40-50	
2/12/2013	WFN-122	8	2	3	50-60	
2/12/2013	WFN-123	9	2	3	60-70	
2/12/2013	WFN-124	10	2	3	70-80	
2/12/2013	WFN-125	11	2	3	80-90	
2/12/2013	WFN-126	1	3	1	0-5	
2/12/2013	WFN-127	2	3	1	5-10	
2/12/2013	WFN-128	3	3	1	10-15	
2/12/2013	WFN-129	4	3	1	15-20	
2/12/2013	WFN-130	5	3	1	20-25	
2/12/2013	WFN-131	6	3	1	25-30	
2/12/2013	WFN-132	7	3	1	30-40	
2/12/2013	WFN-133	8	3	1	40-50	
2/12/2013	WFN-134	9	3	1	50-60	
2/12/2013	WFN-135	10	3	1	60-70	
2/12/2013	WFN-136	11	3	1	70-80	
2/12/2013	WFN-137	12	3	1	80-90	
2/12/2013	WFN-138	13	3	1	90-100	
2/12/2013	WFN-139	14	3	1	100-110	
2/12/2013	WFN-140	15	3	1	110-120	

Appendix B-1 continued. Floodplain cores sample properties.

Collection Date	Code	Sample in Core	Transect	Core	Depth (cm) (min-max)	Munsell Color
2/12/2013	WFN-141	16	3	1	120-130	
2/12/2013	WFN-142	17	3	1	130-140	
2/12/2013	WFN-143	18	3	1	140-150	
2/12/2013	WFN-144	19	3	1	150-170	
2/12/2013	WFN-145	20	3	1	170-190	
2/12/2013	WFN-146	21	3	1	190-210	
2/12/2013	WFN-147	1	3	2	0-5	
2/12/2013	WFN-148	2	3	2	5-10	
2/12/2013	WFN-149	3	3	2	10-20	
2/12/2013	WFN-150	4	3	2	20-30	
2/12/2013	WFN-151	5	3	2	30-40	
2/12/2013	WFN-152	6	3	2	40-50	
2/12/2013	WFN-153	7	3	2	50-60	
2/12/2013	WFN-154	8	3	2	60-70	
2/12/2013	WFN-155	9	3	2	70-80	
2/12/2013	WFN-156	10	3	2	80-90	
2/12/2013	WFN-157	11	3	2	90-100	
2/12/2013	WFN-158	12	3	2	100-110	
2/12/2013	WFN-159	13	3	2	110-120	
2/12/2013	WFN-160	14	3	2	120-130	
2/12/2013	WFN-161	15	3	2	130-140	
2/12/2013	WFN-162	16	3	2	140-150	
2/12/2013	WFN-163	17	3	2	150-160	
2/12/2013	WFN-164	18	3	2	160-170	
2/12/2013	WFN-165	1	3	3	0-5	
2/12/2013	WFN-166	2	3	3	5-10	
2/12/2013	WFN-167	3	3	3	10-15	
2/12/2013	WFN-168	4	3	3	15-20	
2/12/2013	WFN-169	5	3	3	20-30	
2/12/2013	WFN-170	6	3	3	30-40	
2/12/2013	WFN-171	7	3	3	40-50	
2/12/2013	WFN-172	8	3	3	50-60	
2/12/2013	WFN-173	9	3	3	60-70	
2/12/2013	WFN-174	10	3	3	70-80	
2/12/2013	WFN-175	11	3	3	80-90	
2/12/2013	WFN-176	12	3	3	90-100	
2/12/2013	WFN-177	13	3	3	100-115	
2/12/2013	WFN-178	14	3	3	115-130	

Appendix B-1 continued. Floodplain cores sample properties.

Collection Date	Code	Sample in Core	Transect	Core	Depth cm (min-max)	Munsell Color
2/12/2013	WFN-179	15	3	3	130-145	
2/12/2013	WFN-180	16	3	3	145-157	
2/12/2013	WFN-181	1	3	0	0-10	
2/12/2013	WFN-182	2	3	0	10-20	
2/12/2013	WFN-183	3	3	0	20-30	
2/12/2013	WFN-184	4	3	0	30-40	
2/12/2013	WFN-185	5	3	0	40-56	
2/12/2013	WFN-186	1	2	0	0-10	
2/12/2013	WFN-187	2	2	0	10-20	
2/12/2013	WFN-188	3	2	0	20-30	
2/12/2013	WFN-189	4	2	0	30-40	
2/12/2013	WFN-190	5	2	0	40-50	
2/12/2013	WFN-191	6	2	0	50-60	
2/12/2013	WFN-192	7	2	0	60-67	

Appendix B-2. Floodplain grid surface sample properties.

Collection Date	Code	Grid coordinates		Elevation (m)
		X	Y	
6/7/2013	WCG-1	-15	0	351.04
6/7/2013	WCG-2	-10	0	351.12
6/7/2013	WCG-3	-10	10	351.09
6/7/2013	WCG-5	-10	20	350.60
6/7/2013	WCG-6	-10	40	351.00
6/7/2013	WCG-7	-10	50	351.28
6/7/2013	WCG-8	-10	60	351.36
6/7/2013	WCG-10	-10	70	351.19
6/7/2013	WCG-11	-10	80	351.28
6/7/2013	WCG-12	-5	0	351.03
6/7/2013	WCG-13	-5	10	350.96
6/7/2013	WCG-14	-5	20	350.77
6/7/2013	WCG-15	-5	30	351.19
6/7/2013	WCG-16	-5	40	351.37
6/7/2013	WCG-18	-5	50	351.24
6/7/2013	WCG-19	-5	60	351.15
6/7/2013	WCG-20	-5	70	351.14
6/7/2013	WCG-21	-5	80	351.00
6/7/2013	WCG-22	0	0	351.09
6/7/2013	WCG-23	0	10	350.74
6/7/2013	WCG-24	0	20	350.56
6/7/2013	WCG-25	0	30	350.67
6/7/2013	WCG-26	0	40	351.11
6/7/2013	WCG-27	0	50	351.06
6/7/2013	WCG-28	0	60	351.03
6/7/2013	WCG-29	0	70	351.00
6/7/2013	WCG-30	0	80	350.80
6/7/2013	WCG-32	5	30	350.80
6/7/2013	WCG-33	10	0	351.47
6/7/2013	WCG-34	10	10	351.40
6/7/2013	WCG-35	10	20	351.29
6/7/2013	WCG-36	10	30	351.17
6/7/2013	WCG-37	10	40	350.63
6/7/2013	WCG-38	10	50	350.61
6/7/2013	WCG-39	10	60	350.34
6/7/2013	WCG-41	10	70	350.21
6/7/2013	WCG-42	10	80	350.27

Appendix B-2 Continued. Floodplain grid surface sample properties.

Collection Date	Code	Grid coordinates		Elevation (m)
		X	Y	
6/7/2013	WCG-43	20	0	351.50
6/7/2013	WCG-44	20	10	351.57
6/7/2013	WCG-45	20	20	351.55
6/7/2013	WCG-46	20	30	351.52
6/7/2013	WCG-48	20	40	351.50
6/7/2013	WCG-49	20	50	351.44
6/7/2013	WCG-50	20	60	351.43
6/7/2013	WCG-51	20	70	351.44
6/7/2013	WCG-52	20	80	351.38
6/7/2013	WCG-54	30	0	351.44
6/7/2013	WCG-55	30	10	351.49
6/7/2013	WCG-56	30	20	351.53
6/7/2013	WCG-57	30	30	351.54
6/7/2013	WCG-59	30	40	351.55
6/7/2013	WCG-60	30	50	351.53
6/7/2013	WCG-62	30	60	351.50
6/7/2013	WCG-63	30	70	351.47
6/7/2013	WCG-64	30	80	351.43
6/7/2013	WCG-66	40	0	351.41
6/7/2013	WCG-67	40	10	351.39
6/7/2013	WCG-68	40	20	351.47
6/7/2013	WCG-70	40	30	351.48
6/7/2013	WCG-71	40	40	351.54
6/7/2013	WCG-72	40	50	351.56
6/7/2013	WCG-73	40	60	351.55
6/7/2013	WCG-74	40	70	351.56
6/7/2013	WCG-75	40	80	351.52
6/7/2013	WCG-76	50	0	351.52
6/7/2013	WCG-77	50	10	351.36
6/7/2013	WCG-78	50	20	351.22
6/7/2013	WCG-79	50	30	351.27
6/7/2013	WCG-80	50	40	351.32
6/7/2013	WCG-81	50	50	351.34
6/7/2013	WCG-82	50	60	351.36
6/7/2013	WCG-84	50	70	351.34
6/7/2013	WCG-86	50	80	351.32
6/7/2013	WCG-87	60	0	351.91

Appendix B-2 Continued. Floodplain grid surface sample properties.

Collection Date	Code	Grid coordinates		Elevation (m)
		X	Y	
6/7/2013	WCG-88	60	10	351.81
6/7/2013	WCG-89	57	20	351.80
6/7/2013	WCG-90	60	30	351.50
6/7/2013	WCG-92	60	40	351.24
6/7/2013	WCG-93	60	50	351.18
6/7/2013	WCG-94	60	60	351.08
6/7/2013	WCG-95	60	70	351.05
6/7/2013	WCG-96	60	80	351.09

Appendix C. Geochemical Data

Appendix C-1. Ca, Cu, Fe, Pb, and Zn floodplain core samples geochemical data used in this study.

Sample	Ca (ppm)	Cu (ppm)	Fe (ppm)	Pb (ppm)	Zn (ppm)
WFN-1*	7837	14	21609	79	198
WFN-2*	4595	ND	20996	61	124
WFN-3*	3594	ND	21413	ND	112
WFN-4*	3078	12	19627	36	87
WFN-5*	3200	ND	20517	38	81
WFN-6*	3551	10	20176	28	58
WFN-7*	2054	ND	18789	24	42
WFN-8*	2361	ND	18847	33	74
WFN-9*	2774	12	21234	72	208
WFN-10*	2489	19	25262	90	306
WFN-11*	3135	12	24119	92	270
WFN-12*	2344	ND	23107	54	217
WFN-13*	2868	ND	24745	48	164
WFN-14*	3128	ND	24826	55	133
WFN-15*	1881	ND	24830	49	116
WFN-16*	2686	ND	21958	40	99
WFN-17*	3033	ND	23747	49	106
WFN-18*	2384	ND	22621	43	94
WFN-19*	3130	ND	26327	50	83
WFN-20*	2762	ND	24606	ND	79
WFN-21*	2896	ND	22840	39	69
WFN-22*	3163	ND	24851	ND	78
WFN-23*	2818	21	26940	144	290
WFN-24*	3757	34	29915	219	392
WFN-25*	4923	44	30247	287	495
WFN-26*	8961	51	31158	261	479
WFN-27*	10785	47	31404	238	415
WFN-28*	17013	36	33719	228	433
WFN-29*	16442	43	30743	275	461
WFN-30*	9043	31	28834	206	369
WFN-31*	7422	27	25202	186	328
WFN-32*	4636	19	24854	113	242
WFN-33*	4548	ND	25134	118	219
WFN-34*	4428	15	24444	117	216
ND	Below detection limit				
*	Not used in study				

Appendix C-1 Continued. Ca, Cu, Fe, Pb, and Zn floodplain core samples geochemical data used in this study.

Sample	Ca (ppm)	Cu (ppm)	Fe (ppm)	Pb (ppm)	Zn (ppm)
WFN-35*	3562	ND	24275	107	248
WFN-36*	5231	15	33426	135	345
WFN-37*	5989	25	40551	181	371
WFN-38*	5687	34	35805	241	359
WFN-39	28615	58	23493	185	531
WFN-40	24122	242	25260	394	1146
WFN-41	16741	60	23485	149	410
WFN-42	7402	20	22201	74	162
WFN-43	3957	14	21718	49	92
WFN-44	2277	11	20129	42	80
WFN-45	3868	64	20021	134	330
WFN-46	3888	44	20524	98	243
WFN-47	2162	19	18977	44	123
WFN-48	2183	19	20047	44	108
WFN-49	2379	16	19389	49	96
WFN-50	2760	ND	22448	43	92
WFN-51	2953	11	21769	37	86
WFN-52	2475	ND	22379	26	66
WFN-53	11658	38	18838	55	167
WFN-54	9941	30	20143	58	142
WFN-55	4448	13	20629	ND	87
WFN-56	3096	ND	20933	35	62
WFN-57	2349	ND	22059	29	49
WFN-58	2087	ND	22793	32	50
WFN-59*					
WFN-60	2874	43	20608	80	192
WFN-61	1842	46	21786	66	155
WFN-62	2822	41	22732	57	139
WFN-63	3019	51	23480	50	176
WFN-64	3037	39	22251	60	127
WFN-65	2723	17	20652	40	93
WFN-66	1778	ND	20073	38	64
WFN-67	1887	ND	18561	35	50
WFN-68	2307	ND	18731	ND	51
WFN-69	31709	18	24412	96	348

ND Below detection limit
* Not used in study

Appendix C-1 Continued. Ca, Cu, Fe, Pb, and Zn floodplain core samples geochemical data used in this study.

Sample	Ca (ppm)	Cu (ppm)	Fe (ppm)	Pb (ppm)	Zn (ppm)
WFN-69	31709	18	24412	96	348
WFN-70	36857	20	26140	129	365
WFN-71	25245	14	27828	128	327
WFN-72	13991	ND	23834	83	185
WFN-73	3850	ND	21413	37	73
WFN-74	3715	ND	20799	30	61
WFN-75	2973	ND	23067	ND	55
WFN-76	2776	ND	20620	27	43
WFN-77	2869	ND	19219	26	44
WFN-78	3555	ND	21907	ND	58
WFN-79	2468	ND	23893	42	77
WFN-80	2800	ND	23737	34	64
WFN-81	2995	ND	22237	ND	48
WFN-82	2642	ND	21231	31	46
WFN-83	1961	ND	21854	35	59
WFN-84	2970	ND	21444	30	52
WFN-85	2740	ND	21201	28	64
WFN-86	4205	13	24495	87	174
WFN-87	7307	19	36671	545	287
WFN-88	5653	26	31901	147	255
WFN-89	12407	330	21311	135	330
WFN-90	8770	268	21225	101	268
WFN-91	4259	111	20021	49	111
WFN-92	3027	73	22389	46	73
WFN-93	3003	62	24561	24	62
WFN-94	3405	55	24054	23	55
WFN-95	2281	52	26067	37	52
WFN-96	2137	62	26351	29	62
WFN-97	2437	66	27720	29	66
WFN-98	2590	59	27145	27	59
WFN-99	2416	62	27760	31	62
WFN-100	2604	65	28244	ND	65
WFN-101	2186	62	25958	ND	62
WFN-102	4230	112	27429	ND	112
WFN-103	2010	61	24547	27	61
WFN-104	2951	76	25039	25	76

ND Below detection limit

Appendix C-1 Continued. Ca, Cu, Fe, Pb, and Zn floodplain core samples geochemical data used in this study.

Sample	Ca (ppm)	Cu (ppm)	Fe (ppm)	Pb (ppm)	Zn (ppm)
WFN-105	2462	66	25886	ND	66
WFN-106	2382	70	26001	27	70
WFN-107	2600	68	25350	31	68
WFN-108	2871	90	28508	35	90
WFN-109	21075	336	21770	105	336
WFN-110	18130	316	22674	108	316
WFN-111	4593	129	20907	57	129
WFN-112	2753	74	22850	38	74
WFN-113	2711	51	24117	ND	51
WFN-114	2076	51	22590	ND	51
WFN-115	7800	315	20964	109	315
WFN-116	7887	310	21044	109	310
WFN-117	2541	144	19250	62	144
WFN-118	2759	71	19744	34	71
WFN-119	3077	49	21243	ND	49
WFN-120	2813	54	22591	ND	54
WFN-121	2661	55	23640	26	55
WFN-122	2915	60	24531	ND	60
WFN-123	2359	56	25005	ND	56
WFN-124	3277	61	27358	35	61
WFN-125	2348	56	25776	33	56
WFN-126	3731	185	17758	81	185
WFN-127	3098	171	17813	66	171
WFN-128	2642	135	19471	55	135
WFN-129	2669	102	18976	47	102
WFN-130	2583	75	18345	42	75
WFN-131	2787	67	19248	ND	67
WFN-132	2475	59	19625	29	59
WFN-133	2143	51	19985	ND	51
WFN-134	2148	51	19105	17	51
WFN-135	2506	51	19197	21	51
WFN-136	2541	56	19965	ND	56
WFN-137	2008	56	21486	23	56
WFN-138	2487	61	20884	21	61
WFN-139	2180	61	21684	27	61
WFN-140	2549	72	21835	23	72

ND Below detection limit

Appendix C-1 Continued. Ca, Cu, Fe, Pb, and Zn floodplain core samples geochemical data used in this study.

Sample	Ca (ppm)	Cu (ppm)	Fe (ppm)	Pb (ppm)	Zn (ppm)
WFN-141	2198	14	21156	ND	60
WFN-142	1728	66	22071	23	66
WFN-143	2631	66	22785	28	66
WFN-144	2439	57	22899	25	57
WFN-145	2402	57	24013	27	57
WFN-146	2185	55	27400	ND	55
WFN-147	8703	224	20361	86	224
WFN-148	8964	252	21763	98	252
WFN-149	4255	160	21099	73	160
WFN-150	2824	115	21711	77	115
WFN-151	3313	131	21611	58	131
WFN-152	2567	86	20421	38	86
WFN-153	3158	55	21172	31	55
WFN-154	4446	71	22173	26	71
WFN-155	3487	63	21725	ND	63
WFN-156	3565	64	22401	22	64
WFN-157	3276	66	22517	29	66
WFN-158	3031	65	25168	41	65
WFN-159	2576	59	23271	30	59
WFN-160	2764	59	24368	27	59
WFN-161	3078	60	25530	31	60
WFN-162	2679	74	26646	36	74
WFN-163	1972	57	25247	34	57
WFN-164	2022	51	28395	ND	51
WFN-165	3799	101	18077	38	101
WFN-166	2951	82	17401	38	82
WFN-167	1746	63	17339	35	63
WFN-168	2351	62	17328	30	62
WFN-169	2472	45	19082	20	45
WFN-170	1394	43	20413	ND	43
WFN-171	1421	52	22082	29	52
WFN-172	1695	52	24336	18	52
WFN-173	1859	59	25688	19	59
WFN-174	1845	70	26200	ND	70
WFN-175	1828	52	26196	ND	52
WFN-176	1564	46	26024	31	46

ND Below detection limit

Appendix C-1 Continued. Ca, Cu, Fe, Pb, and Zn floodplain core samples geochemical data used in this study.

Sample	Ca (ppm)	Cu (ppm)	Fe (ppm)	Pb (ppm)	Zn (ppm)
WFN-177	2176	57	28094	31	57
WFN-178	2349	69	28577	41	69
WFN-179	2805	64	30268	38	64
WFN-180	2025	57	31271	ND	57
WFN-181	25498	306	25186	135	306
WFN-182	19070	311	30684	169	311
WFN-183	8753	230	28369	145	230
WFN-184	4586	198	23546	118	198
WFN-185	3688	181	22605	70	181
WFN-186	32375	357	28111	112	357
WFN-187	37943	380	28065	123	380
WFN-188	6281	148	24124	52	148
WFN-189	3284	92	23255	35	92
WFN-190	4665	82	23506	36	82
WFN-191	3180	68	24085	36	68
WFN-192	3432	75	25809	34	75

ND Below detection limit

Appendix C-2. Ca, Cu, Fe, Pb, and Zn floodplain surface grid samples geochemical data used in this study.

Sample	Ca (ppm)	Cu (ppm)	Fe (ppm)	Pb (ppm)	Zn (ppm)
WCG-1	13953	15	24757	92	311
WCG-2	18735	20	26020	152	336
WCG-3	29913	14	29275	136	388
WCG-5	50641	16	26336	109	374
WCG-6	26904	9	22355	94	270
WCG-7	28731	20	27259	139	335
WCG-8	40764	13	26991	115	333
WCG-10	30183	15	27105	156	326
WCG-11	30723	16	27120	107	335
WCG-12	34462	21	24779	126	315
WCG-13	36151	115	26019	107	291
WCG-14	36193	15	26629	108	333
WCG-15	33126	ND	28578	140	338
WCG-16	50346	21	25852	115	375
WCG-18	43372	12	25568	116	369
WCG-19	47673	13	25689	106	377
WCG-20	52238	15	25016	122	385
WCG-21	46623	15	24634	120	387
WCG-22	44307	23	24632	102	313
WCG-23	4692	ND	24719	ND	88
WCG-24	18783	ND	25937	80	215
WCG-25	28640	14	23664	94	287
WCG-26	32391	ND	25865	100	287
WCG-27	9879	ND	25766	47	133
WCG-28	35579	20	22694	103	316
WCG-29	43278	15	25484	127	394
WCG-30	29682	11	26497	124	322
WCG-32	33328	16	24560	108	293
WCG-33	16876	15	21934	81	213
WCG-34	18441	13	22166	70	225
WCG-35	3928	ND	18398	34	91
WCG-36	9988	ND	20109	52	150
WCG-37	9164	ND	24790	54	132
WCG-38	12923	ND	24951	53	144
WCG-39	5285	ND	21875	26	91
WCG-41	6652	ND	27800	39	104

ND Below detection limit

Appendix C-2 Continued. Ca, Cu, Fe, Pb, and Zn floodplain surface grid samples geochemical data used in this study.

Sample	Ca (ppm)	Cu (ppm)	Fe (ppm)	Pb (ppm)	Zn (ppm)
WCG-42	2953	13	17049	61	148
WCG-43	19962	45	22270	120	348
WCG-44	3551	ND	21574	62	107
WCG-45	6814	25	18284	74	185
WCG-46	4867	24	20019	60	139
WCG-48	5726	40	20645	90	234
WCG-49	5880	26	17858	96	238
WCG-50	4038	25	18273	87	218
WCG-51	5296	58	20248	146	386
WCG-52	3308	20	16025	71	161
WCG-54	21755	22	21696	114	301
WCG-55	17426	38	22641	121	347
WCG-56	12658	37	22668	106	275
WCG-57	9465	29	18271	86	250
WCG-59	8742	39	18561	77	218
WCG-60	5270	45	18620	107	282
WCG-62	5240	53	19264	136	352
WCG-63	5530	65	18865	131	355
WCG-64	4706	61	20930	135	340
WCG-66	3107	34	16038	95	233
WCG-67	2994	22	17665	60	164
WCG-68	8302	40	19802	94	294
WCG-70	7363	47	22088	115	303
WCG-71	9205	24	20561	71	206
WCG-72	6473	23	21143	64	176
WCG-73	4568	25	19001	65	184
WCG-74	5008	39	18072	68	167
WCG-75	5908	42	21345	104	251
WCG-76	43455	17	25824	130	344
WCG-77	4985	54	19056	134	328
WCG-78	11356	34	22331	84	292
WCG-79	10343	29	21106	94	233
WCG-80	9800	28	20503	82	209
WCG-81	10059	36	21151	87	230
WCG-82	10634	29	19710	80	232
WCG-84	6016	31	21898	89	230

ND Below detection limit

Appendix C-2 Continued. Ca, Cu, Fe, Pb, and Zn floodplain surface grid samples geochemical data used in this study.

Sample	Ca (ppm)	Cu (ppm)	Fe (ppm)	Pb (ppm)	Zn (ppm)
WCG-86	8905	36	20649	96	241
WCG-87	3857	12	17016	36	96
WCG-88	3035	36	18546	102	209
WCG-89	3983	23	16027	63	153
WCG-90	6055	14	20760	70	176
WCG-92	6510	10	19792	57	173
WCG-93	5675	24	21551	93	216
WCG-94	7359	22	21894	105	255
WCG-95	5716	30	22296	80	235
WCG-96	4973	27	20393	93	237

Appendix C-3. Co, Cr, Mn, Mo, Sr, Ti, and Zr floodplain core samples geochemical data not used in this study.

Sample	Co (ppm)	Cr (ppm)	Mn (ppm)	Mo (ppm)	Sr (ppm)	Ti (ppm)	Zr (ppm)
1*	47	ND	1216	22	67	5044	516
2*	ND	ND	1377	33	64	5058	496
3*	ND	ND	1292	30	67	5872	536
4*	ND	ND	1111	27	66	5798	503
5*	44	22	1152	21	68	5853	539
6*	54	ND	1296	29	67	6116	544
7*	50	ND	1286	34	64	5264	587
8*	ND	47	1258	34	55	5366	566
9*	45	0	1263	27	58	5263	545
10*	ND	ND	1185	28	64	5465	516
11*	ND	ND	1311	21	62	4980	480
12*	ND	2	1298	24	59	5614	495
13*	81	ND	1503	18	63	5534	504
14*	89	44	1471	26	67	5443	513
15*	71	ND	1999	18	61	5167	467
16*	42	50	1559	22	60	5549	510
17*	63	ND	1723	33	66	5565	478
18*	52	ND	1422	25	65	5274	466
19*	69	ND	1993	20	70	5380	445
20*	ND	7	1700	26	60	5799	450
21*	60	7	1462	27	69	5371	497
22*	ND	ND	1607	17	70	5394	455
23*	77	ND	1402	29	66	5717	519
24*	ND	33	1274	19	61	5260	475
25*	50	ND	1286	28	63	4977	467
26*	ND	25	1353	25	59	5135	453
27*	ND	ND	1466	27	63	4430	423
28*	76	ND	1811	20	72	4053	453
29*	ND	ND	1633	29	65	4425	445
30*	68	39	1228	25	61	4324	403
31*	ND	ND	1237	27	63	4722	503
32*	61	ND	1784	27	65	5372	513
33*	62	2	1838	29	66	5582	532
34*	ND	ND	1246	33	67	5527	516
35*	ND	ND	1729	33	64	5443	489

ND Below detection limit
* Not used in study

Appendix C-3 Continued. Co, Cr, Mn, Mo, Sr, Ti, and Zr floodplain core samples geochemical data not used in this study.

Sample	Co (ppm)	Cr (ppm)	Mn (ppm)	Mo (ppm)	Sr (ppm)	Ti (ppm)	Zr (ppm)
36*	74	27	3596	16	48	5157	371
37*	ND	ND	4578	25	61	4269	305
38*	ND	ND	2779	24	58	4486	363
39	ND	52	1524	27	70	3877	423
40	ND	268	1023	35	80	4999	436
41	47	76	1330	36	74	4998	528
42	ND	15	1255	30	72	5426	524
43	50	ND	1199	28	70	5447	545
44	45	36	1335	32	69	5636	545
45	ND	90	1084	24	68	5126	495
46	ND	55	1216	26	66	5470	536
47	59	ND	1351	32	70	4378	559
48	ND	ND	1273	31	63	5439	546
49	61	22	1363	34	65	5051	537
50	67	22	1205	26	69	6013	519
51	47	ND	1286	30	74	5760	553
52	48	ND	1051	38	71	5618	508
53	ND	ND	1038	25	62	4680	525
54	47	ND	1386	32	70	4857	541
55	53	ND	1398	31	59	5052	579
56	80	ND	1311	31	60	5639	627
57	ND	1	1105	26	67	5028	552
58	54	33	1041	22	60	5600	536
59*							
60	ND	22	1546	37	70	5289	519
61	ND	58	1670	28	64	5007	524
62	47	46	1819	29	75	5031	567
63	ND	34	1965	27	70	5005	545
64	60	1	1885	28	71	5259	574
65	39	7	1811	27	73	5520	563
66	68	ND	1648	25	73	5754	547
67	ND	ND	1400	26	70	5141	527
68	ND	3	1271	30	67	5308	542
89	64	78	1425	34	71	4233	518
90	ND	40	1428	30	71	5242	514

ND Below detection limit
* Not used in study

Appendix C-3 Continued. Co, Cr, Mn, Mo, Sr, Ti, and Zr floodplain core samples geochemical data not used in this study.

Sample	Co (ppm)	Cr (ppm)	Mn (ppm)	Mo (ppm)	Sr (ppm)	Ti (ppm)	Zr (ppm)
91	67	ND	1284	39	64	5042	520
92	ND	39	1819	30	66	5189	499
93	44	31	1765	36	62	5696	498
94	48	ND	1184	23	66	5398	493
95	77	10	1580	32	71	5827	472
96	46	ND	1211	27	66	5660	468
97	43	24	1184	30	69	5753	453
98	57	ND	1000	31	68	5411	449
99	43	54	1040	22	73	5677	458
100	56	ND	1014	28	72	5862	449
101	49	ND	926	33	75	5481	460
102	50	35	1198	20	73	5930	475
103	ND	34	934	29	76	5417	459
104	68	1	1099	37	74	5645	438
105	75	30	1077	31	79	5934	455
106	43	ND	1058	22	81	5899	469
107	74	10	1104	29	79	5603	447
108	67	5	1759	26	78	5618	447
109	0	0	0	0	0	0	0
110	ND	9	1392	34	71	4649	519
111	53	ND	1344	37	71	4879	525
112	45	14	1426	25	67	5888	513
113	42	7	1552	22	62	5607	493
114	48	ND	1689	25	51	4491	410
115	57	8	1414	34	66	4667	453
116	ND	37	1354	31	73	4795	462
117	47	ND	1230	33	74	4732	534
118	44	ND	1190	35	76	5570	517
119	49	ND	1209	25	70	5527	467
120	61	0	1233	31	72	5381	481
121	42	40	1343	32	73	5343	481
122	92	ND	1262	37	69	5240	463
123	52	15	1321	32	66	5371	476
124	78	8	1921	23	75	5978	473
125	81	30	1371	24	56	4831	382
126	41	0	1319	32	65	5067	508

ND Below detection limit

Appendix C-3 Continued. Co, Cr, Mn, Mo, Sr, Ti, and Zr floodplain core samples geochemical data not used in this study.

Sample	Co (ppm)	Cr (ppm)	Mn (ppm)	Mo (ppm)	Sr (ppm)	Ti (ppm)	Zr (ppm)
127	42	ND	1328	36	65	5194	520
128	ND	44	1482	29	73	5622	577
129	ND	23	1467	27	73	5589	569
130	98	0	1454	32	77	5883	572
131	37	ND	1570	28	75	5677	516
132	43	2	1657	30	77	6213	537
133	ND	16	1529	31	77	5991	535
134	69	ND	1257	29	75	5802	533
135	61	15	1119	31	73	5689	490
136	62	45	1248	33	76	5818	509
137	68	26	1318	28	79	5626	510
138	73	8	1151	33	65	5475	482
139	55	25	1046	26	75	5537	513
140	37	ND	926	30	70	5863	494
141	52	ND	542	30	66	5789	488
142	93	1	412	31	75	5763	481
143	56	9	426	33	71	5640	475
144	63	ND	862	32	75	5774	495
145	62	21	1262	26	75	5630	470
146	76	46	1357	32	62	5196	381
147	69	ND	1374	34	70	4062	412
148	ND	37	1513	31	69	4695	457
149	50	15	1533	35	63	4949	493
150	41	ND	1646	25	67	5397	543
151	64	10	1518	32	68	5429	494
152	ND	20	1315	34	72	5217	495
153	65	2	1592	31	75	5850	481
154	52	1	1883	25	75	5712	485
155	58	ND	1548	35	67	5457	458
156	ND	ND	1441	30	78	5579	468
157	58	ND	1481	23	74	5708	477
158	53	27	1679	30	71	6415	496
159	53	49	1263	22	72	5680	469
160	88	ND	1299	26	75	5710	468
161	79	ND	1256	28	71	5544	455
162	61	ND	1529	30	74	5734	454

ND Below detection limit

Appendix C-3 Continued. Co, Cr, Mn, Mo, Sr, Ti, and Zr floodplain core samples geochemical data not used in this study.

Sample	Co (ppm)	Cr (ppm)	Mn (ppm)	Mo (ppm)	Sr (ppm)	Ti (ppm)	Zr (ppm)
163	83	ND	1710	35	62	4673	391
164	100	14	1547	30	57	4243	334
165	59	ND	1263	33	71	5510	598
166	48	ND	1261	30	70	5342	573
167	ND	1	1239	25	72	5697	582
168	38	ND	1257	29	71	5710	583
169	ND	16	1184	28	83	6080	568
170	ND	ND	649	28	66	5566	515
171	53	18	601	28	79	5628	531
172	80	ND	808	30	71	5889	495
173	ND	38	759	26	79	5894	454
174	61	38	736	28	78	5752	484
175	54	10	732	35	76	5620	460
176	68	ND	771	29	77	5949	465
177	105	15	964	32	76	6087	456
178	74	10	1082	23	71	5522	400
179	85	5	1437	24	80	5315	451
180	81	11	1189	31	76	4949	406
181	50	ND	1869	30	70	4024	480
182	ND	ND	2020	32	79	4833	523
183	67	ND	1767	28	60	4367	468
184	72	ND	1680	28	66	5168	503
185	53	7	1187	25	65	5727	522
186	89	ND	2157	24	71	4104	418
187	89	ND	2115	24	66	4136	437
188	81	ND	1345	35	68	5438	446
189	60	28	1253	24	74	5545	460
190	61	21	1182	33	69	5331	450
191	54	ND	1708	27	67	5684	447
192	55	ND	2037	23	71	5552	417

ND Below detection limit

Appendix C-4. Co, Cr, Mn, Mo, Sr, Ti, and Zr floodplain surface grid samples geochemical data not used in this study.

Sample	Co (ppm)	Cr (ppm)	Mn (ppm)	Mo (ppm)	Sr (ppm)	Ti (ppm)	Zr (ppm)
WCG-1	73	ND	1526	27	67	4426	533
WCG-2	96	ND	1434	25	70	4305	524
WCG-3	76	ND	1882	29	72	4570	444
WCG-5	63	ND	1912	32	66	3178	403
WCG-6	73	ND	1890	22	61	3682	399
WCG-7	63	15	1952	27	63	4104	445
WCG-8	65	27	2060	25	75	3712	459
WCG-10	75	26	2129	35	63	4017	477
WCG-11	ND	ND	1898	28	65	4089	440
WCG-12	67	ND	1661	23	65	4072	436
WCG-13	45	ND	2170	30	66	4203	411
WCG-14	69	ND	2015	29	66	3576	404
WCG-15	ND	ND	2133	29	67	3282	401
WCG-16	48	ND	1976	23	72	3215	447
WCG-18	69	ND	2055	25	67	3343	418
WCG-19	60	ND	1833	31	71	3330	436
WCG-20	48	ND	1956	31	81	3563	409
WCG-21	72	ND	1859	28	72	3204	420
WCG-22	ND	ND	1664	26	70	3384	432
WCG-23	52	11	849	18	62	5172	407
WCG-24	ND	ND	1518	36	71	4424	435
WCG-25	ND	ND	2101	29	59	3310	350
WCG-26	ND	2	2031	25	71	3793	383
WCG-27	57	ND	1050	30	60	4819	404
WCG-28	53	ND	1705	27	60	2942	366
WCG-29	59	ND	1905	32	70	3790	442
WCG-30	101	ND	2077	22	68	3946	445
WCG-32	ND	ND	1669	32	69	4052	438
WCG-33	ND	ND	1647	30	66	4415	482
WCG-34	ND	ND	1472	23	63	4502	489
WCG-35	42	ND	1017	17	51	4718	421
WCG-36	ND	ND	1395	25	54	4362	433
WCG-37	100	ND	1766	32	63	4647	437
WCG-38	60	25	1248	26	63	4746	427
WCG-39	ND	18	863	26	55	4452	360
WCG-41	ND	ND	1116	27	76	5185	423

ND Below detection limit

Appendix C-4 Continued. Co, Cr, Mn, Mo, Sr, Ti, and Zr floodplain surface grid samples geochemical data not used in this study.

Sample	Co (ppm)	Cr (ppm)	Mn (ppm)	Mo (ppm)	Sr (ppm)	Ti (ppm)	Zr (ppm)
WCG-42	45	17	1190	29	62	4116	432
WCG-43	ND	28	1434	33	68	4415	462
WCG-44	56	ND	1433	31	68	5772	513
WCG-45	56	ND	1184	28	56	4277	430
WCG-46	66	ND	1485	31	60	5172	521
WCG-48	ND	48	1469	28	61	5050	483
WCG-49	ND	47	1291	32	54	4372	416
WCG-50	49	57	1275	29	51	4373	419
WCG-51	ND	50	1337	29	66	4896	481
WCG-52	ND	18	1098	29	46	4293	385
WCG-54	38	51	1638	28	66	3839	462
WCG-55	66	24	1510	25	78	4279	503
WCG-56	58	20	1531	32	68	4907	506
WCG-57	38	42	1350	22	54	3798	435
WCG-59	47	57	1210	31	53	4036	451
WCG-60	ND	58	1473	32	57	4380	445
WCG-62	ND	60	1179	30	59	4390	428
WCG-63	ND	109	1205	31	63	4637	435
WCG-64	ND	55	1493	34	65	5205	487
WCG-66	ND	17	1131	27	55	4011	441
WCG-67	46	22	1450	26	59	4703	459
WCG-68	52	25	1258	28	59	4335	432
WCG-70	ND	67	1585	25	72	5092	512
WCG-71	ND	ND	1416	29	62	4547	493
WCG-72	ND	ND	1528	26	68	5033	508
WCG-73	53	ND	1351	26	62	5471	488
WCG-74	ND	ND	1289	24	58	4724	460
WCG-75	ND	36	1543	31	69	5435	549
WCG-76	52	ND	2086	29	72	3602	426
WCG-77	41	77	1262	34	66	4826	470
WCG-78	ND	ND	1463	21	67	4357	442
WCG-79	ND	2	1357	25	71	5178	498
WCG-80	ND	ND	1328	25	64	4990	521
WCG-81	ND	9	1605	29	68	4900	545
WCG-82	ND	35	1448	28	60	4456	449
WCG-84	66	ND	1347	32	65	5107	540

ND Below detection limit

Appendix C-4 Continued. Co, Cr, Mn, Mo, Sr, Ti, and Zr floodplain surface grid samples geochemical data not used in this study.

Sample	Co (ppm)	Cr (ppm)	Mn (ppm)	Mo (ppm)	Sr (ppm)	Ti (ppm)	Zr (ppm)
WCG-86	37	7	1646	28	67	4871	508
WCG-87	61	ND	1587	26	67	4163	456
WCG-88	41	24	1589	29	72	5239	521
WCG-89	44	13	1209	25	62	4040	372
WCG-90	74	ND	2245	21	76	4958	519
WCG-92	40	ND	1397	28	66	4895	471
WCG-93	59	29	1683	35	72	5020	470
WCG-94	ND	ND	1764	29	74	4853	449
WCG-95	94	63	1724	26	72	5360	456
WCG-96	ND	8	1498	30	64	5004	462

ND Below detection limit

Appendix D. Textural Data

Appendix D. Textural data used in this study.

	Particle Size			
Sample	Sand % (2000-62.5μm)	Silt % (62.5-3.9μm)	Clay % (<3.9μm)	Mean (am)
WFN-69	5	71	23	33
WFN-70	4	72	24	33
WFN-71	5	70	26	33
WFN-72	1	71	28	33
WFN-73	0	71	29	33
WFN-74	0	70	30	33
WFN-75	0	70	30	33
WFN-76	0	69	31	33
WFN-77	0	70	30	33
WFN-78	0	69	31	33
WFN-79	0	69	31	33
WFN-80	0	69	31	33
WFN-81	0	69	31	33
WFN-82	0	70	30	33
WFN-83	0	69	31	33
WFN-84	0	69	31	33
WFN-85	0	71	28	33
WFN-86	44	39	17	33
WFN-87	44	41	16	33
WFN-88	50	34	15	33

Appendix E. Total Carbon and Inorganic Carbon Data

Appendix E. Carbon data used in this study.

	Depth (cm)				
Sample	Min	Max	Total Carbon (%)	Inorganic Carbon (%)	Organic Carbon (%)
WFN-69	0	5	3.59	1.51	2.08
WFN-70	5	10	2.52	1.47	1.04
WFN-71	10	15	1.87	1.11	0.76
WFN-72	15	25	1.44	0.58	0.86
WFN-73	25	35	0.99	0.17	0.82
WFN-74	35	45	1.17	0.08	1.08
WFN-75	45	55	1.07	0.08	0.99
WFN-76	55	65	0.95	0.08	0.87
WFN-77	65	75	0.87	0.08	0.79
WFN-78	75	85	1.06	0.10	0.97
WFN-79	85	95	1.19	0.08	1.11
WFN-80	95	105	1.10	0.12	0.98
WFN-81	105	115	0.87	0.12	0.76
WFN-82	115	125	0.78	0.09	0.69
WFN-83	125	135	1.17	0.10	1.06
WFN-84	135	145	1.10	0.08	1.02
WFN-85	145	155	0.97	0.12	0.85
WFN-86	155	165	13.33	7.97	5.35
WFN-87	165	175	16.85	4.57	12.28
WFN-88	175	187	6.32	3.65	2.67